AD-A071 716 FLORIDA UNIV GAINESVILLE ROTORDYNAMICS LAB F/G 20/11
INVESTIGATION OF LOAD-INDUCED NON-SYNCHRONOUS WHIRL INSTABILITI--ETC(U)
MAR 79 J M VANCE, G N SANDOR, K E ARD DAAG29-77-G-0217
UNCLASSIFIED ARO-15041.2-E NL

1 OF 2
AD A071716

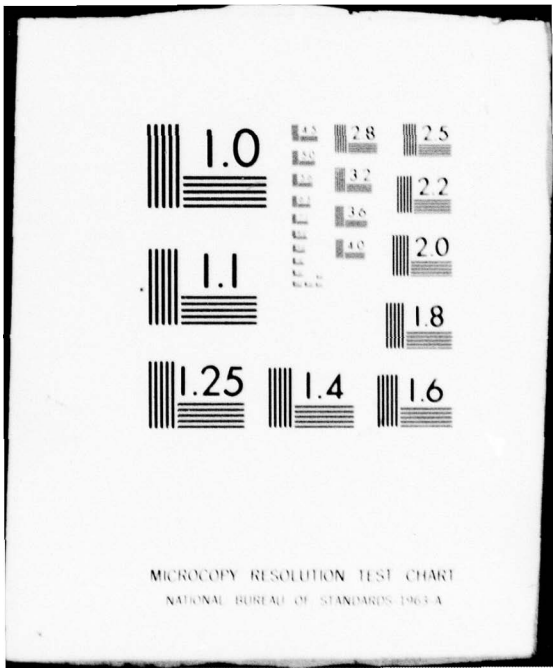
1.0
1.1
1.25
1.4
1.6
2.8
3.2
3.6
4.0
2.5
2.2
2.0
1.8
MICROCOPY RESOLUTION TEST CHART
NATIONAL BUREAU OF STANDARDS 1963-A

LEVEL

ARO. 1504.2-E

12

FINAL REPORT

U. S. ARO GRANT No. DAAG29-77-G-0217

INVESTIGATION OF LOAD-INDUCED NON-SYNCHRONOUS WHIRL INSTABILITIES IN ROTATING MACHINERY

09/15/77 - 03/31/79

J. M. VANCE and G. N. SANDOR
with K. E. ARD and F. J. LAUDADIO

Unclassified

SECURITY CLASSIFICATION OF THIS PAGE (When Data Entered)

REPORT DOCUMENTATION PAGE

READ INSTRUCTIONS BEFORE COMPLETING FORM

1. REPORT NUMBER: 15041.2-E (19) (18) ARO
2. GOVT ACCESSION NO.
3. RECIPIENT'S CATALOG NUMBER (9)

4. TITLE (and Subtitle) (6): INVESTIGATION OF LOAD-INDUCED NON-SYNCHRONOUS WHIRL INSTABILITIES IN ROTATING MACHINERY.

5. TYPE OF REPORT & PERIOD COVERED: Final Report. 15 Sep 77 - 31 Mar 79

6. PERFORMING ORG. REPORT NUMBER

7. AUTHOR(s) (10): John M. Vance, Kenneth E. Ard, George N. Sandor, Frank J. Laudadio

8. CONTRACT OR GRANT NUMBER(s) (15): DAAG29-77-G-0217

9. PERFORMING ORGANIZATION NAME AND ADDRESS
University of Florida
Gainesville, Florida 32611
Rotordynamics Lab

10. PROGRAM ELEMENT, PROJECT, TASK AREA & WORK UNIT NUMBERS

11. CONTROLLING OFFICE NAME AND ADDRESS (11)
U. S. Army Research Office
P. O. Box 12211
Research Triangle Park, NC 27709

12. REPORT DATE: Mar 79
13. NUMBER OF PAGES: 121

14. MONITORING AGENCY NAME & ADDRESS (if different from Controlling Office) (12) 126p.

15. SECURITY CLASS. (of this report): Unclassified
15a. DECLASSIFICATION/DOWNGRADING SCHEDULE

16. DISTRIBUTION STATEMENT (of this Report)

Approved for public release; distribution unlimited.

17. DISTRIBUTION STATEMENT (of the abstract entered in Block 20, if different from Report)

18. SUPPLEMENTARY NOTES

The view, opinions, and/or findings contained in this report are those of the author(s) and should not be construed as an official Department of the Army position, policy, or decision, unless so designated by other documentation.

19. KEY WORDS (Continue on reverse side if necessary and identify by block number)

multiple-disk rotors
flexible shafts
rotating machinery
whirl instabilities
torquewhirl
damping coefficients
shaft flexibility

411300

20. ABSTRACT (Continue on reverse side if necessary and identify by block number)

Seven tasks are described which were designed to reach the objectives. At the time of termination of the grant, these tasks were in various stages of completion, as described in this report.
Tasks 1 and 2: Experimental Verification of "Torquewhirl"; Task 3: Measurement of the Alford Force; Task 4: Comparison of Test Data with Theory; Task 5: Inclusion of a More General Shaft Flexibility in the "Torquewhirl" Theory; Task 6: Derivation of the Linearized Stiffness Damping, and Cross-Coupling for Use in a Computer Stability Analysis; and Task 7: Load-Dependent Stability Predictions for a Machine of Realistic Complexity.

DD FORM 1 JAN 73 1473 EDITION OF 1 NOV 65 IS OBSOLETE

Unclassified

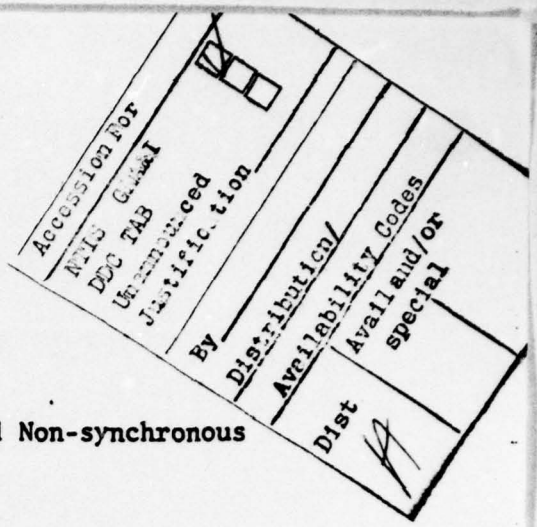

FINAL REPORT

1. ARO PROPOSAL NUMBER DRXRO-PR P-15041-E

2. PERIOD COVERED: 09/15/77 - 03/31/79

3. TITLE OF PROPOSAL: Investigation of Load-Induced Non-synchronous Whirl Instabilities in Rotating Machinery

4. GRANT NUMBER: DAAG29-77-G-0217

5. NAME OF INSTITUTION: Rotordynamics Laboratory, Department of Mechanical Engineering, University of Florida, Gainesville, Florida 32611

6. AUTHORS OF REPORT: Drs. J. M. Vance and G. N. Sandor, with Kenneth E. Ard and Frank J. Laudadio

7. LIST OF MANUSCRIPTS SUBMITTED OR PUBLISHED UNDER ARO SPONSORSHIP DURING THIS PERIOD, INCLUDING JOURNAL REFERENCES:
Vance, J. M. and Tison, J. D.,
"Analysis and Interpretation of Nonsynchronous Whirling in Turbomachinery", presented in the session organized by the Petroleum Division of the American Society of Mechanical Engineers, Houston, Texas at the Energy Technology Conference and Exhibition, November 5-9, 1978

8. SCIENTIFIC PERSONNEL SUPPORTED BY THIS PROJECT AND DEGREES AWARDED DURING THIS REPORTING PERIOD:
   i. Dr. John M. Vance, First Principal Investigator, (to September, 1978)
   ii. Dr. George N. Sandor, 2nd Principal Investigator, (to September, 1978)
   iii. Mr. Kenneth E. Ard, BSME, Graduate Research Assistant, (Masters Degree Candidate), (to September, 1978)
   iv. Mr. Frank J. Laudadio, Student Assistant, BSME degree candidate at senior level (to September, 1978)

   Note: Although funding was withdrawn in September, all four of the above-listed researchers continued working on the project: Dr. Vance at Texas A & M University, the other three here in the Department of Mechanical Engineering at the University of Florida, Gainesville, Florida 32611. Also, Mr. Mark S. Darlow of Mechanical Technology, Inc. (MTI), Rotordynamicist, now Ph.D. candidate at U.F., served as consultant without remuneration, as did also Mr. Mike Dove, Student Assistant, BSME degree candidate at the senior level.

   There were no degrees awarded during this period to personnel on this project.

9. The FINAL TECHNICAL REPORT is attached.

March 31, 1979

FINAL TECHNICAL REPORT

Contents

FINAL REPORT: ARO Grant No. DAAG29-77-G-0217,
"Investigation of Load-Induced Nonsynchronous
Whirl Instabilities in Rotating Machinery"

Background

The grant for this investigation was made to the University of Florida (EIES) in the amount of $70,469, for a period of two years beginning in September 1977. A third year of funding was made optional at the discretion of the Army. The Principal Investigators were Drs. J. M. Vance and G. N. Sandor.

At the end of the first year, Dr. Vance joined the Mechanical Engineering faculty at Texas A&M University, leaving the grant under the direction of Dr. Sandor. Several months later, the grant was terminated by the Army.

This report gives results accomplished up to the termination date, and also gives certain material required for a possible future completion of the work.

Objectives

The overall objective of this investigation was to experimentally verify (or modify) and analytically extend the two available theories which can explain torque-load-dependent nonsynchronous shaft whirling in turbomachinery, so as to develop an improved methodology for design of compressors and turboshaft engines.

The specific technical objectives were:

1. To experimentally verify in a controlled test apparatus the mathematical solution of reference 1, called "torquewhirl".

2. To experimentally verify the existence of the aerodynamic tip-clearance effect hypothesized by Alford in reference 7, and determine the direction of the induced tangential force.
3. To extend the analysis of reference 1 to include the effects of a more general type of shaft flexibility.
4. To derive the linearized stiffness and damping coefficients resulting from the "torquewhirl" generalized forces, for use in a linearized stability analysis, such as the one developed by Lund (reference 14) for multiple-disk rotors with flexible shafts and other realistic complexities.
5. To verify the usefulness of the theory by incorporating the linearized "torquewhirl" and Alford coefficients into a stability analysis (such as the computer program of reference 14) to predict the threshold of whirl instability for a rotating machine with an available background of test data for comparison and/or verification.

Results and/or Status at the Termination Date

There are seven tasks described in the grant's Statement of Work which are designed to reach the above objectives. At the time of termination of the grant, these tasks were in various stages of completion, as described below. Wherever the results or description of status involve extensive details, they are relegated to referenced appendices.

Tasks 1 and 2: Experimental Verification of "Torquewhirl"

A test rig capable of producing torquewhirl under controlled and measured

conditions in the laboratory has been designed. The basic test problem addressed by the design is that torquewhirl normally occurs only in rotating machines with extremely high levels of load torque and horsepower, a condition which is expensive to simulate in the laboratory. This problem was overcome by designing the rig with very low damping and very high susceptibility to torquewhirl.

Drawings are now ready to begin shop construction. The design is the result of an extensive optimization study to produce measurable levels of torque-excited whirl with the relatively low levels of torque available in the laboratory from a 15 HP aircraft electric motor. The design includes a unique concept to apply the torque in a controllable manner. See Appendix A for a detailed description of the design procedure and the resulting test rig design.

Task 3: Measurement of the Alford Force

A test rig to measure Alfrod's force has been redesigned and rebuilt with a flexibly-mounted fan rotor, adjustable housing offset, variable-speed motor, and instrumentation to measure the deflection produced by Alford's force. The instrumentation includes a special filter circuit to enable the very small DC deflection signal from Alford's force to be measured in the presence of unavoidable vibration from shaft unbalance, runout, and bearing roughness.

Measurements from the original test rig did produce indications that the force was in the direction predicted by Alford, but the data was considered inconclusive because of surging, large standard deviation, and the

presence of a large synchronous vibration component in the signal.

In the new rig, vibration has been minimized by the use of instrument quality bearings, and by precision balancing of the rotor.

The new rig was just ready to begin providing data at the time of writing this report.

Details of the rig design and results obtained to date are given in Appendix B.

Task 4: Comparison of Test Data with Theory

This task is dependent on future completion of Tasks 2 and 3.

Task 5: Inclusion of a More General Shaft Flexibility in the "Torquewhirl" Theory

This task is a modification of the original Task 5, in keeping with a suggestion by one of the Proposed Reviewers that the single-joint shaft flexibility model in reference 1 is too restrictive. (Documented by letter correspondence with Dr. Ed Saibel).

There are two ways one can take a more general shaft flexibility model into account. One is to expand the three degree of freedom model of reference 1 to four (or five) degrees of freedom, allowing the shaft to bend in a general manner, and attempting to find an exact solution to satisfy the non-linear differential equations of motion (as in reference 1). The generalized coordinates are chosen to render the functional solutions tractable.

The second approach is to first derive generalized forces in a cartesian coordinate system from a virtual work expression which includes the four degrees of freedom allowed by the flexible shaft. Linearized stiffness and

damping (Lund) coefficients are then derived from the generalized forces, and can be used in a computer program such as the one described in reference 14.

The two approaches are radically different, mathematically, because of the different choice of generalized coordinates to describe the motion.

The former approach is outlined in Appendix C.

The latter approach is the subject of Task 6, and is described in Appendix D.

Final results have not been obtained as of the termination date, but work on these tasks is being continued at Texas A&M University by Dr. Vance and Mr. Brian Murphy.

Task 6: Derivation of the Linearized Stiffness Damping, and Cross-Coupling for Use in a Computer Stability Analysis

These coefficients have been derived for the "Torquewhirl" model of reference 1, and are given in Appendix "D".

Derivation of the coefficients for the extended flexible-shaft model is still in progress. The approach is outlined in Appendix D.

Task 7: Load-Dependent Stability Predictions for a Machine of Realistic Complexity

Part of this task, as stated in the Proposal, was to "improve the computational speed and accuracy by incorporating the method of reference 15 to generate the coefficients of the characteristic polynomial, which can then be numerically solved for the complex roots." The proposed method involves using the transfer matrices to generate the polynominal coefficients.

Since this is conceptually difficult for the general rotor dynamic problem with four boundary conditions and complex roots, work was started by applying the method to torsional vibration problems. Results of this initial work are given in Appendix D.

The major part of Task 7, a comparison of stability predictions with test results from an unstable machine, had not been addressed as of the termination date, since it is dependent on results from Task 6.

References

1. Vance, J. M., "Torquewhirl - A Theory to Explain Nonsynchronous Whirling Failures of Rotors with High Load Torque", ASME Paper No. 76-DE-29, Design Engineering Conference, Chicago, April 5-8, 1976.

2. Rankine, W. A., "On the Centrifugal Force of Rotating Shafts", Engineer, London, Vol. 27, 1869, p. 249.

3. Hori, Y., "A Theory of Oil Whip", ASME Journal of Applied Mechanics, June 1959, pp. 189-198.

4. Crandall, S. H., and Brosens, P.J., "On the Stability of Rotation of a Rotor With Rotationally Unsymmetric Inertia and Stiffness Properties", ASME Journal of Applied Mechanics, December 1961, pp. 567-570.

5. Gunter, E. J., Jr., Dynamic Stability of Rotor-Bearing Systems, NASA-SP-113, 1966.

6. Sternlicht, B., "Stability and Dynamics of Rotors Supported on Fluid-Film Bearings, ASME Journal of Engineering for Power, October 1963, pp. 331-342.

7. Alford, J. S., "Protecting Turbomachinery From Self-Excited Rotor Whirl", ASME Journal of Engineering for Power, October 1965, pp. 333-344.

8. Ehrich, F. F., "Identification and Avoidance of Instabilities and Self-Excited Vibrations in Rotating Machinery," ASME Paper No. 72-DE-21, Design Engineering Conference, Chicago, May 8-11, 1972.

9. Smith, D. M., Journal Bearings in Turbomachinery, Chapman and Hall, London, 1969, pg. 127.

10. Ehrich, F. F., "An Aeroelastic Whirl Phenomenon in Turbomachinery Rotors", ASME Paper No. 73-DET-97, Design Engineering Technical Conference, Cincinnati, Ohio, September 9-12, 1973.

11. Wachel, J. C., "Nonsynchronous Instability of Centrifugal Compressors", ASME Paper No. 75-PET-22, Petroleum Mechanical Engineering Conference, Tulsa, Oklahoma, September 21-25, 1975.

12. Fowlie, D. W., and Miles, D. D., "Vibration Problems with High Pressure Centrifugal Compressors", ASME Paper No. 75-PET-28, Petroleum Mechanical Engineering Conference, Tulsa, Oklahoma, September 21-25, 1975.

13. Vance, J. M., "High-Speed Rotor Dynamics-An Assessment of Current Technology for Small Turboshaft Engines", USAAMRDL-TR-74-66, July 1974, pg. 35.

14. Lund, J. W., "Stability and Damped Critical Speeds of a Flexible Rotor in Fluid-Film Bearings", ASME Journal of Engineering for Industry, May 1974, pp. 509-517.

15. Pilkey, W., and Chang, P. Y., "Avoiding Iterative Searches to Find Critical Speeds of Rotating Shafts with the Transfer Matrix Method", ASME Paper No. 71-VIBR-53, Vibrations Conference, Toronto, September 8-10, 1971.

16. Vance, J. M., and Sitchin, A., "Derivation of First-Order Difference Equations for Dynamical Systems by Direct Application of Hamilton's Principle," ASME Journal of Applied Mechanics, June 1970, pp. 276-278.

17. Vance, J. M., and Sitchin, A., "Numerical Solution of Dynamical Systems by Direct Application of Hamilton's Principle", International Journal for Numerical Methods in Engineering, Vol. 4, 1972, pp. 207-216.

18. Seireg, Ali, Mechanical Systems Analysis, International Textbook Co., Scranton, Pa., 1969, pp. 371-373.

Appendix A

TORQUEWHIRL THEORY

TEST RIG DESIGN REPORT

KENNETH E. ARD

JUNE 1, 1978

Abstract

The recently published Torquewhirl theory defines a possible source of driving energy which may help cause failure due to non-synchronous shaft whirling. In an effort to investigate this possible driving source, a test rig must be designed. The design of the test rig is followed from the beginning to the present. Numerous problems have been encountered and are presented along with their proposed solutions. A detailed description of the test rig, as now envisioned, is included.

conditions in the laboratory has been designed. The basic test problem addressed by the design is that torquewhirl normally occurs only in rotating machines with extremely high levels of load torque and horsepower, a condition which is expensive to simulate in the laboratory. This problem was overcome by designing the rig with very low damping and very high susceptibility to torquewhirl.

Drawings are now ready to begin shop construction. The design is the result of an extensive optimization study to produce measurable levels of torque-excited whirl with the relatively low levels of torque available in the laboratory from a 15 HP aircraft electric motor. The design includes a unique concept to apply the torque in a controllable manner. See Appendix A for a detailed description of the design procedure and the resulting test rig design.

Task 3: Measurement of the Alford Force

A test rig to measure Alfrod's force has been redesigned and rebuilt with a flexibly-mounted fan rotor, adjustable housing offset, variable-speed motor, and instrumentation to measure the deflection produced by Alford's force. The instrumentation includes a special filter circuit to enable the very small DC deflection signal from Alford's force to be measured in the presence of unavoidable vibration from shaft unbalance, runout, and bearing roughness.

Measurements from the original test rig did produce indications that the force was in the direction predicted by Alford, but the data was considered inconclusive because of surging, large standard deviation, and the

presence of a large synchronous vibration component in the signal.

In the new rig, vibration has been minimized by the use of instrument quality bearings, and by precision balancing of the rotor.

The new rig was just ready to begin providing data at the time of writing this report.

Details of the rig design and results obtained to date are given in Appendix B.

Task 4: Comparison of Test Data with Theory

This task is dependent on future completion of Tasks 2 and 3.

Task 5: Inclusion of a More General Shaft Flexibility in the "Torquewhirl" Theory

This task is a modification of the original Task 5, in keeping with a suggestion by one of the Proposed Reviewers that the single-joint shaft flexibility model in reference 1 is too restrictive. (Documented by letter correspondence with Dr. Ed Saibel).

There are two ways one can take a more general shaft flexibility model into account. One is to expand the three degree of freedom model of reference 1 to four (or five) degrees of freedom, allowing the shaft to bend in a general manner, and attempting to find an exact solution to satisfy the non-linear differential equations of motion (as in reference 1). The generalized coordinates are chosen to render the functional solutions tractable.

The second approach is to first derive generalized forces in a cartesian coordinate system from a virtual work expression which includes the four degrees of freedom allowed by the flexible shaft. Linearized stiffness and

that many of the parameters used in the design of a test rig are coupled. The nature of the coupling is rather complex and can best be seen in Figure A-2. There are further couplings between parameters that are not readily visible from Figure A-2. For example, it is not obvious that an increase in the moment of inertia about the point of angular deflection results in an increase in the amount of horsepower required to produce torquewhirl. Nor is it obvious that this same increase in the moment of inertia reduces the shaft speed required for torquewhirl. Hidden relations such as these make it extremely difficult to get a rig design.

FIGURE A-2

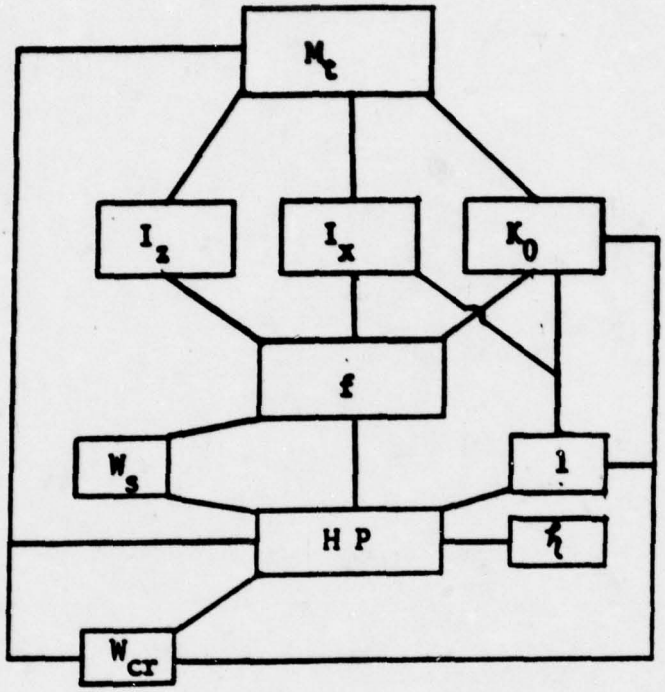

M_t = total mass
I_z = moment of inertia about axis of rotation
I_x = moment of inertia about point of angular deflection
K_0 = stiffness refered to point of angular deflection
f = whirling speed ratio
W_s = shaft speed
l = shaft length
H P = horse power required to produce Torquewhirl
ζ = damping ratio
W_{cr} = natural frequency of system

Design Concepts

Before the complex nature of the parameter relations was understood, a test rig was constructed by another investigative team. Not surprisingly, this rig failed to produce torquewhirl. The reason, of course, was that many of the important relations were completely overlooked. A sketch of this system is shown in Figure A-3. While this rig was basically a failure, it did provide this effort with a starting place.

It was known beforehand that the maximum power available would be around 15 H.P. This fact put limitations on the system design that were not fully understood at the time. The first attempts at the system development were based on power dissipation. The basic design was to have some sort of power dissipation unit suspended on a shaft. This shaft was to be coupled to the main drive shaft at the point of angular deflection. (See Fig. A-4) The outside of the dissipation unit was not to turn but was to be held by springs that were grounded to the support frame. The reason for this was so that the whirl motion could be ovserved without any rotation. This also was the easiest way of applying a reaction load torque to the dissipation unit. The type of dissipation could be either coulomb friction or viscous friction. Viscous friction was chosen for this system. It was thought that an impeller could be placed inside of a housing that was supported by the same shaft that was used to drive the

FIGURE A-3

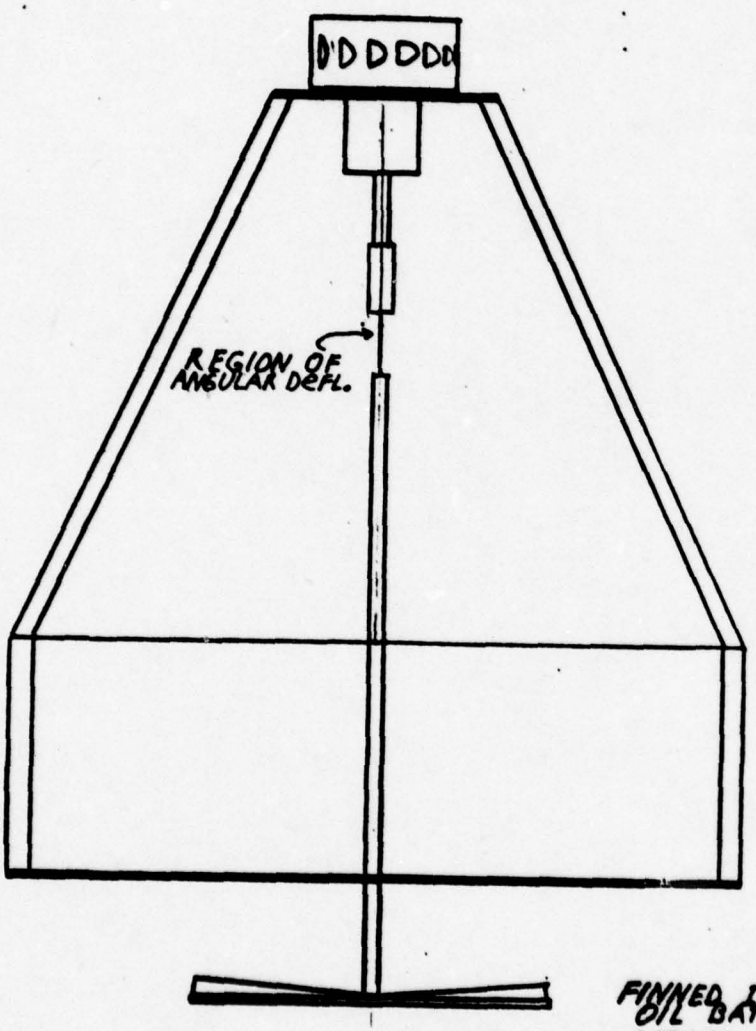

FINNED IMPELLER IN OIL BATH
WEIGHT ≈ 50 LBS
SHAFT LENGTH ≈ 25"

FIGURE A-4

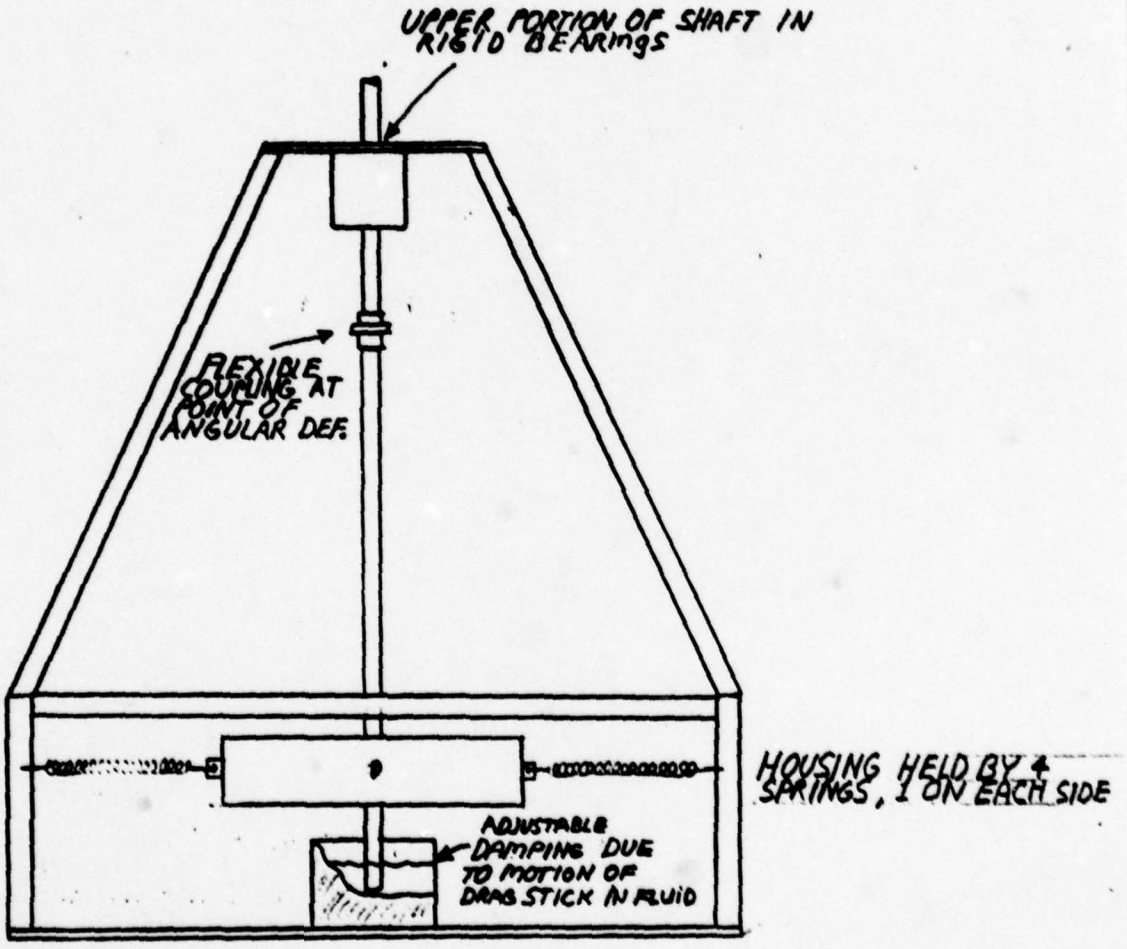
UPPER PORTION OF SHAFT IN RIGID BEARINGS
FLEXIBLE COUPLING AT POINT OF ANGULAR DEF.
HOUSING HELD BY 4 SPRINGS, 1 ON EACH SIDE
ADJUSTABLE DAMPING DUE TO MOTION OF DRAG STICK IN FLUID

impeller. The power was to be dissipated by pumping the fluid from the center out to the edges and then recirculating it back to the center. This method was dropped because of the many problems associated with power dissipation calculations and the possibility of pump stall or cavitation. Other fluid pumping ideas were abandoned for the same general reasons. The second approach was based on viscous shear. In this idea, the housing fit very close to the rotating impeller. The power was to be dissipated by the shearing of a thin film of fluid between the housing and the impeller. This method would dissipate a good deal of horsepower, but required a large diameter impeller because it was desired to dissipate approximately 15 H.P. An operational speed of 250 rpm was arbitrarily assigned. These limitations were placed on the system before the relations between them was known. Because of the low rpm of the system, a large impeller was required. For this reason the idea was rejected. This idea may be more viable when viewed in the light of higher speeds, which appear to be possible. A review of this idea is warranted before the go ahead is given to any other design.

Another idea based on viscous friction was put forward at a design meeting on January 17, 1978. In this idea the impeller took the form of a conical plug. (See fig. A-5) The plug fit inside of a mating housing. The shape of the outside of the housing was not determined at the time but was assumed to be boxlike. Power dissipation in this system was adjustable. The adjustment was made by moving the plug in or out slightly and thereby changing the thickness of the viscous shear film. This is basically the form of the system today.

FIGURE A-5

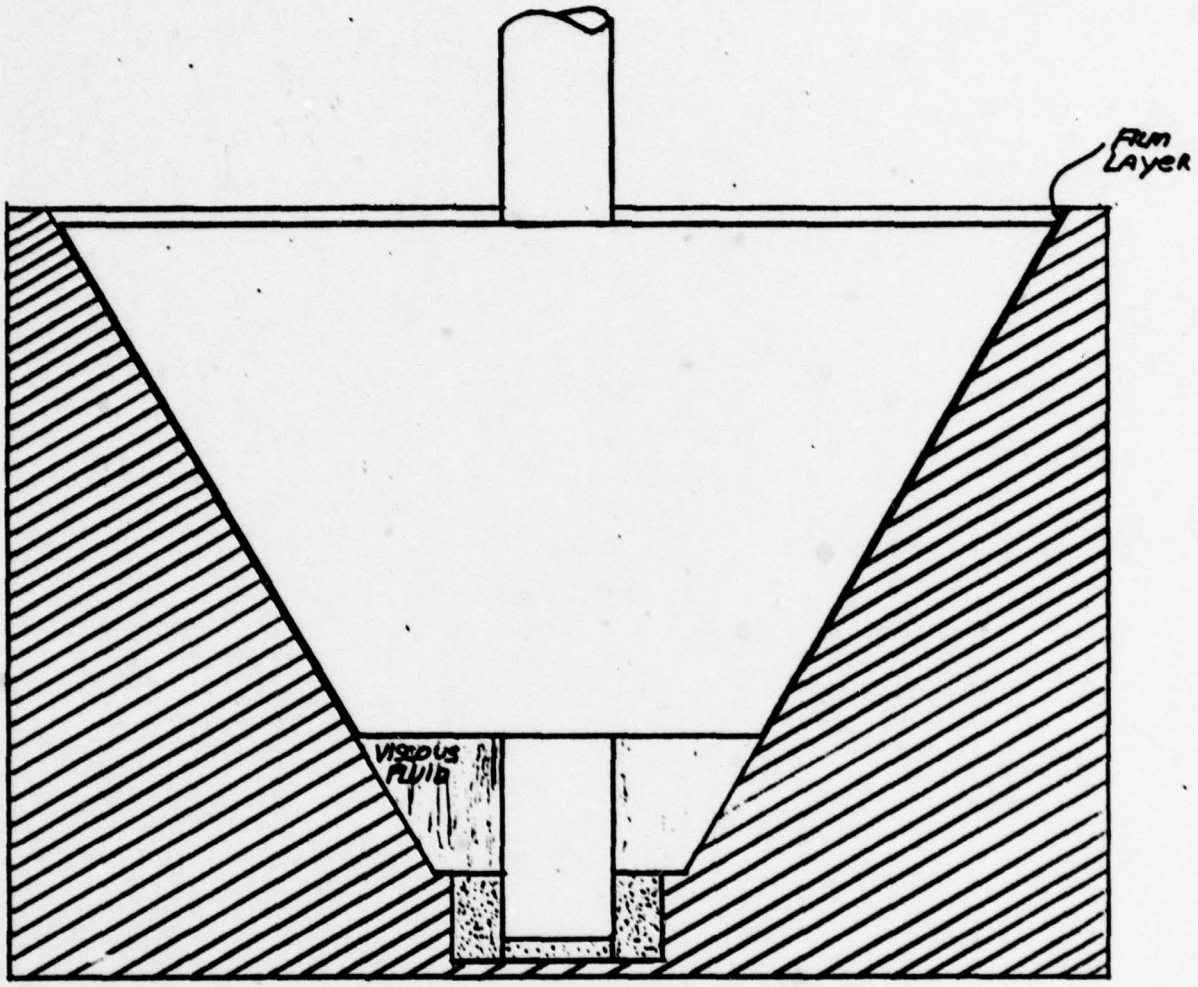

CONICAL PLUG IN MATING HOUSING
VISCOUS SHEAR DISSIPATION

At the time, the size of the system was still unknown. In an effort to get some feel for how large or small the system should be, several mathematical models were set up. An equation was developed which related horsepower dissipation to size, film thickness, viscosity, shaft speed and angle of plug cone.

This equation was used to develop horsepower dissipation vs. speed curves for the various models. To do this, the viscosity was assumed to be 56 micro reyns (Dow Corning silicon fluid 1000). The film thickness was taken as .003 inches. The cone half angle was taken as 30^0. It is important to note that during the design process the value of f, the whirling frequency ratio was limited to be between .4 and .7 so as to resemble actual field date. The curves were reviewed in light of this limitation on f and the assumed horsepower available. From the review, one system was chosen as most desirable. At the time this selection was made, most of the relations between parameters were still to be uncovered. (For example, though the system selected from the curves would dissipate an adequate amount of horsepower at a certain rpm, it would not be dissipating enough at that speed for torquewhirl to be produced.) The selected system was then analyzed more carefully. The effect of changing the shaft length, the effect of changing the speed, and most other parameters as well, were investigated. This is when the relationships began to appear between power, speed and moment of inertia about the coupling (located at a point of angular deflection). The selected system was continually modified. The purpose of all modifications was to increase

speed and decrease the power required for torquewhirl.* The result of all the basic modifications was a reduction in size and removal of the shaft from the couple to the dissipation unit in favor of a direct connection. A sketch of the basic unit as was perceived at this stage is shown in Figure A-6.

* Note: there are two powers with which we are concerned. One is the power the unit will dissipate at a given rpm, and the other is the power required for torquewhirl.

FIGURE A-6

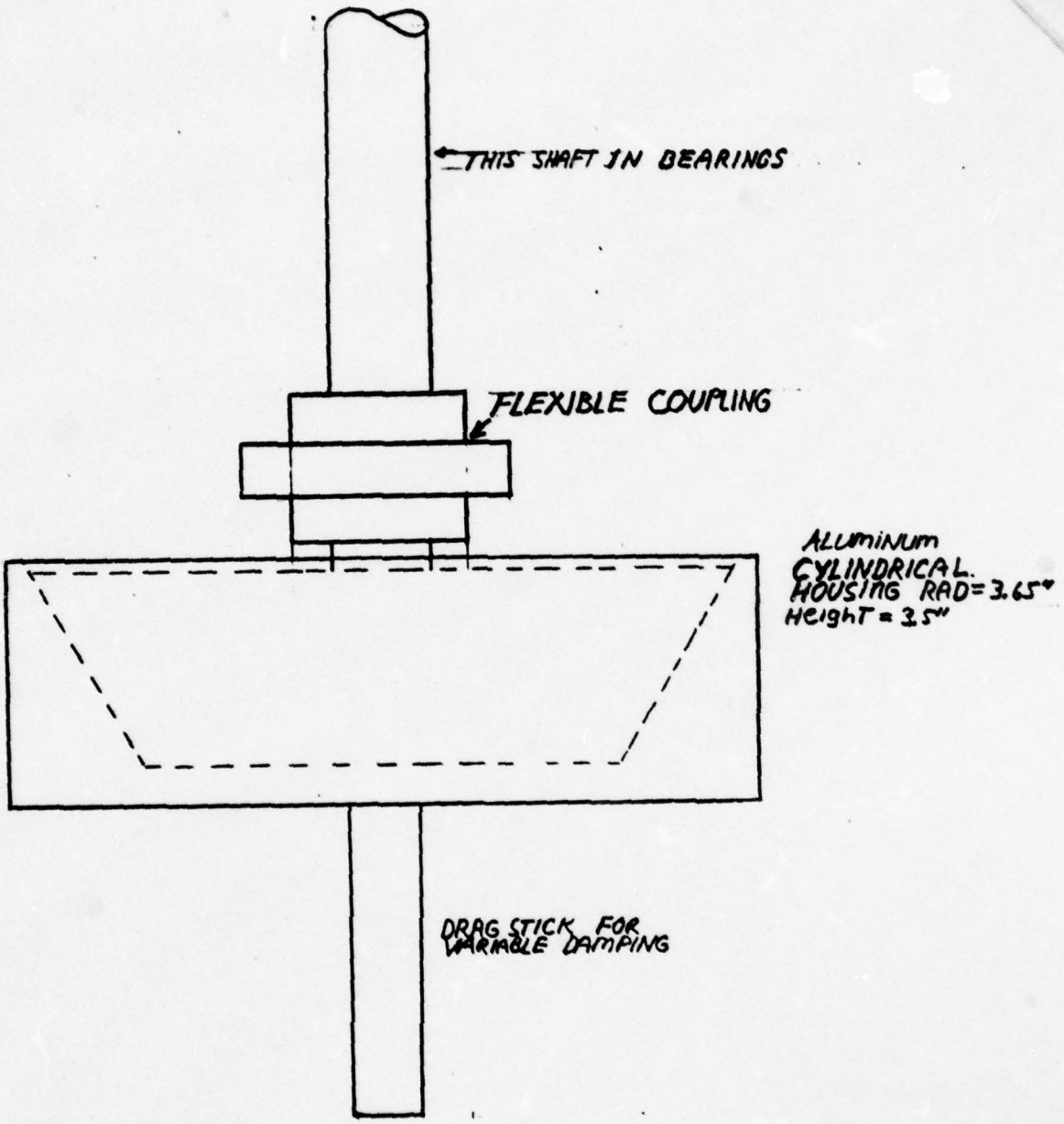
THIS SHAFT IN BEARINGS
FLEXIBLE COUPLING
ALUMINUM CYLINDRICAL HOUSING RAD = 3.65"
HEIGHT = 3.5"
DRAG STICK FOR VARIABLE DAMPING

Problems with the Basic Unit

For any machine, the percent of critical damping that will be present in the final construction is very difficult to determine. For the torquewhirl test rig the percent of damping is a very important parameter. It has a direct effect on the amount of horsepower that is required for torquewhirl. Before any finalized design can be developed the value of ζ must be determined. To do this a rig model was constructed and the percent critical damping was determined by the log decrement method. The value obtained was ζ = .24%. This very low value enables the system to function at much higher speeds since it requires less power to produce torquewhirl.

The system in its present form will dissipate approximately 12 H.P. This brings up an obvious problem. How to get rid of 12 H.P. worth of heat. It was at first hoped that the thermal capacity of the aluminum plug and housing would be sufficient to absorb the heat while the necessary readings were taken. This did not prove to be the case. Based on thermal capacitance alone, the operating time before a temperature in excess of 250^0 F was reached, was only 59 seconds. Some method of heat transfer would have to be devised. Calculation for free convection showed no improvement, so forced convection was considered. It was decided that fins would be necessary to get the rate of heat transfer required. The fins are to be machined into the

previously cylindrical housing as shown in Figure A-7. Forced flow was assumed at six feet per second, based on experimental results from a standard blower. Analysis for the fins was carried out apart from the rest of the housing. Based on the flow velocity and an assumed steady state temperature difference of 175°, a convective heat transfer coefficient of 197.5 BTU/hr-ft^{2}-°F was obtained. The non-finned portion of the housing was analyzed based on the flat plate assumptions. It turned out that eight fins, 3/8 of an inch thick would be sufficient when combined with other surface transfer rates. The forced convection is to be developed by attaching a small fan to the portion of the shaft that is rigidly fixed in the bearings above the coupling. The fan will turn at the shaft speed of the system. Air will be drawn up through a large tube that surrounds the dissipation unit (see Fig. A-8). The flow velocity can be controlled by ports at the bottom of the tube. Partitions will be placed in the tube to ensure that the flow is turbulent before it reaches the dissipation unit.

Another problem, not quite as obvious as the heating problem, is a result of the centrifugal effect the rotating plug imparts to the viscous film layer. This centrifugal effect causes the fluid to, in effect, be pumped out from under the plug. The net result is that the plug is sucked down with more and more force. This continues until the plug seizes. To alleviate this problem, the plug is fitted with two return ducts which can be seen in Figure A-9. These ducts insure that the fluid will be able to get back down under the plug. The angled portions of the ducts act as centrifugal pumps in themselves. The use of this solution to the seizure problem requires a level

FIGURE A-7

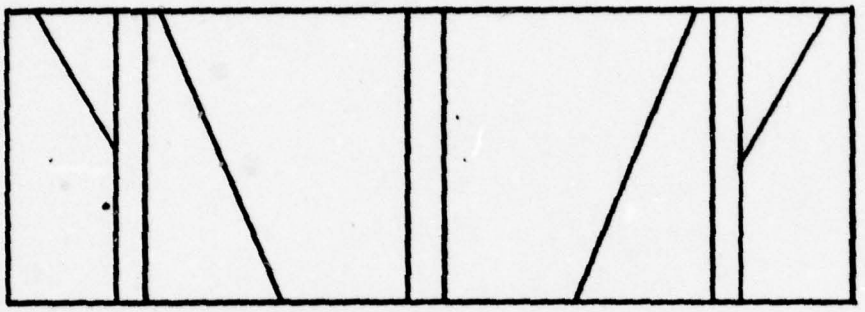

FINS ARE MACHINED INTO CYLINDRICAL HOUSING

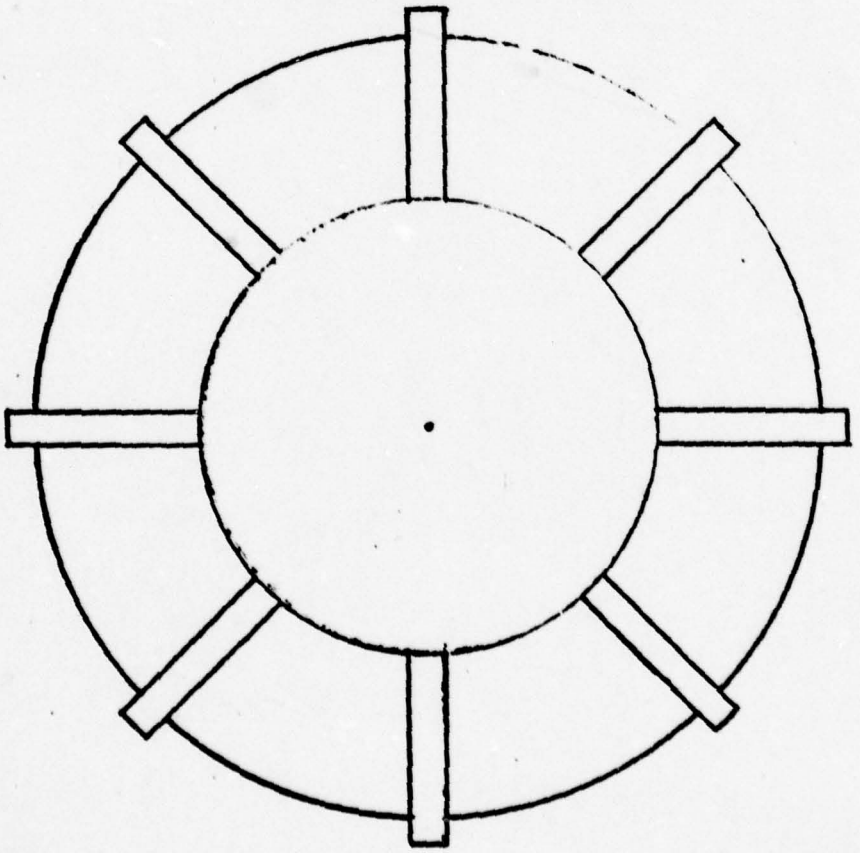

FIGURE A-8

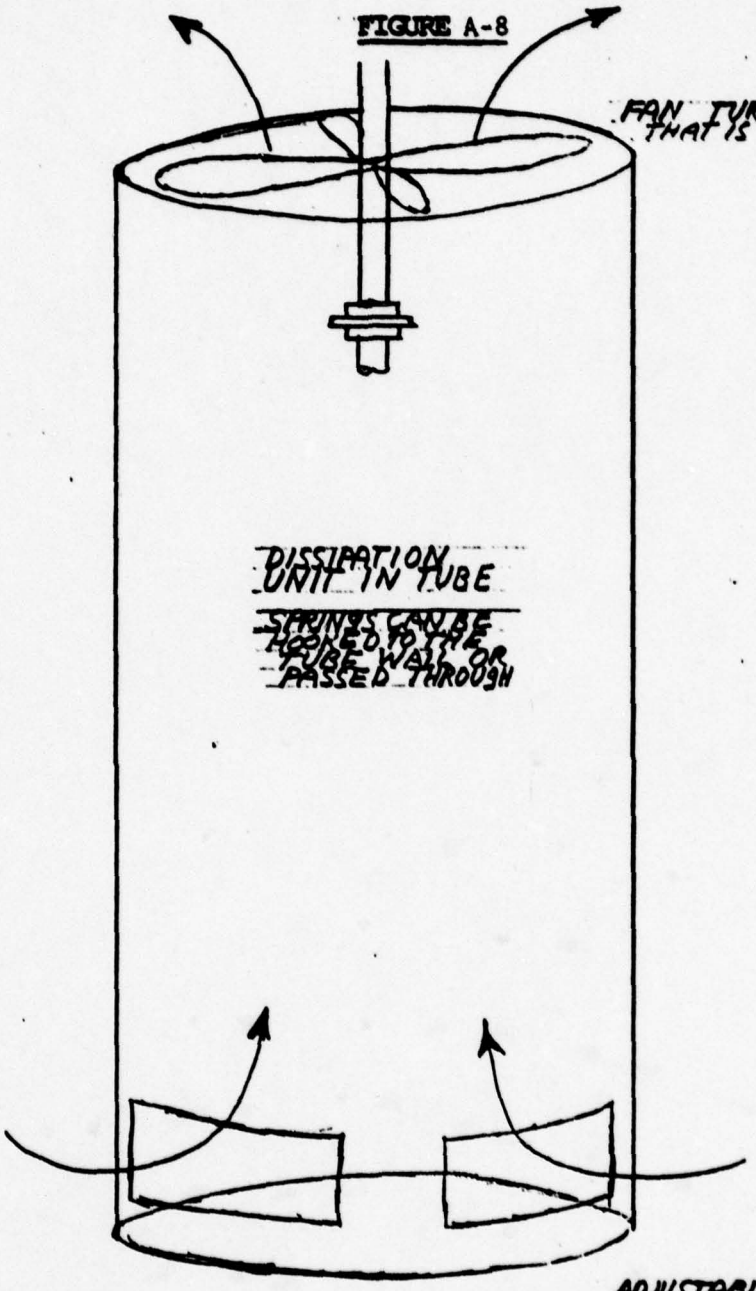
FAN TURNS WITH SHAFT THAT IS IN BEARINGS
DISSIPATION UNIT IN TUBE
STRUTS CAN BE WELDED TO THE TUBE WALL OR PASSED THROUGH
ADJUSTABLE INTAKE PORTS CONTROL FLOW RATE

FIGURE A-9

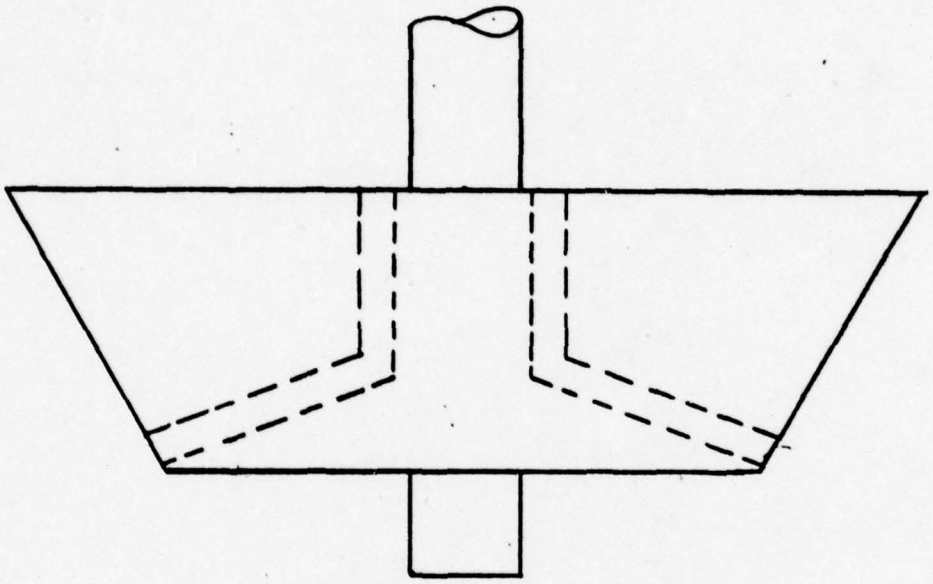

2 RETURN PORTS 180° APART ACT AS PUMP TO FORCE FLUID BELOW PLUG

of fluid to cover the top of the plug. In order to prevent this fluid from being slung out it is necessary to put a cap over the entire housing. This plate serves two purposes. First, of course, it keeps the fluid from being slung out, and second, it provides a seat for the top bearing. This top bearing is included to ensure alignment and prevent housing wobble. (See Fig. A-10)

In order to make adjustments to the power dissipation it is necessary to be able to adjust the film thickness. In the original basic design this was done by tightening a nut that turned with the bottom of the shaft. Naturally a more desirable method would be one that allowed adjustments while the rig was in operation. For this purpose, a device was developed that utilizes two wedges. (See Fig. A-10). The top wedge is fixed with respect to the cover plate. The bottom wedge is free to slide. The bottom wedge applies pressure to the bearing in the cover plate. This bearing sits on a shoulder on the shaft. It has a sliding fit between its outer race and the cover plate. When the lower wedge is slid in, the bearing and therefor the shaft and plug are forced down. The film clearance is reduced. The lower wedge is controlled by two thumb screws, one on either side, that are grounded to the plate. The wedges have an angle of 1.78^{o}. It requires 1/2 inch of linear wedge motion to produce .015 in. of axial plug motion. This corresponds to full adjustment of the film thickness. Two bevel springs are located beneath the bearing and contact the bearings outer race and the plate. The purpose of these two springs is to aid gravity in holding the film gap at the desired

FIGURE A-10

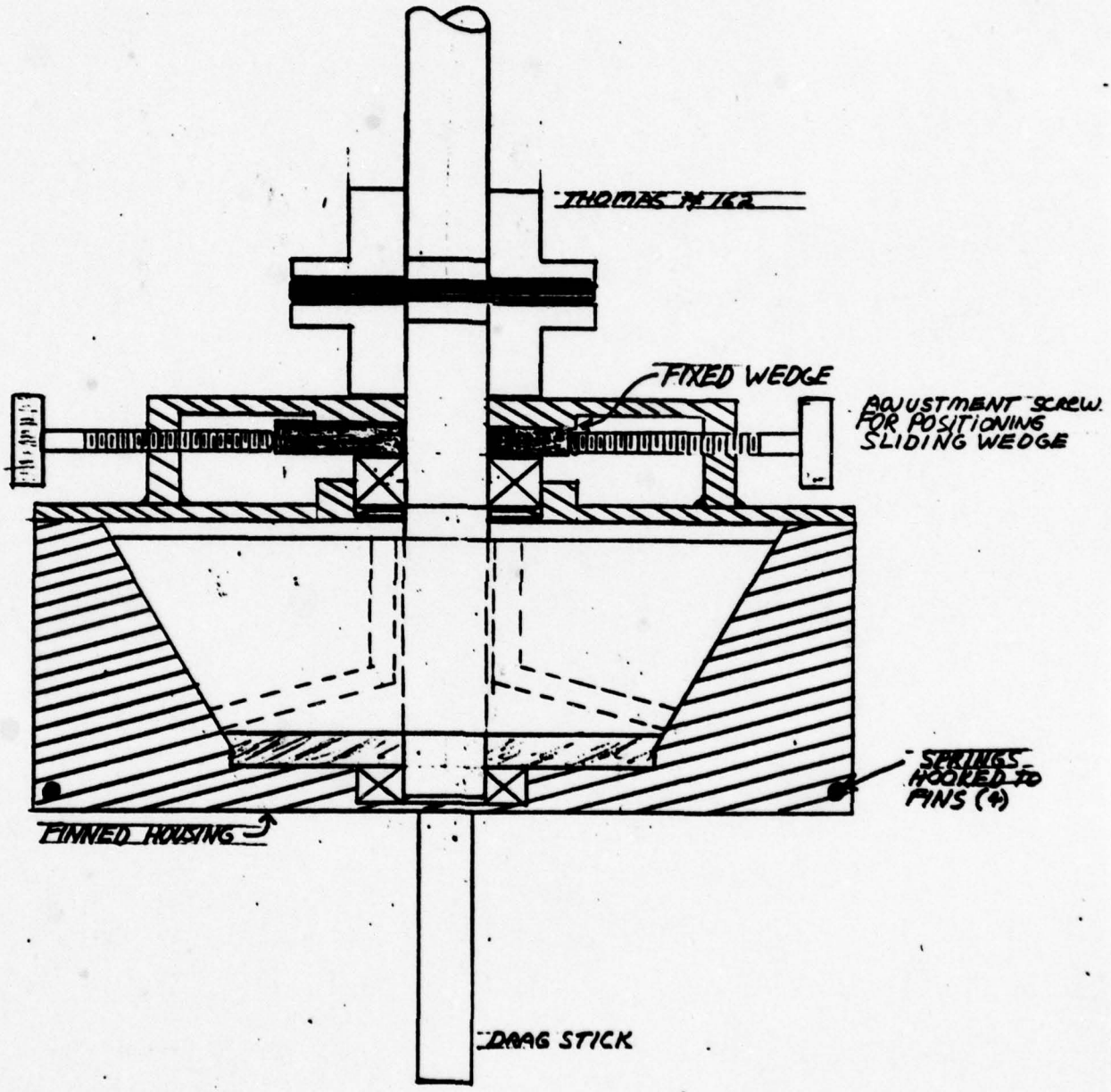
THOMAS #162
FIXED WEDGE
ADJUSTMENT SCREW FOR POSITIONING SLIDING WEDGE
SPRINGS HOOKED TO PINS (4)
FINNED HOUSING
DRAG STICK

A good deal of searching was required to find a coupling that would handle the anticipated 68 ft. lb. of torque and also the expected 4^0 of angular misalignment. Parallel misalignment features found on most couplings are not desirable for this application. The first choice was a universal joint. However, universals do not transmit a constant velocity and were therefor deemed unsatisfactory. Numerous other coupling styles were investigated. The final choice was a Thomas Model 162. The Thomas coupling is of the standard disc pack construction and will handle the expected loads. One possible problem that requires testing is the added damping due to this type of coupling. It is hoped it is not sufficient to raise the horsepower requirement out of the range of the selected drive motor. Should this damping prove too large, the coupling search will continue.

For powering the system, a 14 H.P. aircraft generator was selected. The basis for this selection was primarily price, but also because some experience has been had with this type of power drive from other projects.

Summary

The primary design of the torquewhirl test rig is very near completion. The design calculations are in the process of being checked out. Material selection has, for the most part, been completed. Almost certainly there will be unexpected problems that will arise during and after construction. These will be dealt with as they develop. Every precaution has been taken so that nothing has been overlooked.

At this time the project is nearing the construction phase. What remains to be done is a final check of all calculations. A recheck of the speed and power requirements for the system with all the changes included in the calculations and the necessary parts and assembly drawings will be done. If all goes as expected, construction will begin within the next two months. Figure A-10 is a sketch of the system as now designed.

Final Design of Torquewhirl Test Rig

The design of the Torquewhirl test rig proved to be far more complicated than originally assumed. A thorough examination of the Torquewhirl equations reveals a high degree of cross-coupling between the variable design parameters. This coupling became a major problem in the early stages of the design, when initial sizing of the rig was necessary. The diagram on the following page (Fig. A-1A) gives an overview of the linking of variable design parameters. Once the nature of the parameter coupling was understood, the design process advanced more rapidly. Thus, changes and new ideas could be considered in light of their overall system effect. (See Appendix A, page A3.)

It was known beforehand that the maximum power available would be around 15 h.p. This fact put limitations on the system design. The exact nature of these limitations was not fully understood at the early stage of design. The first attempts at system development were based on power dissipation alone. The basic system was to have some sort of power dissipation unit suspended on a shaft. This shaft was to be coupled to a main drive shaft at a point of concentrated flexural elasticity (see Fig. A-2A). The outside of the dissipation unit was not to rotate, but was to be held by springs which were grounded to the support frame. These springs afford a method for measuring the torque developed by the power dissipation device. This is accomplished by observing the rotational displacement of the housing of the dissipation device. With this type of setup it would be possible to observe the expected whirl motion without rotation. The method of power dissipation could be the result of either Coulomb or viscous friction. Viscous friction was chosen as the preferred method. In the early stage of the design it was thought that an impeller

FIGURE A-1A

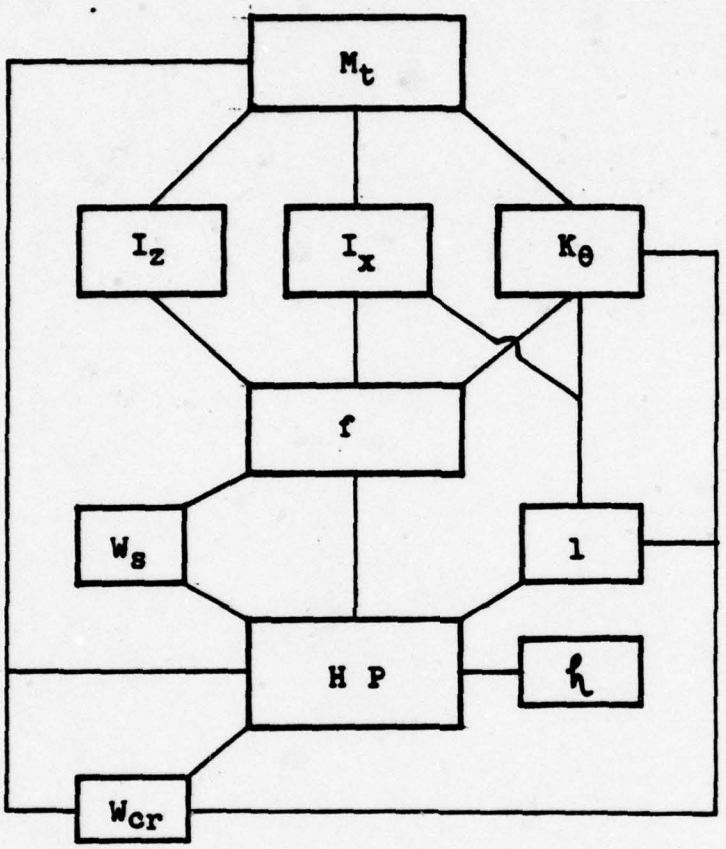

M_t = total mass

I_z = moment of inertia about axis of rotation

I_x = moment of inertia about point of angular deflection

K_θ = stiffness refered to point of angular deflection

f = whirling speed ratio

W_s = shaft speed

l = shaft length

HP = horsepower required to produce Torquewhirl

η = damping ratio

FIGURE A-2A

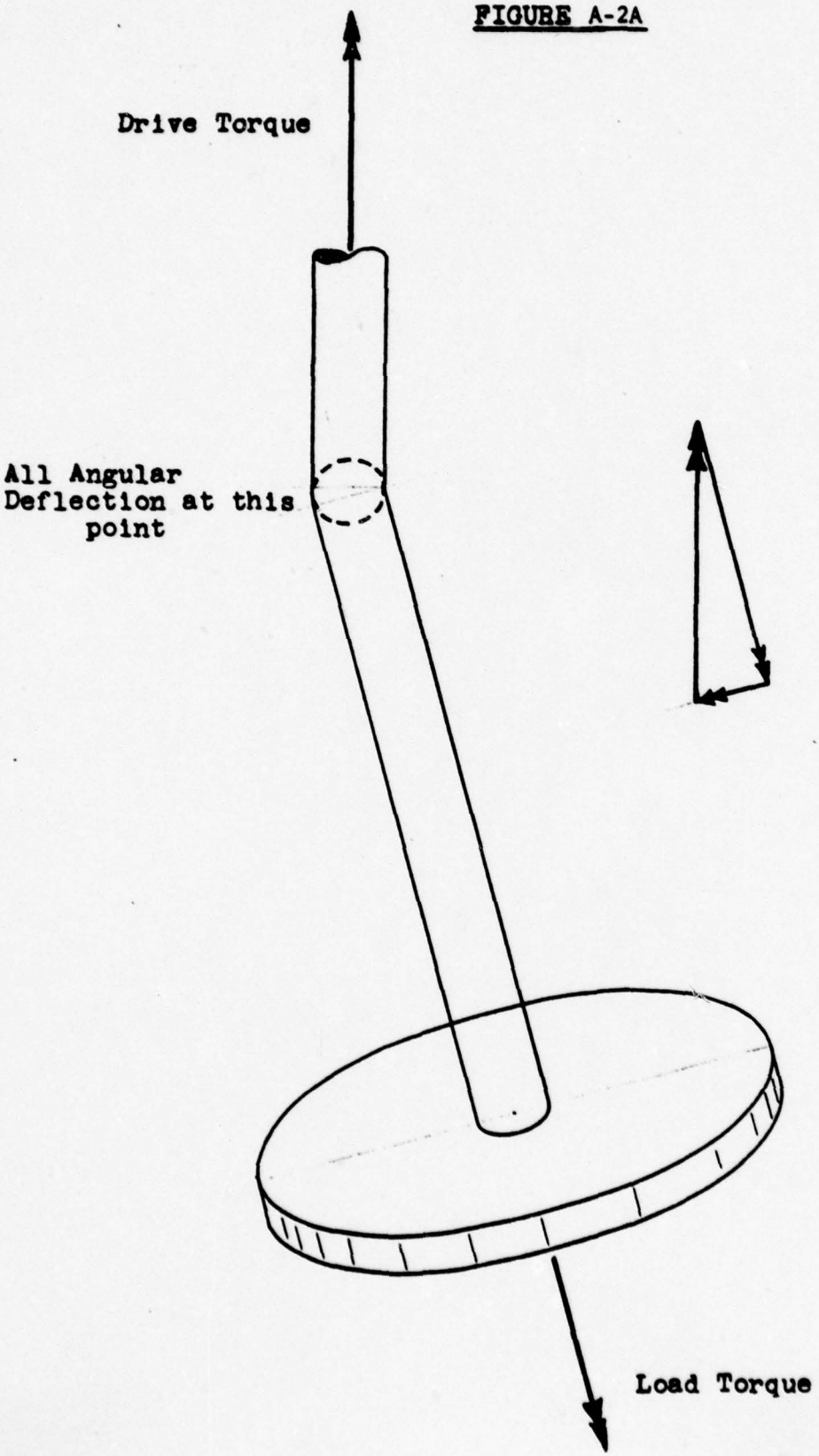
Drive Torque
All Angular Deflection at this point
Load Torque

could be placed inside of a housing, supported on the same shaft that was used to drive the impeller. The power was to be dissipated by pumping the viscous fluid. There were numerous problems with this method, particularly with the accurate calculation of power dissipation. Consequently this idea was dropped. It was replaced by a system based on thin film viscous shear. In this thin film shear idea, the housing fit very close to a flat rotating disk. Power would be dissipated by the shearing of a very thin film of viscous fluid. A good deal of power can be absorbed by this technique. At the same time this idea was being investigated, the complex interrelationships of the many variable design parameters were not understood, and the method appeared to require a system of impractical size. In hindsight, this method does indeed seem to be workable; however, a design idea, put forward at a meeting* in mid-January of '78, forms the basis of the current system. In this idea the impeller took the form of a conical plug (Fig. A-3A). The plug fit inside of a closely mated housing. The shape of the outside of the housing was not known at the time, but was assumed to be boxlike. Power dissipation in this system was adjustable. The adjustment could be effected by raising or lowering the plug thereby changing the thickness of the fluid film. Still, at the time, the size of the actual system had not been determined. Mathematical models of different sized systems were developed and investigated. The relation of the various design variables was developed from these models. An equation relating several of the parameters was used to generate required h.p. dissipation vs. speed curves for the various models.

For all calculations the fluid viscosity was assumed to be 56 micro reyns (Dow Corning silicone 1000). The film thickness was taken to be 0.003 in. and

*The meeting was comprised of Dr. J. M. Vance, Dr. G. N. Sandor, and Mr. Ken Ard.

FIGURE A-3A

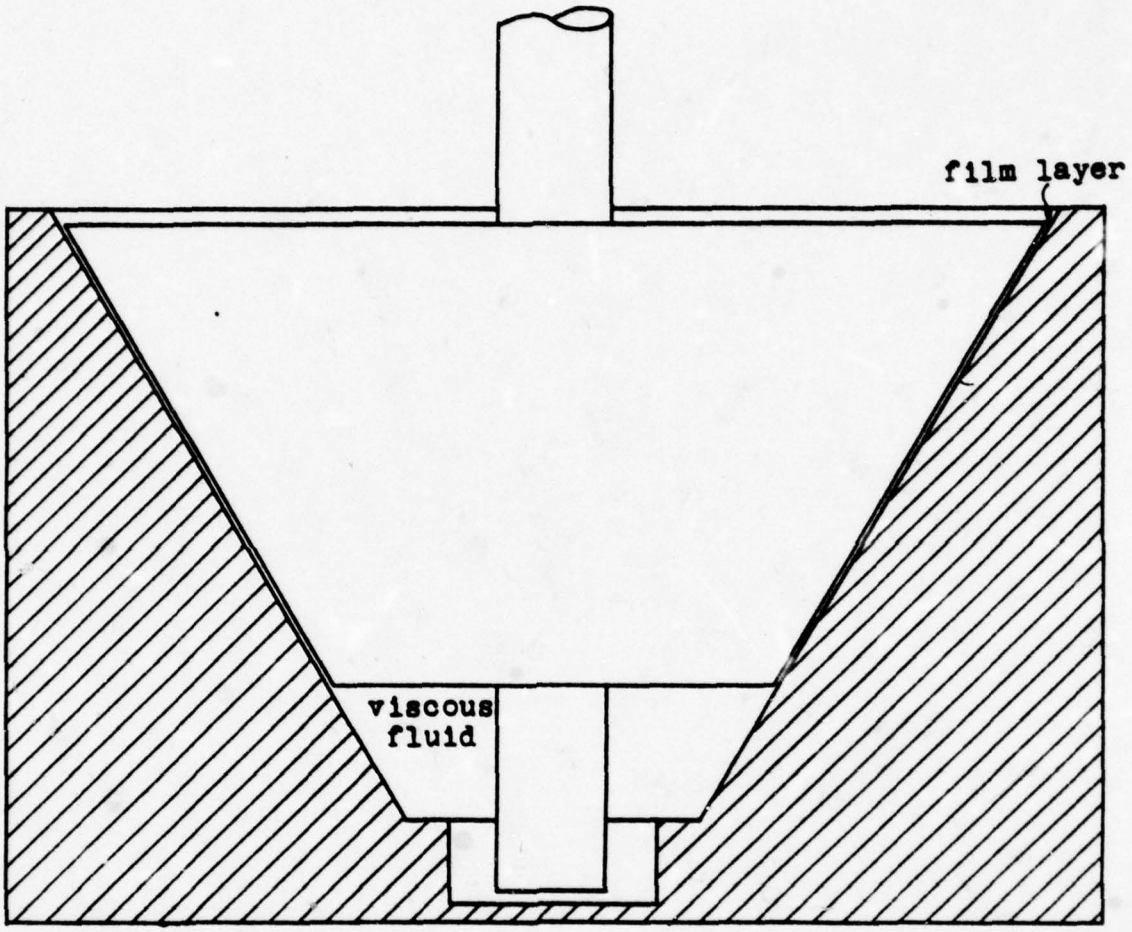

CONICAL PLUG IN MATING HOUSING
VISCOUS SHEAR DISSIPATION

and the cone plug half angle was 30 degrees. Throughout the entire design process the whirling speed ratio was limited to values between 0.4 and 0.7, so as to resemble actual field measurements. From a review of the resultant data, one system was chosen as the most desirable. At the time this selection was made most of the parameter relations were not known. It was through careful examination of the effects of changing parameters that the relations became apparent. The selected system was continually modified. The purpose of all modifications was to increase speed and to reduce required horsepower. The result of the basic modifications was an overall decrease in size and the removal of the shaft length from the coupling to the dissipation housing. A sketch of the basic unit as perceived at this time is shown in Fig. A-4A.

Problems with the Basic Unit

For any machine, the percent critical damping that will be present in the final construction is very difficult to determine. In the Torquewhirl rig damping is very important. The greater the damping, the greater the power required to produce the whirl. Before any design could be developed, it was necessary to find some approximation of the percent of critical damping that would be present in the basic system. To gain this information a simple model was constructed and test measurements were made. From the results of the tests it was determined that the damping was low enough to result in an acceptable power requirement.

The system in its present form will dissipate close to 12 h.p. The immediate problem is, of course, how to get rid of 12 h.p. worth of heat. It was first hoped that the thermal capacity of the housing would be sufficient to allow the time necessary to take data without excessive temperature rise. This proved not to be the case. The housing would reach temperatures in excess of 250 degrees F in less than 59 seconds. When the effects of natural convection

FIGURE A-4A

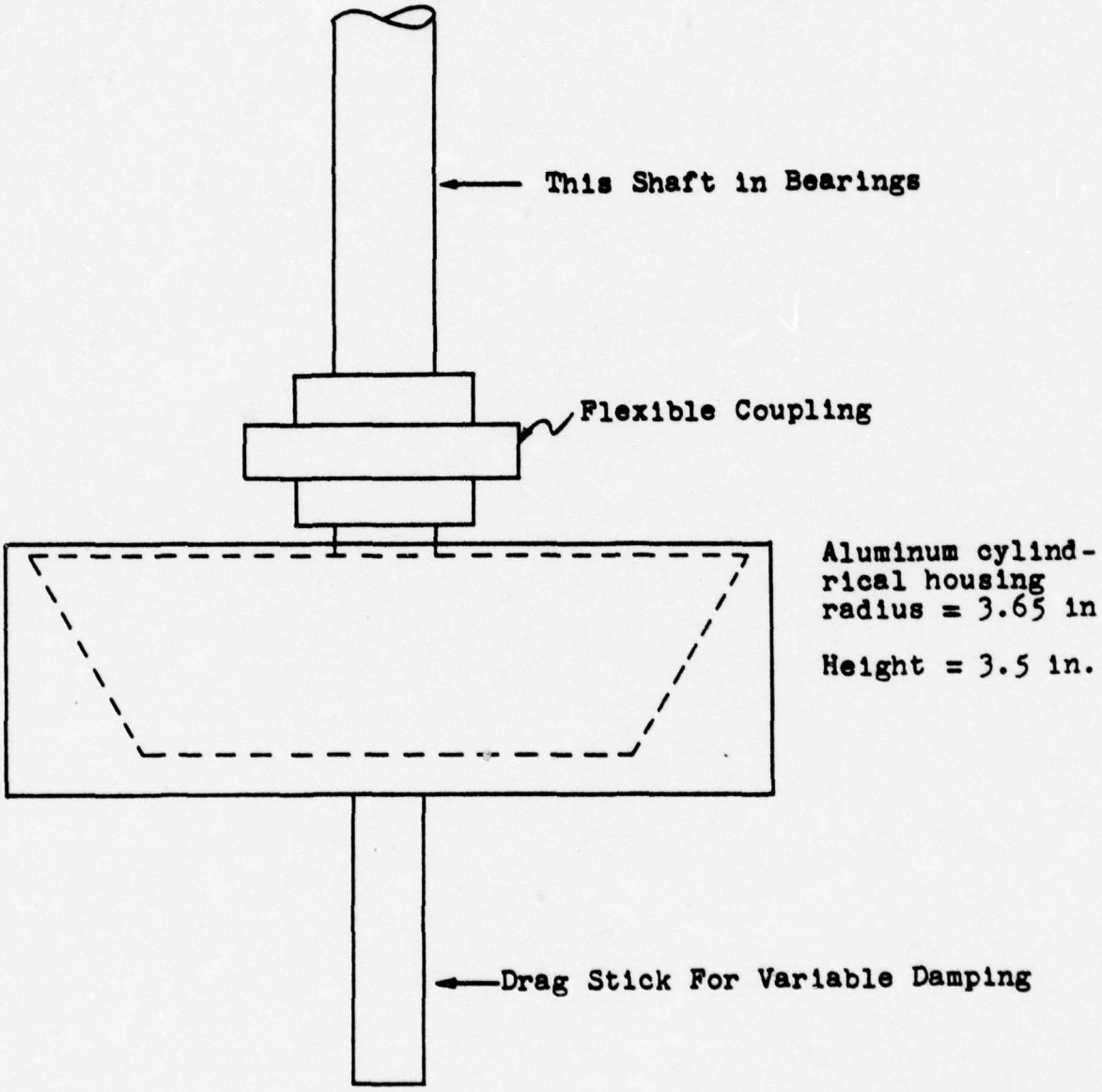
This Shaft in Bearings
Flexible Coupling
Aluminum cylindrical housing radius = 3.65 in
Height = 3.5 in.
Drag Stick For Variable Damping

are included, no significant improvement is realized. Forced convection was the natural alternative. Fins were considered necessary in order to achieve the required heat transfer rate. Forced flow was assumed to be around 6 ft./sec based on the flow velocity of a standard blower. Assuming a steady state temperature of 197 degrees F, eight fins would be required. The final design has sixteen fins and will operate well below 175 degrees.

Another problem, not quite as obvious as the heating problem, is a result of the centrifugal effect imparted to the fluid by the rapidly rotating plug. This centrifugal effect tends to drive the fluid out from beneath the plug. The result of this motion is to create a suction which pulls the plug down into the housing, the final result being seizure. This problem is avoided by drilling return ports in the plug itself to allow the pumped fluid to return. The pumped fluid would be slung out of the housing if a cover plate were not included. This plate serves two purposes; first, it prevents the fluid from being thrown out, but it also serves as a place to mount the upper bearing of the cone-shaped rotor. The upper bearing is necessary for the gap control apparatus. It also helps ensure proper alignment and prevents wobble.

In order to change the power dissipation independently from the speed, it is necessary to change the fluid film thickness. In the preliminary design this was accomplished through the tightening of a nut below the housing which raised or lowered the housing with respect to the plug. In the final design this same basic idea is applied in a different form. The raising or lowering of the housing is done by using two wedges. One wedge is grounded to the housing while the other is free to slide. Due to the angle of the wedge the horizontal motion is converted into vertical motion of the housing. A half inch of wedge travel is required to produce 0.007 inches of film gap change.

A coupling selection was made based on an estimated 4 degrees of angular misalignment, while transmitting 70 ft. lbs. of torque.

Standard universal joints could not be used, since when deflected they do not transmit at constant angular velocity. After some searching, the Thomas model 162 coupling was chosen. It is of the standard disk pack construction and will handle the expected torque and misalignment.

To power the rig, a 15 h.p. aircraft generator was purchased to serve as a prime mover. The basis for this selection was primarily price, but also because some experience has been gained with this type of power drive.

The included drawings are self-explanatory and provide a detailed description of all the parts of a test rig as they will be fabricated. Some parts, such as the bearings and the coupling, have either been ordered or already purchased. The major portion of the support structure and safety cage has been constructed.

A general idea of the test rig can be derived through inspection of the assembly drawings. The assembly drawing has been divided into two parts — the upper half and the lower half. The upper half assembly shows the upper drive shaft (Dwg. 5), the upper shaft bearings, and mounting plates (Dwg. 3). The mounting plates are held apart by spacer blocks (Dwg. 4). The upper shaft is rigidly held in position by the precision Barden bearings and the all steel support structure of the upper half. The upper mounting plates are to be positioned during construction. They will then be firmly clamped to each other and to the support frame by four one half inch socket headed cap screws and nuts. Further positive location is assured through the use of four one quarter inch dowel pins which are set in the spacer blocks through the mounting plates.

The upper half of the Thomas coupling is attached to the lower end of the upper drive by a key and setscrew. A clear representation of the drive shaft

shaft can be seen in Drawing No. 5. The design is such that accurate machining is specified only where necessary along the shaft (e.g. bearing seats). The purpose of this is to save both time and money.

The lower portion of the assembly is the most important part as far as Torquewhirl considerations are concerned. The dynamic parameters of this half determine the power and speed combinations that will satisfy the Torquewhirl theory. These important values have been carefully calculated. However, the actual parameters are expected to vary slightly from the calculations. In view of this fact, some items necessary for rig operation have not been included in the present set of drawings. The actual dimensions of these small and inexpensive parts will not be known until measurements can be made on the completed lower assembly. The lower assembly (Dwg. 2) consists of a finned housing (Dwg. 10) enclosing a conical plug (Dwg. 9) which is free to rotate in the housing. There is a housing cover (Dwg. 8), a slide adjustment assembly (Dwg. 7), the lower drive shaft (Dwg. 12), lower shaft bearings, and the lower half of the flexible coupling (Dwg. 6).

The lower shaft design is similar to that of the upper drive shaft. The reasons for this type of design are again, time and expense. The flexible coupling is pressed onto the end of the lower shaft and keyed to resist the load torque. Other than the shaft, bearings, and assorted bolts, the entire lower assembly is made of aluminum. The object of this feature is to lower the weight, and therefore moment of inertia, of the lower portion of the system. This lower weight is required in order to keep the power and speed combination required to produce Torquewhirl to a reasonable value. (Note Linking in Fig. A-1A).

The conical plug is also keyed to the shaft in order to stand the load torque. The plug is basically a truncated cone of 30° half angle. Holes are drilled into and through the cone, to lighten it and to provide return ports for fluid which is pumped to the top of the cone due to its rotation. The cone

fits snugly into a mating finned housing (Dwg. 10). The housing holds the shearing fluid and is finned to provide for adequate cooling. Cooling of the lower housing will be accomplished by the use of a standard blower whose blast will be directed at the base of the finned housing. There is a cap plate (Dwg. 8) that covers the top of the housing to prevent spillage of the shearing fluid. This cap also holds the upper bearing for the lower shaft.

There is an assemblage of two wedges which is fastened to the top of the housing cap plate (Dwg. 7).

These wedges are used to provide adjustment of the film thickness of the shearing fluid. This adjustment allows the independent control of power dissipation. Changes in the film thickness are effected by sliding the wedge in a horizontal direction. The wedge angle is such that one half inch in wedge motion results in seven thousandths of an inch of film gap change. The sliding wedge is held in position by an overhanging ledge that fits over the fixed wedge. The adjusting screws also aid in maintaining the wedge position.

A part which is not shown in this assembly drawing is the drag rod, which is used in adjusting the damping value of the whirling motion. The drag rod is nothing more than a solid circular rod extending downward from the bottom of the finned housing. The damping will be adjusted by raising or lowering the level of viscous fluid in a container in which the lower part of the drag rod is immersed. The drag rod is to be attached to the bottom of the housing by adhesive.

The test rig as described is expected to operate at speeds between one and two thousand revolutions per minute. Power dissipation is calculated to be between eight and twelve horsepower. Theory predicts that, with the above limits on speed and power, there will exist numerous combinations that will produce Torquewhirl in the system. The amplitude and stability of this whirl

motion are to be measured using either capacitance or magnetic transducers which are available. It is expected that this rig, as designed, will answer the need for formal verification of the Torquewhirl theory.

Caption for Figure A-1A Page A25

The general method used to size the Torquewhirl test rig is outlined in figure A-1A, Page A25. First it was necessary to choose a size and shape for the rig. The required values I_x and I_z were calculated. K_θ was known between limits, and was used along with W_s to force the system within the bounds defined by f. If K_θ and W_s turned out to be reasonable, the system then seemed to be within design limits. Next it was necessary to test to see if the horsepower required to produce Torquewhirl was less than the twelve horsepower limit. If the system required less than twleve h.p., it was examined to determine if it would actually dissipate the required amount. The lower the h.p. requirement the better since numerous combinations of speed and power that satisfy the Torquewhirl theory would then exist below the twelve h.p. limit. The selection of the final design was an itterative process, which was followed until all requirements of the theory were satisfied.

TORQUEWHIRL RIG

WORKING DRAWINGS

PARTS LIST

NO.	QUANTITY	NAME	DESCRIPTION/REMARKS
1	2 PCS.	MOUNTING PLATES	SEE DWG. NO. 8
2	2 PCS.	SPACER BLOCKS	SEE DWG. NO. 4
3	1 PC.	BRNG RETAINER	SEE DWG. NO 11
4	1 PC.	UPPER DRIVE SHAFT	SEE DWG. NO 5
5	1 SET	COUPLING	"REXNORD"-TYPE ST SIZE NO. 162 ; SEE DWG NO. 6 REXNORD, 1262 BROAD ST., BLOOMFIELD, N.J. 07003
6	1 PC.	SLIDE GUIDE	SEE DWG. NO. 7
7	1 PC.	SLIDE	SEE DWG. NO 7
8	1 PC.	HOUSING COVER	SEE DWG. NO. 8
9	1 PC.	CONE	SEE DWG. NO. 9
10	1 PC.	HOUSING	SEE DWG. NO. 10
11	1 PC.	END WASHER	SEE DWG. NO. 11
12	1 PC.	END BOLT	3/8" UNF-24 SELF-LOCKING BOLT; SEE DWG. NO. 11
13	1 PC	SPACER	SEE DWG. NO. 11
14	1 PC.	LOWER SHAFT	SEE DWG. NO. 12
15	1 PC.	WAVE SPRING	"ASSOC. SPRING CO." CATALOG NO. W1819-020 18 MAIN ST. BRISTOL, CONNECTICUT 06010
MISC:			
	1 PC.	ANGULAR CONTACT BRG.	BARDEN 105 T / BARDEN 105 — BARDEN BRG. CO DANBURY, CONNECTICUT
	3 PCS.	DEEP GROOVE BALL BRGS.	
	3 PCS.	SQUARE KEYS	1/4" x 1/4" x 2" LONG
	2 PCS.	ADJUSTING SCREWS	NO. 40 UNF-44 x 1 1/4" LONG SHCS
	2 PCS.	BRG. RETAINER SCREWS	1/4" UNC-20 X 1" LONG SHCS WITH LOCK WASHER
	4 PCS.	SLIDE HOLDING SCREWS	NO. 10 UNC-24 X 3/8" LONG SHCS WITH LOCKWASHERS
	8 PCS.	HOUSING COVER SCREWS	NO. 10 UNC-24 x 5/8" LONG SHCS WITH LOCKWASHERS
	4 PCS.	MOUNTING PLATE BOLTS	1/2" UNC-13X 3" LONG SHCS WITH LOCKWASHERS & NUT
	2 PCS.	SET SCREWS	1/4" UNC-20 X 1/2" LONG CONE HEAD SETSREW
	4 PCS.	DOWEL PINS	3/8" DIA. X 1 1/4" LONG
	1 PC.	MOTOR PLATE	SEE DWG. 13

TORQUEWHIRL RIG		
PARTS LISTING		

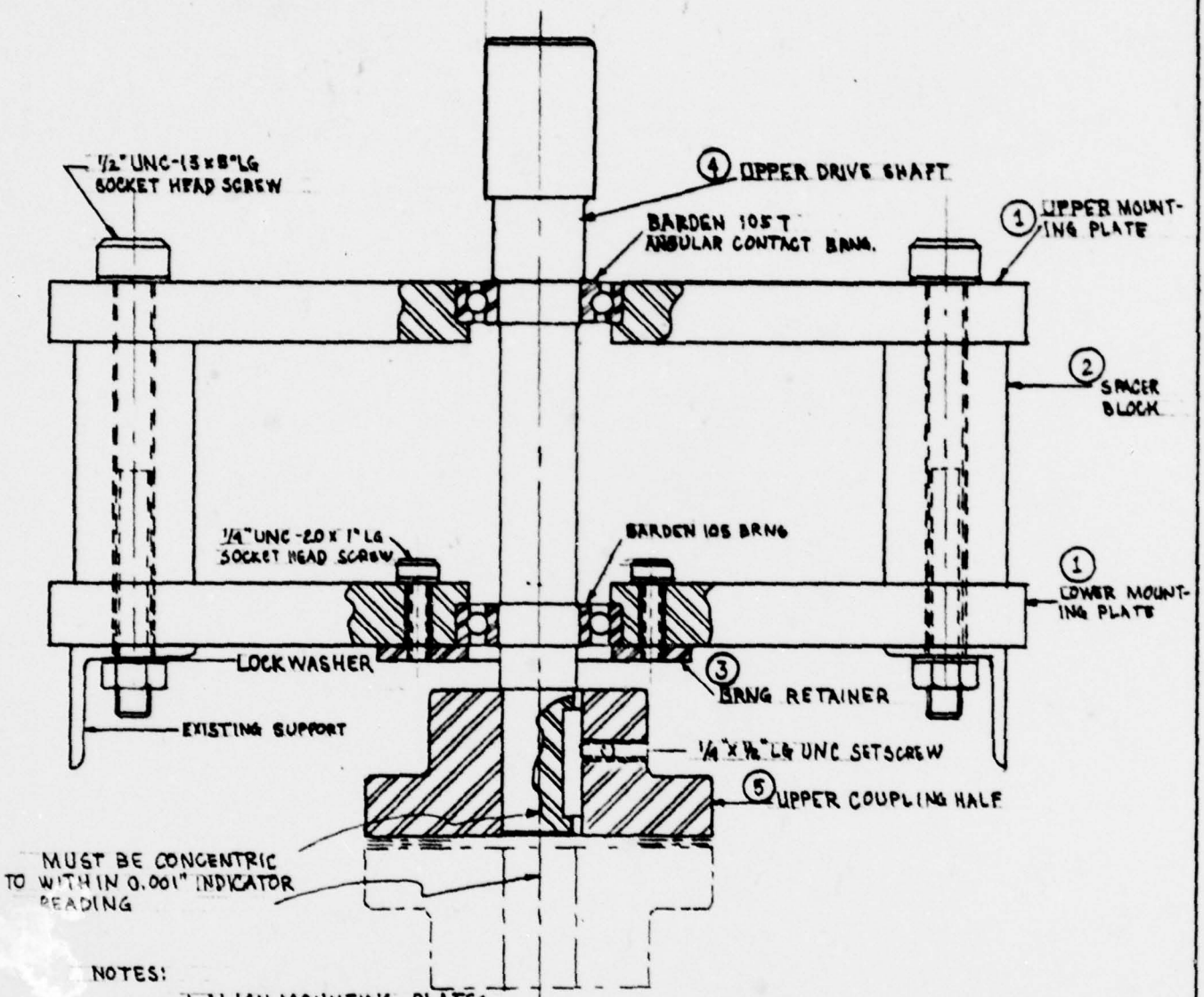

NOTES:

1. ALIGN MOUNTING PLATES ON ASSEMBLY.
2. DRILL HOLES THRU MOUNTING AND ON SPACER FOR 2 DOWELS AFTER ASSEMBLY & ALIGNMENT.

TORQUE WHIRL RIG		
PART NAME : UPPER HALF-ASSY		QUAN. 1
MAT'L : SEE DETAILS		SCALE : 1/2 SIZE
		DWG. NO. 1

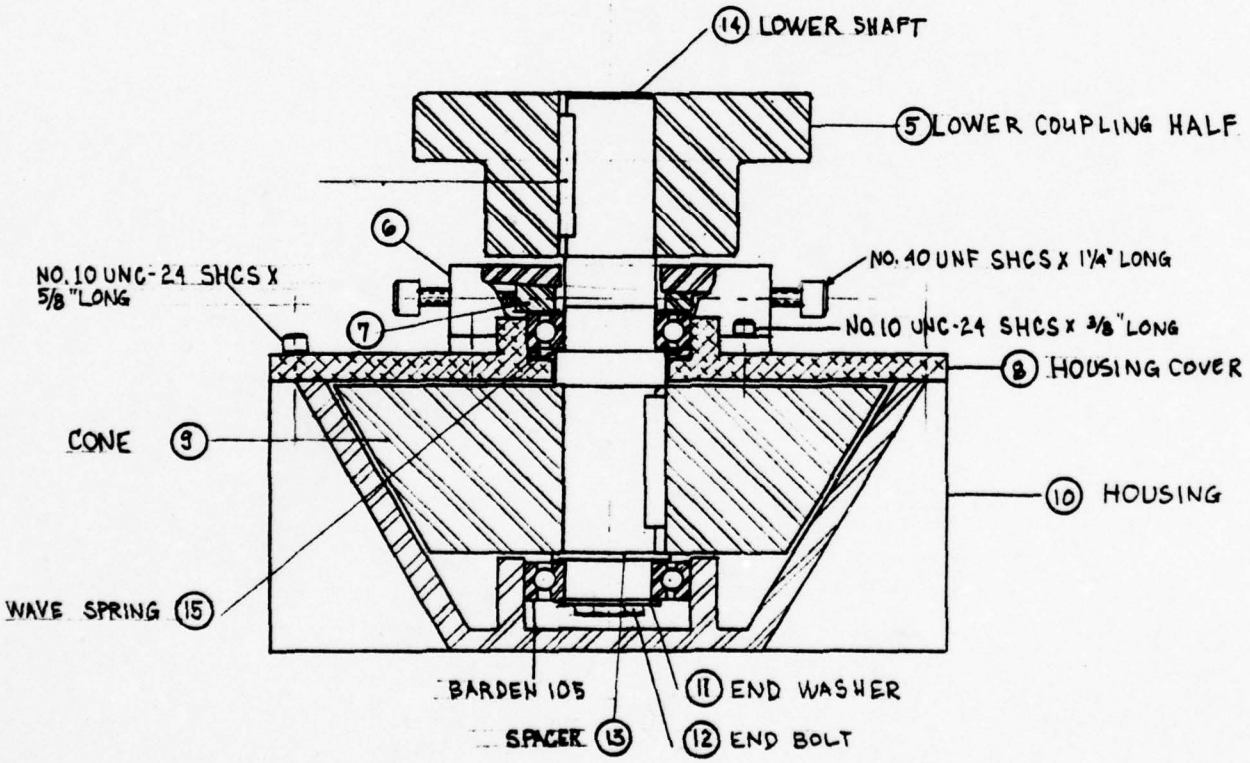

TORQUEWHIRL RIG		
PART: LOWER HALF ASSY	QUAN: 1	
MAT'L: SEE DETAILS	SCALE: ½ SIZE	
		DWG. NO. 2

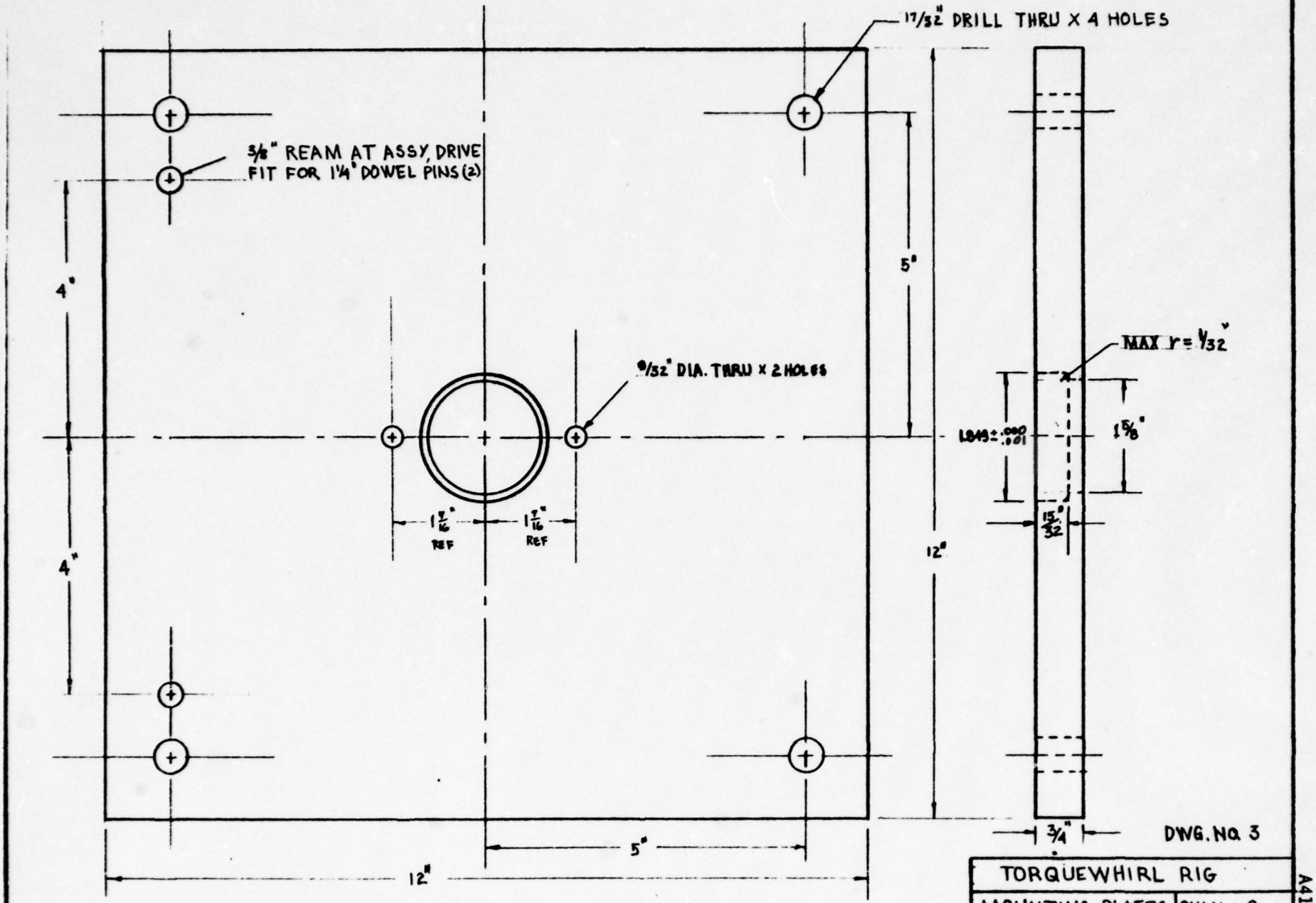

NOTES: ALL DIMENSIONS ±.015" UNLESS INDICATED.
BREAK OFF ALL CORNERS.

TORQUEWHIRL RIG	
MOUNTING PLATES	QUAN. 2
MAT'L: STEEL	SCALE: ½ SIZE

A41

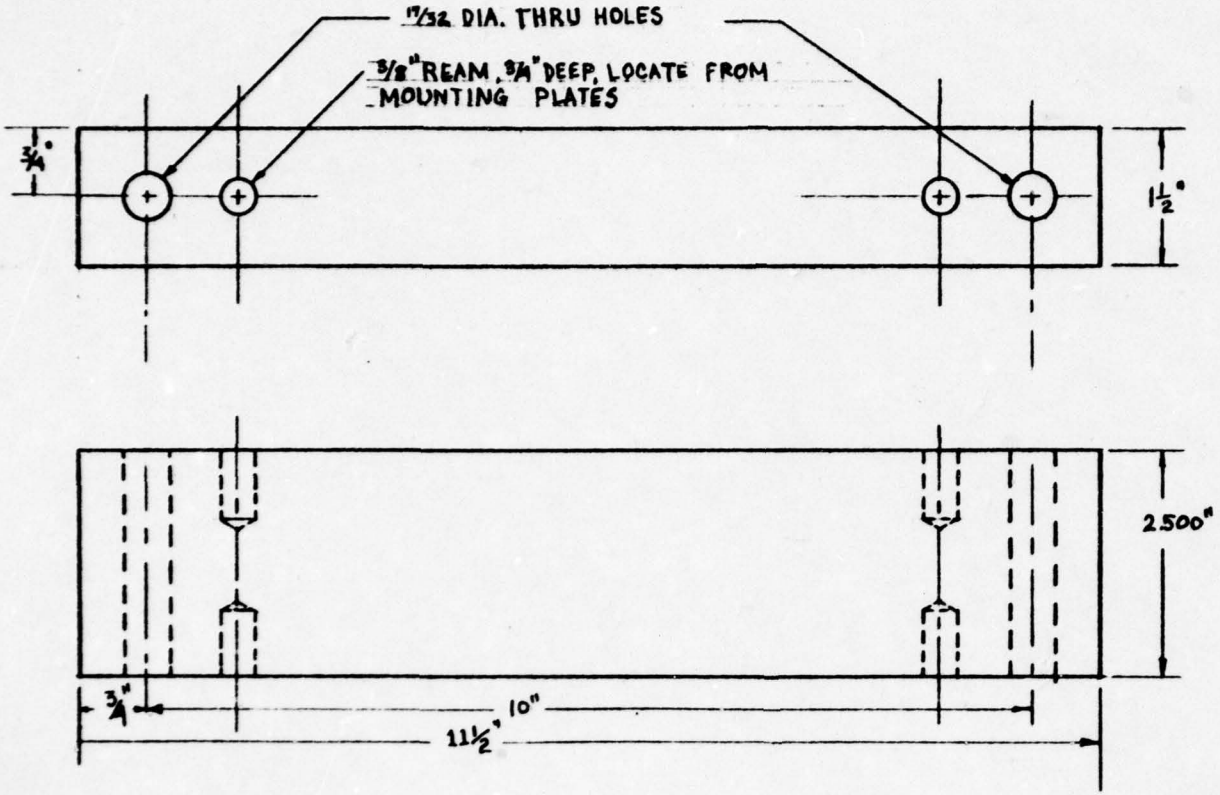

NOTES:

1 TWO PCS. OF THE ABOVE PART ARE REQ'D, MACHINE IN PAIRS TO THE SAME HEIGHT OF 2.50"

TORQUE WHIRL RIG		
PART 2 - SPACER BLOCK		QUAN: 2
MAT'L: STEEL		SCALE: 1/2 SIZE
		DWG. NO. 4

A42

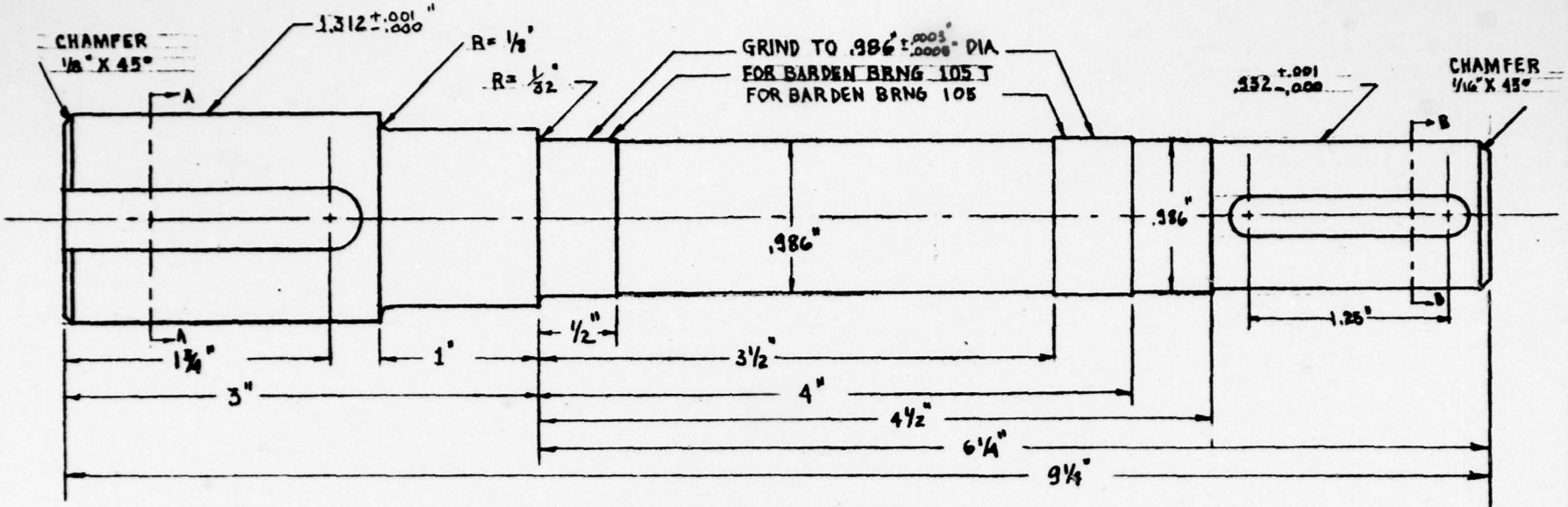

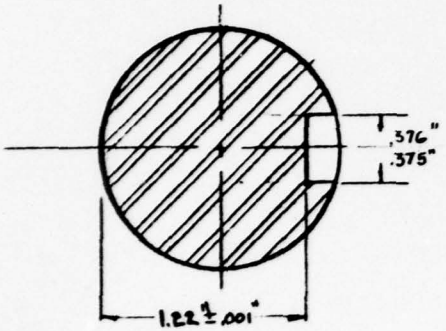

SECTION A-A

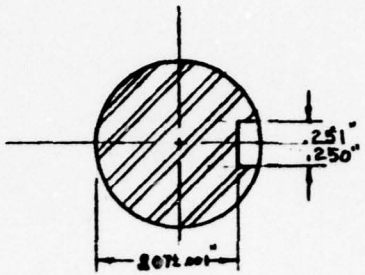

SECTION B-B

NOTE:

ALL DIMENSIONS ±.010"
UNLESS INDICATED

TORQUEWHIRL RIG		
PART: 4 - DRIVE SHAFT		QUAN. 1
MAT'L: STEEL		SCALE: FULL
		DWG. NO. 5

A43

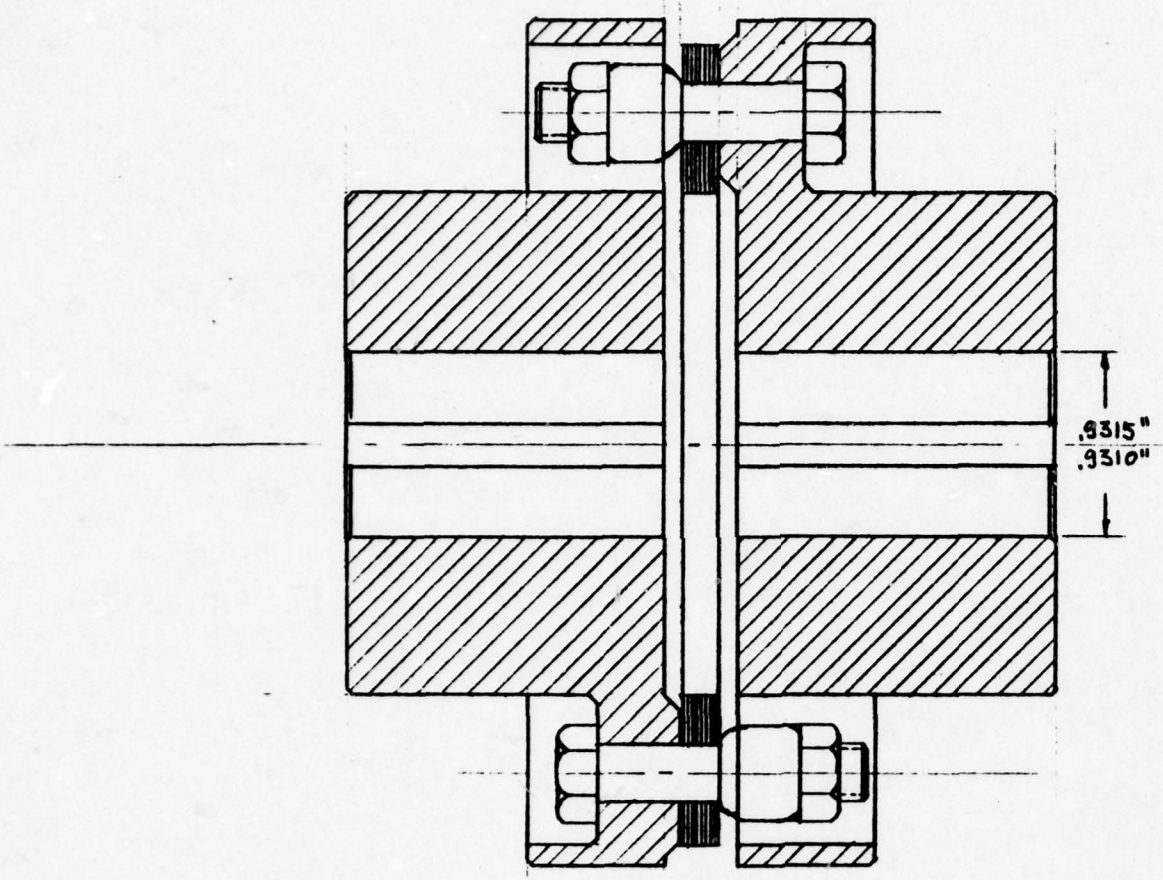

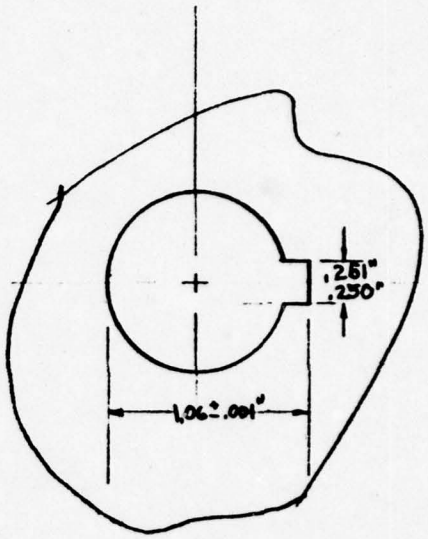

REXNORD -TYPE ST SIZE NO. 162 COUPLING

TORQUE WHIRL RIG		
PART: 5 - COUPLING		QUAN: 1 SET
MAT'L: STEEL		SCALE: FULL SIZE
		DWG. NO. 6

A44

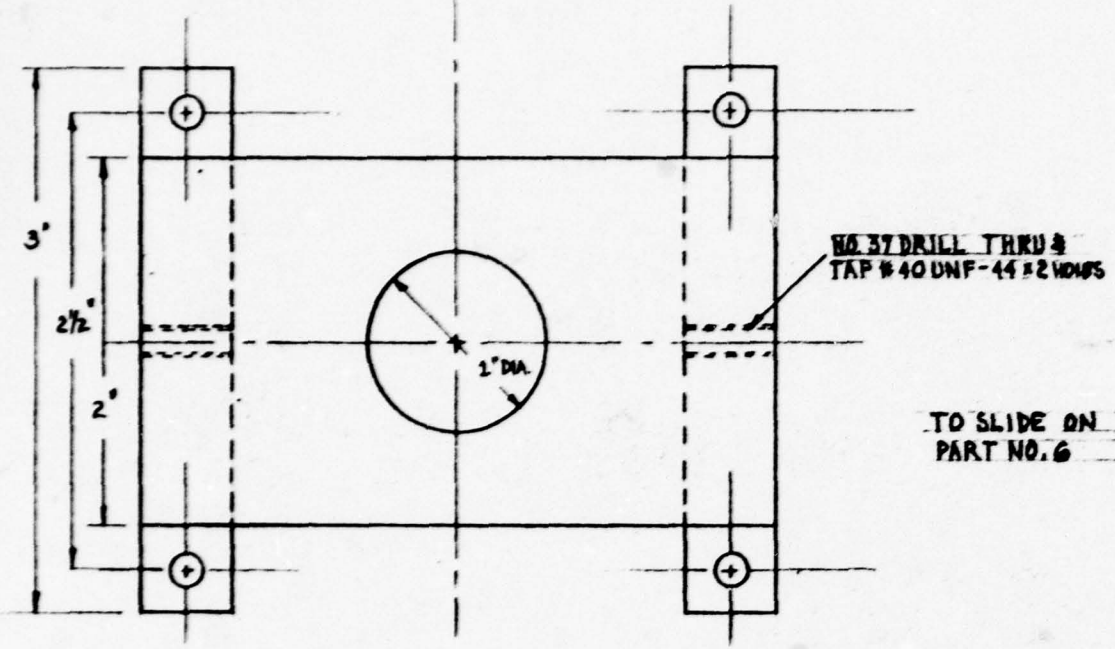

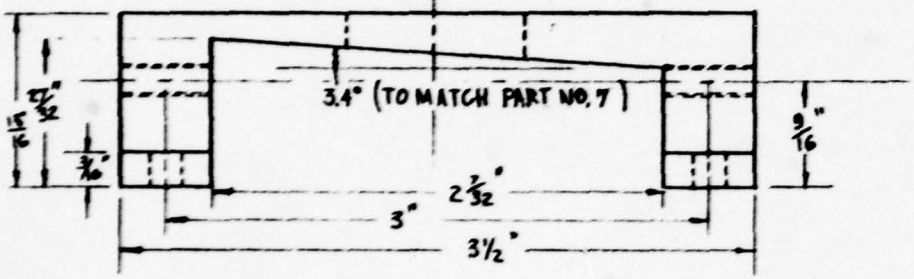

⑥ SLIDE GUIDE

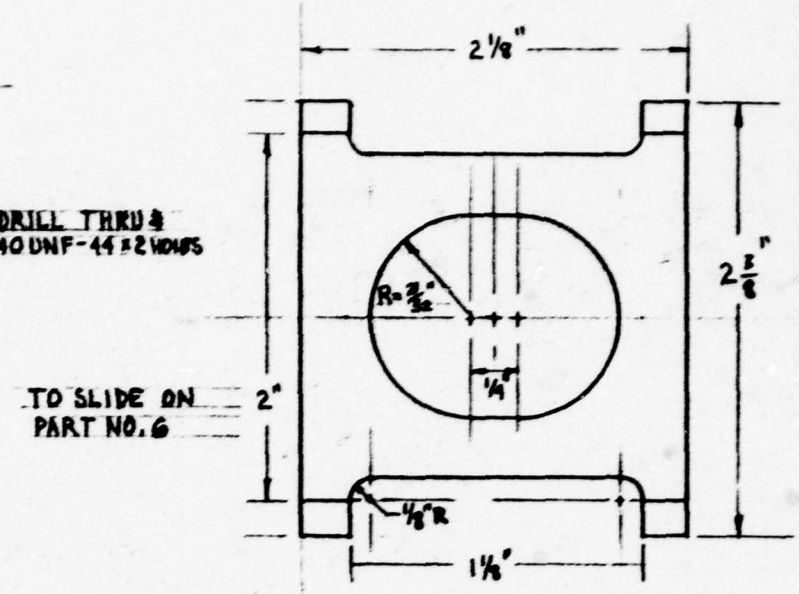

⑦ SLIDE

TORQUEWHIRL RIG		
PART: G&7-SLIDE SET		QUAN: 1 SET
MATL: ALUMINUM		SCALE: FULL SIZE
		DWG. NO. 7

A45

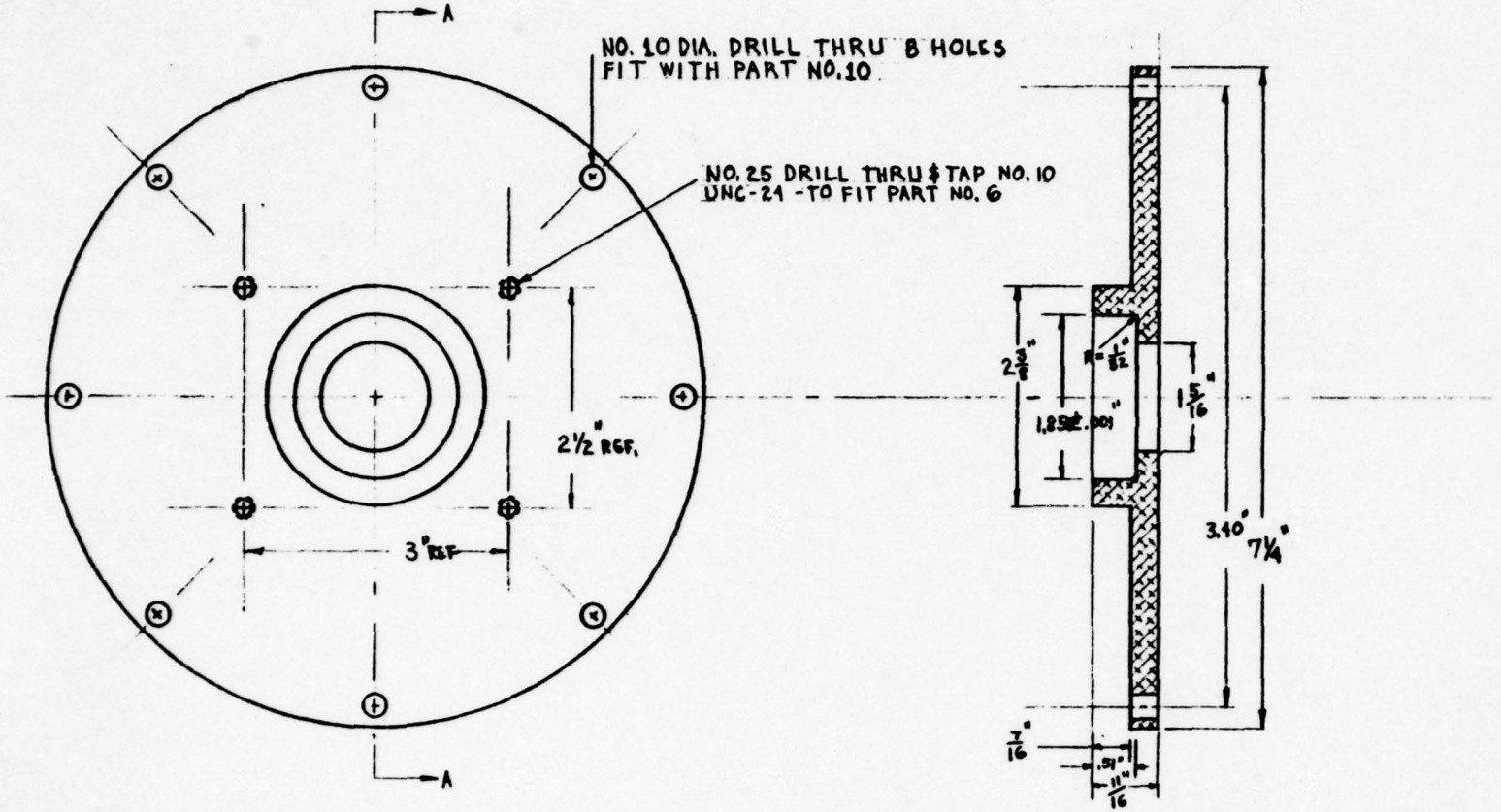

SECTION A-A

TORQUEWHIRL RIG		
PART: 8-HOUSING COVER		QUAN: 1
MAT'L: ALUMINUM		SCALE: ½ SIZE
		DWG. NO. 8

A46

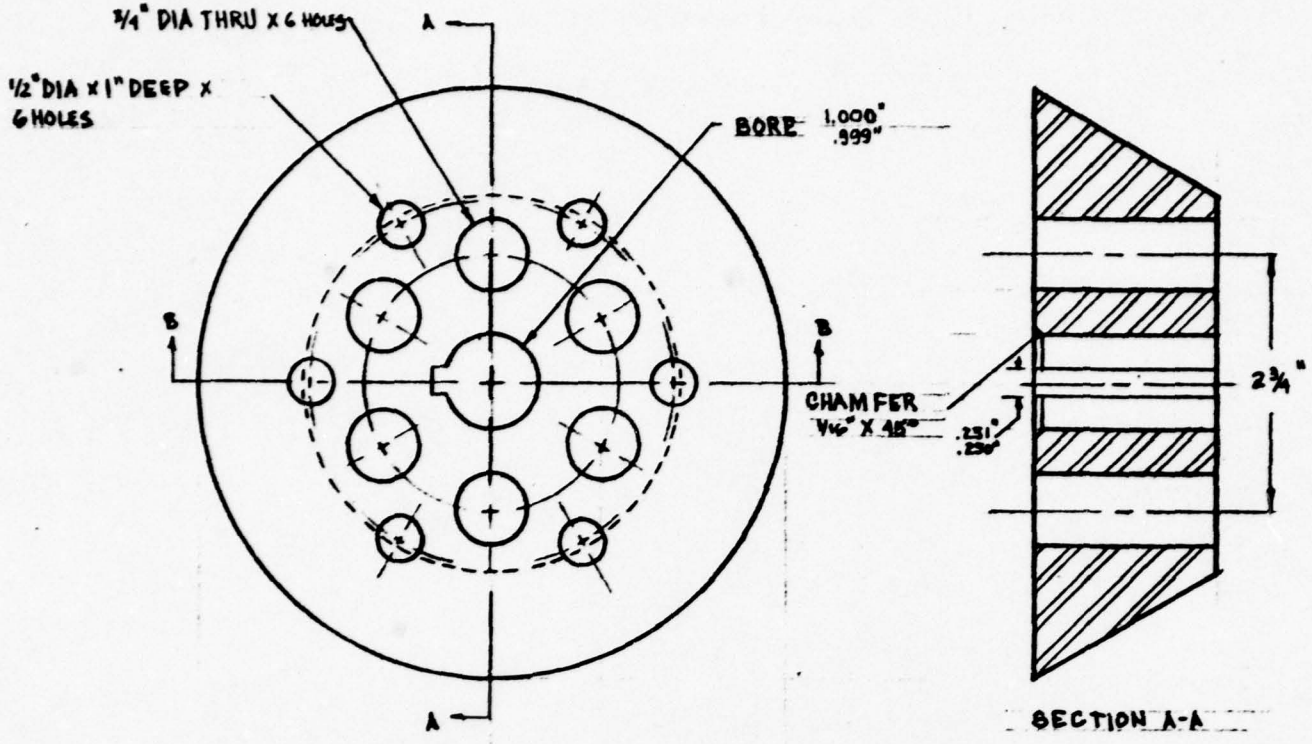

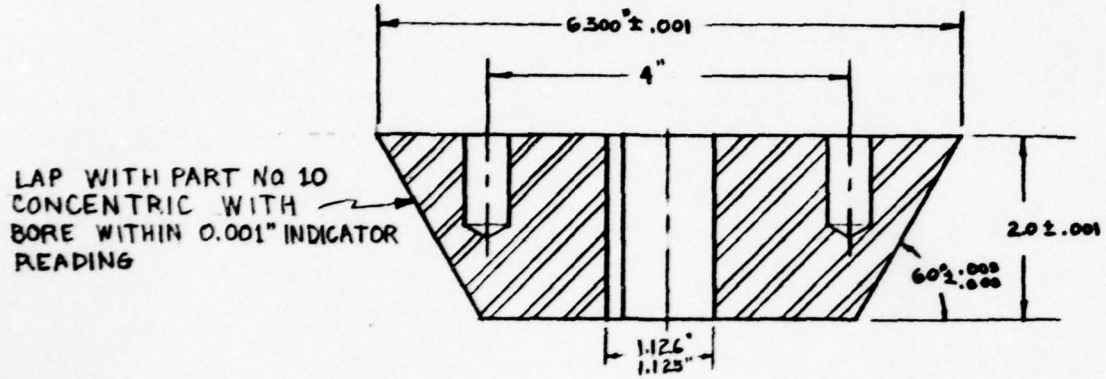

SECTION B-B

NOTE:

ALL DIMENSIONS ± .010" UNLESS INDICATED

TORQUEWHIRL RIG		
PART: 9 - CONE		QUAN. 1
MAT'L: ALUMINUM		SCALE: ½ SIZE
		DWG. NO. 9

A47

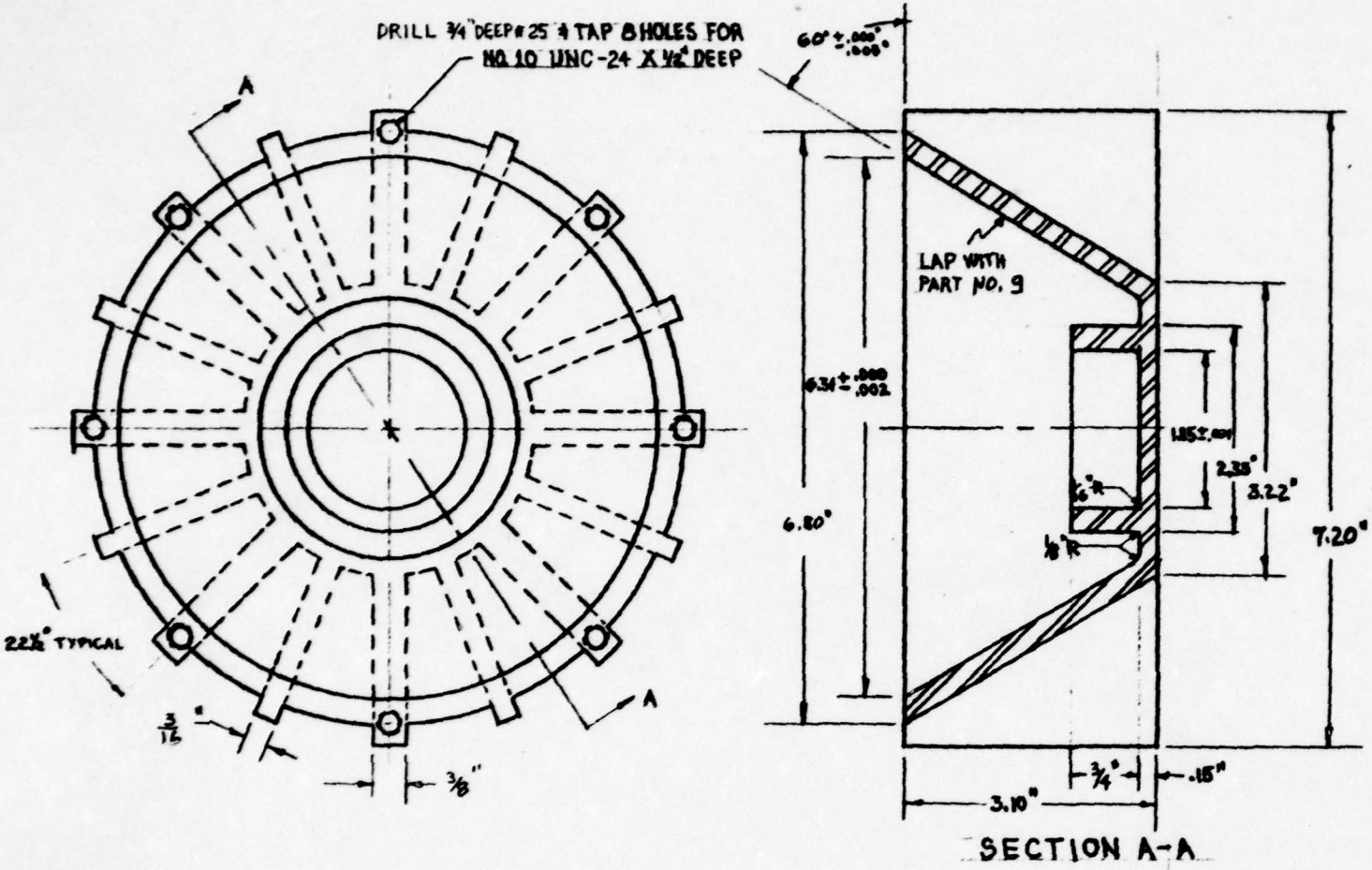

SECTION A-A

NOTE:

ALL DIMENSIONS ± .010" UNLESS INDICATED

TORQUEWHIRL RIG		
PART: 10 - HOUSING		QUAN. 1
MAT'L: ALUMINUM		SCALE: ½ SIZE
		DWG. NO 10

A48

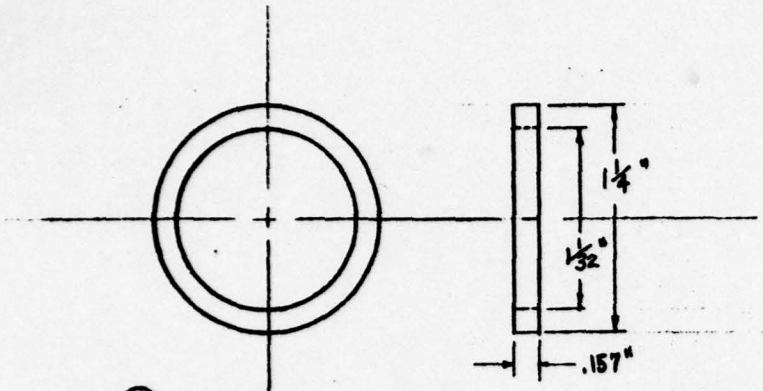

(13) SPACER

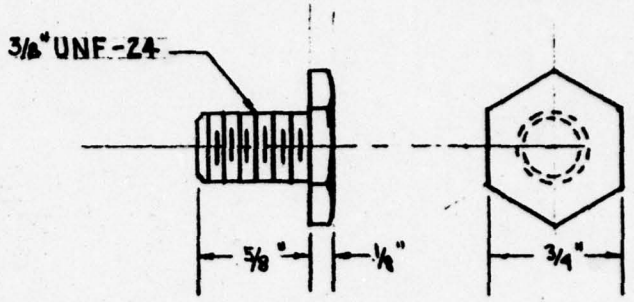

(12) LOWER SHAFT END BOLT

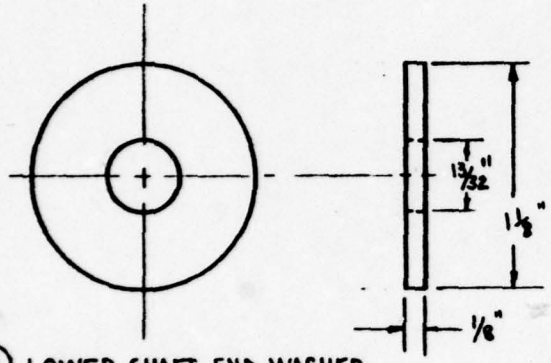

(11) LOWER SHAFT END WASHER

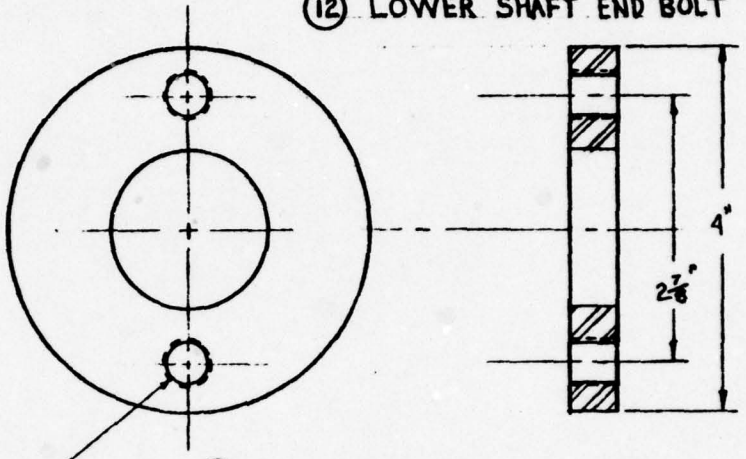

NO.7 DRILL THRU
& TAP ¼" UNC-20

(3) BRNG RETAINER : ½ SIZE

TORQUEWHIRL RIG		
PART NAME: SPACERS & BOLT		QUAN: 1 EA.
MAT'L: STEEL		SCALE: FULL
		DWG. NO. 11

A49

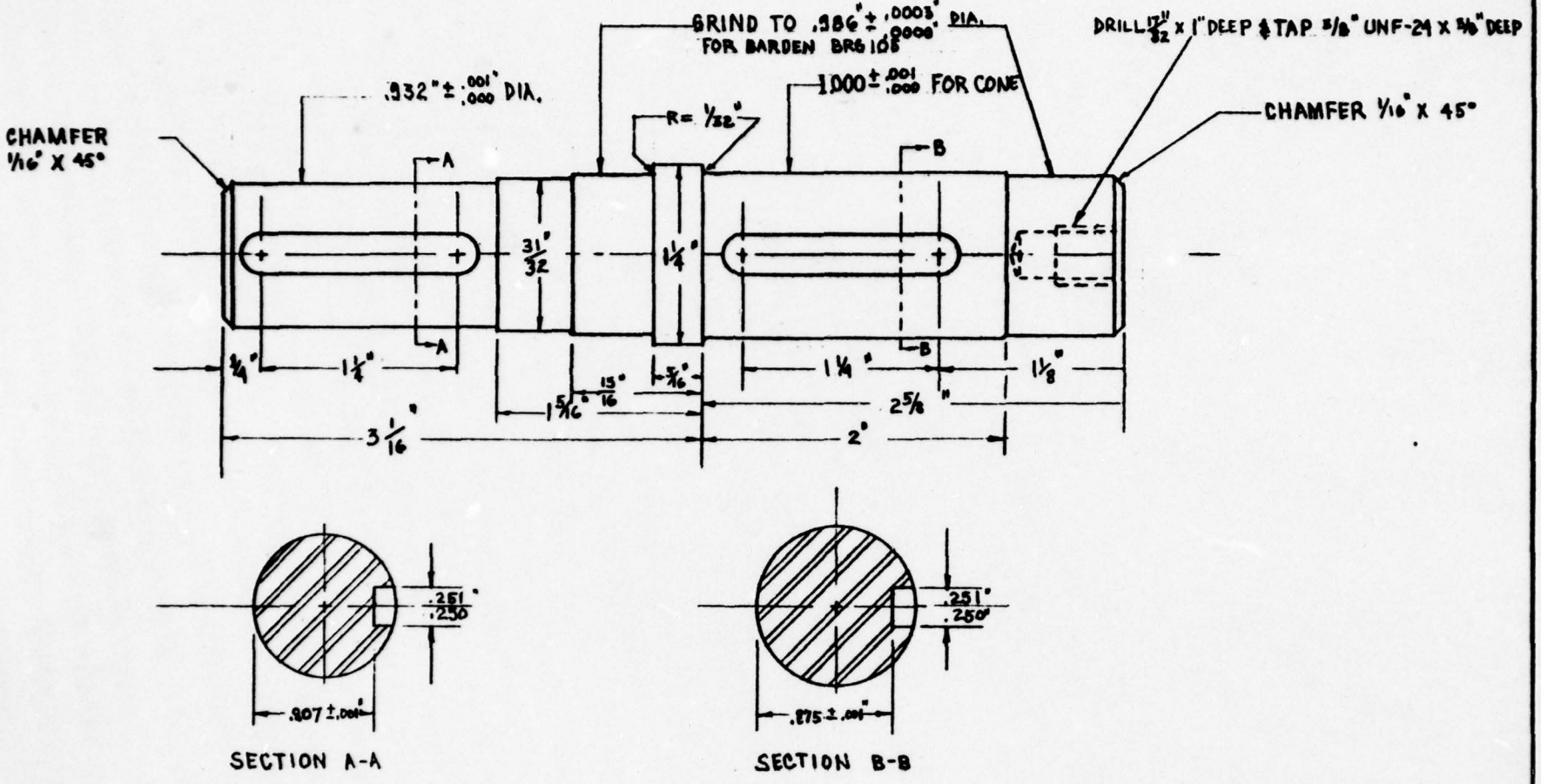

SECTION A-A

SECTION B-B

NOTE:

ALL DIMENSIONS ± .010"
UNLESS INDICATED

TORQUEWHIRL RIG		
PART 14 - LOWER SHAFT		QUAN. 1
MAT'L: STEEL		SCALE: FULL
		DWG. NO. 12

A50

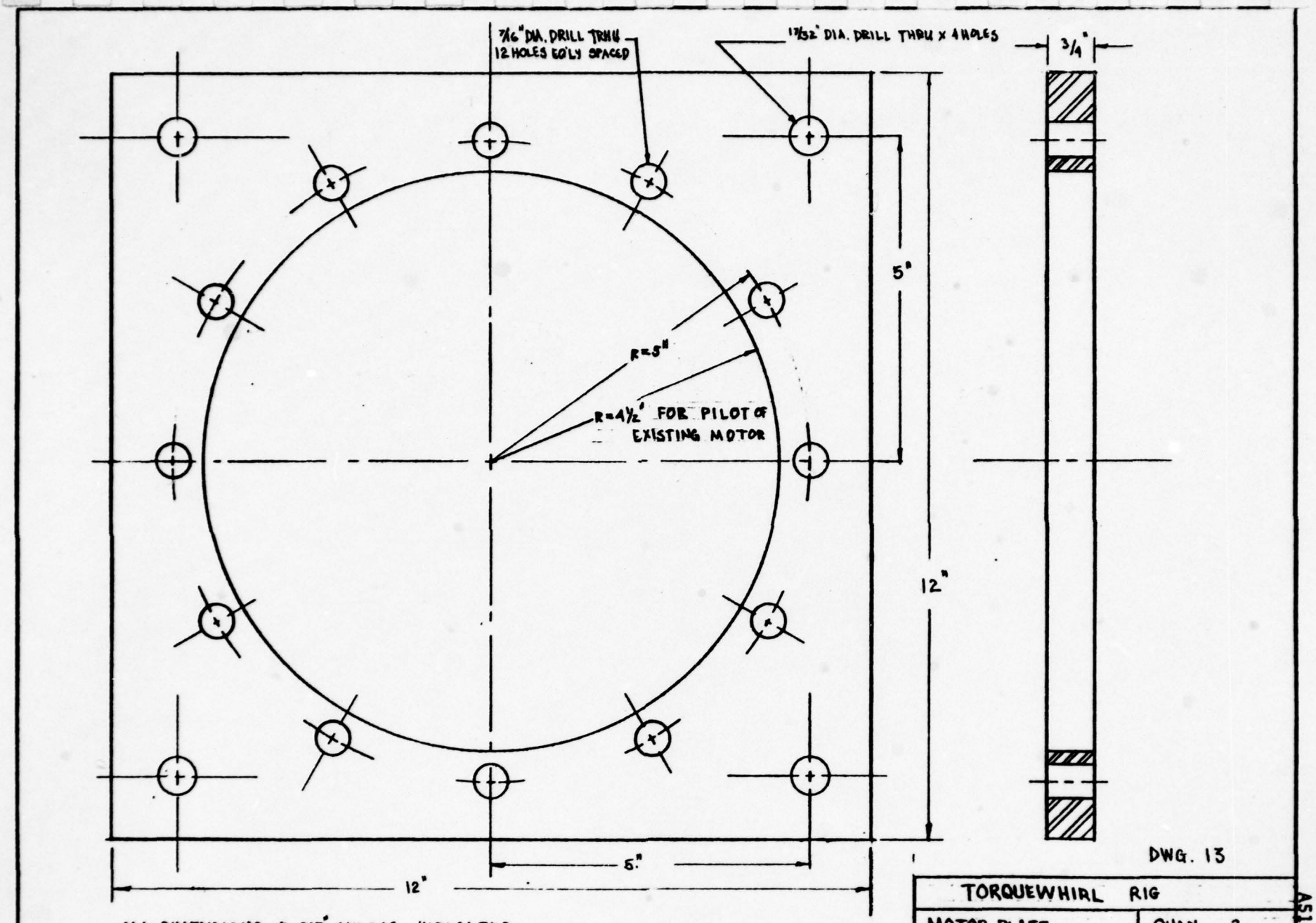

ALL DIMENSIONS ±.015" UNLESS INDICATED

DWG. 13

TORQUEWHIRL RIG	
MOTOR PLATE	QUAN. 2
MAT'L: STEEL	SCALE: ½ SIZE

A51

Appendix B

Theory and Description of Test Rig Used to Measure Alford's Force

by

Frank J. Laudadio

TABLE OF CONTENTS

Theory and Description of Test Rig

Figure B-1 is a representation showing that as the radial tip clearance of the blades of a compressor varies, there is a corresponding variation in efficiency. Large radial clearances cause low efficiency, which in turn requires increased work input in the form of large blade forces to produce the required static-pressure rise. The output required of an axial-flow compressor is such that the axial pressure rise is the same for every portion of the circumference.

The local clearance in the X-direction is shown in Figure B-2. The following is taken from the Journal of Engineering for Power (Ref. 1):

> "Assuming rotor and stator to be perfect circles, rotor displacement x will result in a circumferential variation of blade-tip clearance. The local clearance at position θ is
>
> $$\delta = \delta_m + x \cos \theta, \quad \text{where } \delta_m = \text{mean clearance.}$$
>
> "Thermodynamic stage efficiency is a function of tip clearance, the variation being proportional to ratio of eccentricity to blade or bucket height. The local efficiency is
>
> $$\eta = \eta_m\left(1 + \frac{\beta x}{H}\cos\theta\right)$$
>
> where η_m is the average or mean efficiency corresponding to the average or mean clearance, δ_m. H is the axial height of the blade. For turbines, β has a value of about 1.0 to 1.5. For compressors with adequate stall margin, β also has similar values.

Multistage axial compressors with some stages close to stall may have substantially higher values. This results from the effect of tip clearance on stall pressure ratio."

"For a turbine with constant speed and constant entrance and exit conditions, the output torque is directly proportional to the local efficiency. The local torque per radian, τ_θ, is then related to the average or mean torque, τ_m, by the relation

$$\tau_\theta = \tau_m(1 + \frac{\beta x}{H}\cos\theta).$$

The component of force taken in the direction perpendicular to the instantaneous displacement, x, is per radian

$$\Delta F_y = \frac{\tau_\theta}{r}\cos\theta$$

$$= \frac{\tau_m}{r}(1 + \frac{\beta x}{H}\cos\theta)\cos\theta$$

The net force on the rotor perpendicular to the instantaneous displacement is

$$F_y = \frac{\tau_m}{r}\int_0^{2\pi}(1 + \frac{\beta x}{H}\cos\theta)\cos\theta d\theta$$

$$F_y = \frac{\pi\tau_m\beta}{Hr} \qquad (48)$$

Total torque

$$\tau = \int_0^{2\pi} \tau_\theta d\theta = \int_0^{2\pi}\tau_m(1 + \frac{\beta}{H}\cos\theta)d\theta$$

$$= 2\pi\tau_m \qquad (49)$$

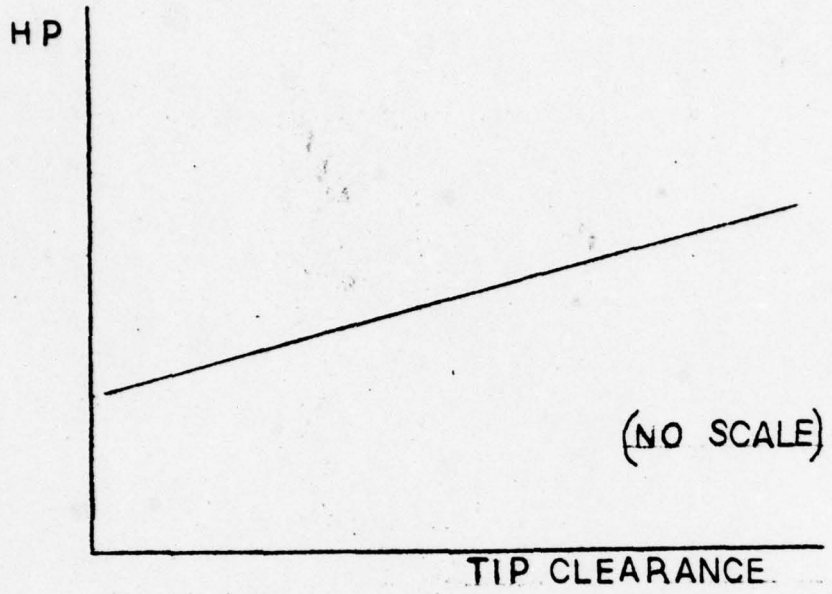

FIGURE B-1,... HP VS. TIP CLEARANCE

$F_{T2} > F_{T1}$

$C_{T2} > C_{T1}$

$R = F_{T2} = F_{T1}$

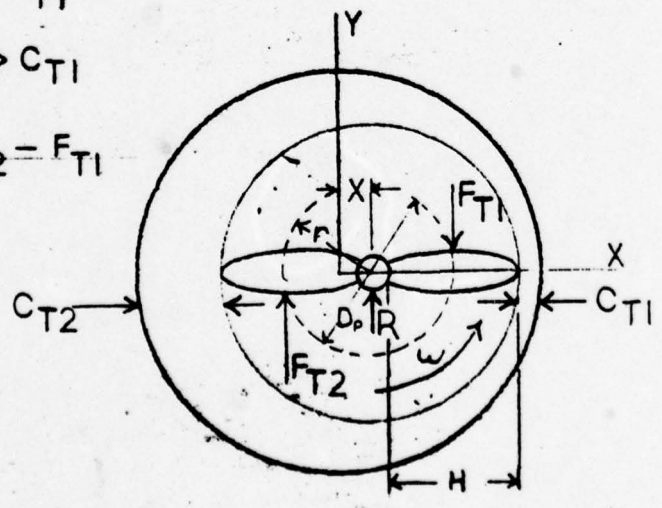

FIGURE B-2 ,...RESULTANT FORCE DUE TO BLADE ECCENTRICITY

Combining equations (48) and (49) gives

$$F_y = \frac{\tau\beta x}{2Hr} = \frac{\tau\beta}{D_p H} = qx \qquad (50)$$

where

$$q = \frac{\tau\beta}{D_p H}$$

The total torque is related to hp and engine rpm by

$$\tau = \frac{hp \times 33{,}000 \times 12}{2\pi rpm}$$

$$= 63{,}000 \frac{(hp)}{(rpm)}, \text{ in-lb}$$

Therefore

$$q = \frac{63{,}000(hp)\beta}{D_p \times H \times (rpm)}$$

Rotation is assumed counterclockwise. A positive displacement along the x-axis causes a positive force in the y-direction. A positive displacement along the y-axis causes a negative force in the x-direction."

Two test rigs have been built for the purpose of verifying equation 50. The first test rig had several shortcomings which were corrected in the second test rig as follows. The design of the second test rig incorporated the salient features of the first, but had many added features, such as a heavy rigid frame to support the electric motor, shaft and rotor. The new frame kept the vibration down to a minimum. A better lock mechanism was provided to keep the shroud surrounding the rotor in place after the eccentricity was introduced. Sturdy probe mounts were added, again to keep the vibration down to a minimum. Slotted motor mounts were also added to give the motor 5 degrees of freedom (3 translations and 2 rotations about

horizontal axes) for easy aligning of the motor shaft, quill shaft and rotor shaft with each other and for the use of different length quill shafts (see Sheet No. 20). Most important, what prompted the evolution of the second test rig, the mean clearance between the blade tips and the shroud was reduced by 0.28 inches to a mean clearance of 0.050 inches. It was felt that the large clearance caused the rotor to surge, which in turn made it difficult to observe any aerodynamic changes due to Alford's force. The pitfalls of the first test rig were thus eliminated in the second test rig.

The eccentricity was imparted to the rotor by moving the shroud in a horizontal direction. It varied from 0.001 to 0.099 inches and could be held in place anywhere in between. A probe used was a Bently proximeter probe which measured horizontal displacement perpendicular to the eccentricity. The "balancing top" (see Sheet No. 16) served as a surface for the probe to act.

The rotor itself was mounted on an elastic beam (see Sheet No. 18) which allowed it to move in a horizontal direction perpendicular to the blade eccentricity when a small force was applied at the rotor blades.

Due to the non-concentric circumference of the balancing top, it was necessary to build an L. C. Low-Pass filter to attenuate the A. C. component of the signal produced by the Bently proximeter probe. The signal was displayed on an oscilloscope. The L. C. filter consisted of a 10 henry choke in series with a lead to the oscilloscope and a 50 microfarad non-polarized capacitor connected across the 2 leads entering the oscilloscope (in a parallel configuration).

In order to verify equation 50 (Alford's equation) it was necessary to know the hp output of the electric motor at various rpm-s. A dynamometer was

designed and built for this purpose. It was an Eddy-Current dynamometer (Ref.2) and the details of the design can be seen on Sheet No. 22 of the assembly drawing. The eddy current brake has many advantages over the band or rope methods of motor-testing. Among these are:

a. Sensitivity combined with convenience of adjustment (a virtually infinite adjustment in torque)

b. Exact constancy after final temperature conditions have been reached

c. Heat produced in energy-absorbing element not conducted to the bearings

d. Absence of wear

The first three arise from the nature of the retarding force employed, and from the simplicity and fineness of rheostatic control. The continual stream of air outward past the copper disc carries away the heat. This is the advantage referred to in c.

The next phase of the research on this project will be to verify equation 50. The previous design work mentioned above will lead to an auspicious beginning of this phase. The Alford's equation will be compared with the measured plot of Alford's force vs. motor rpm (eccentricity held constant) and also by a plot of the measured Alford's force vs. eccentricity with motor rpm held constant. If Alford's equation does not predict the actual values, than a new equation will be derived using the experimental data obtained from the Alford test rig.

REFERENCES

1. Alford, J.S., "Protecting Turbomachinery From Self-Excited Rotor Whirl," Journal of Engineering for Power, October 1965, pp. 337, 342.

2. Morris, D. K., and G. A. Lister, "The Eddy-Current Brake for Testing Motors," Journal of the Institution of Electrical Engineers, Vol. 35, No. 175, April 1905, pp. 445-474.

SHEET 1 OF SHEETS 34

BILL of MATERIAL

PART NO.	QUANTITY	SHEET NO.	DESCRIPTION
A1	1	02	SLIDING PLATE
A2	1	03	STATOR
A3	2	04	SLIDE GUIDE
A4	4	05	CLAMP
A5	1	06	BOTTOM PLATE
A6	2	07	ANGLE BAR 2" × 2" × ¼"
A7	1	08	MOTOR MOUNT
A8	1	09	MOTER MOUNT BRACKET
A9	2	09	PROBE MOUNT SUPPORT
A10	1	10	ROTOR FRAME
A11	1	11	ROTOR SHAFT
A12	2	12	ANGLE BRACKET
A13	2	13	SIDE PLATE
A14	1	14	UPPER FAN UNIT
A15	1	15	ELASTIC BEAM
		HEXAGON SOCKET - HEAD CAP SCREW (HSHCS)	
A16	30		¼"UNC-20 × ¾"LONG (HSHCS)
A17	4		¼"UNC-20 × 1½" LONG (HSHCS)
		HEXAGON HEAD BOLT (HHB)	
A18	12		¼"UNC-20 × 1½" LONG (HHB)
		HEX JAM NUT (HJN)	
A19	4		¼"UNC-20 (HJN)
A20	1		5/16"UNC-20 (HJN)
A21		FLEXIBLE COUPLING NO. CC1-5 WINFRED M. BERG INC. 499 OCEAN AVENUE EAST ROCKAWAY, L.I., NY 11518 PHONE (516) 599-5010	
A22	1	ELECTRIC MOTOR CAT. NO. B2110 FRAME NO. 13 BODINE ELECTRIC COMP., 2500 WEST BRADLEY PLACE, CHICAGO, ILL 60618 (312) 478-3515	
A23	1	BLOWER MODEL 1-6-4-32A JOY MANUF. COMP 338 S. BROADWAY P.O. BOX 431 NEW PHILADELPHIA, OHIO, 44663	
A24	1	16	BALANCING TOP
A25	1	17	QUILL SHAFT

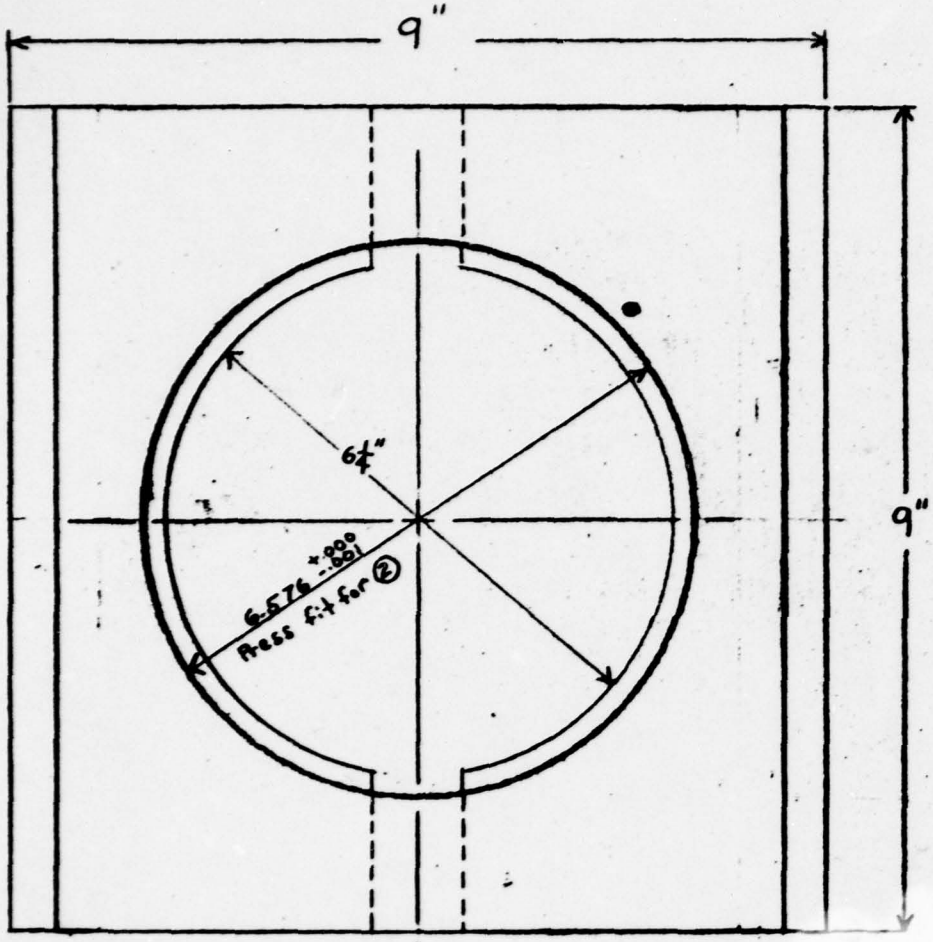

45° SURFACES ARE SLIDING FIT WITH PART NO. 3

SLOT IS SLIDING FIT WITH PART NUMBER 15

SEE ASSEMBLY DRAWING SHEET NO. 19

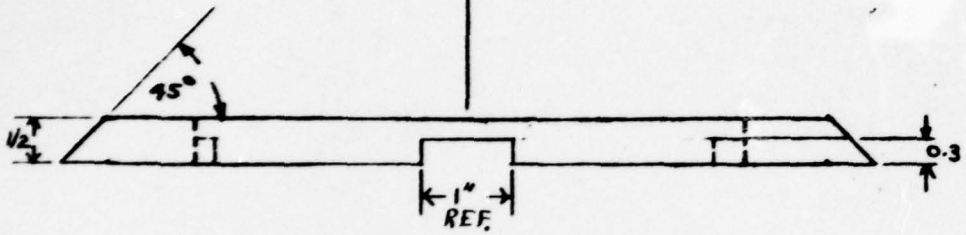

UNIVERSITY of FLORIDA	
NAME: SLIDING PLATE	NO A1
MAT'L ALUMINUM	
SCALE 1" = 2"	DATE: 2-1-78
BY FRANK LAUDADIO	

SHEET 03 OF SHEETS 34

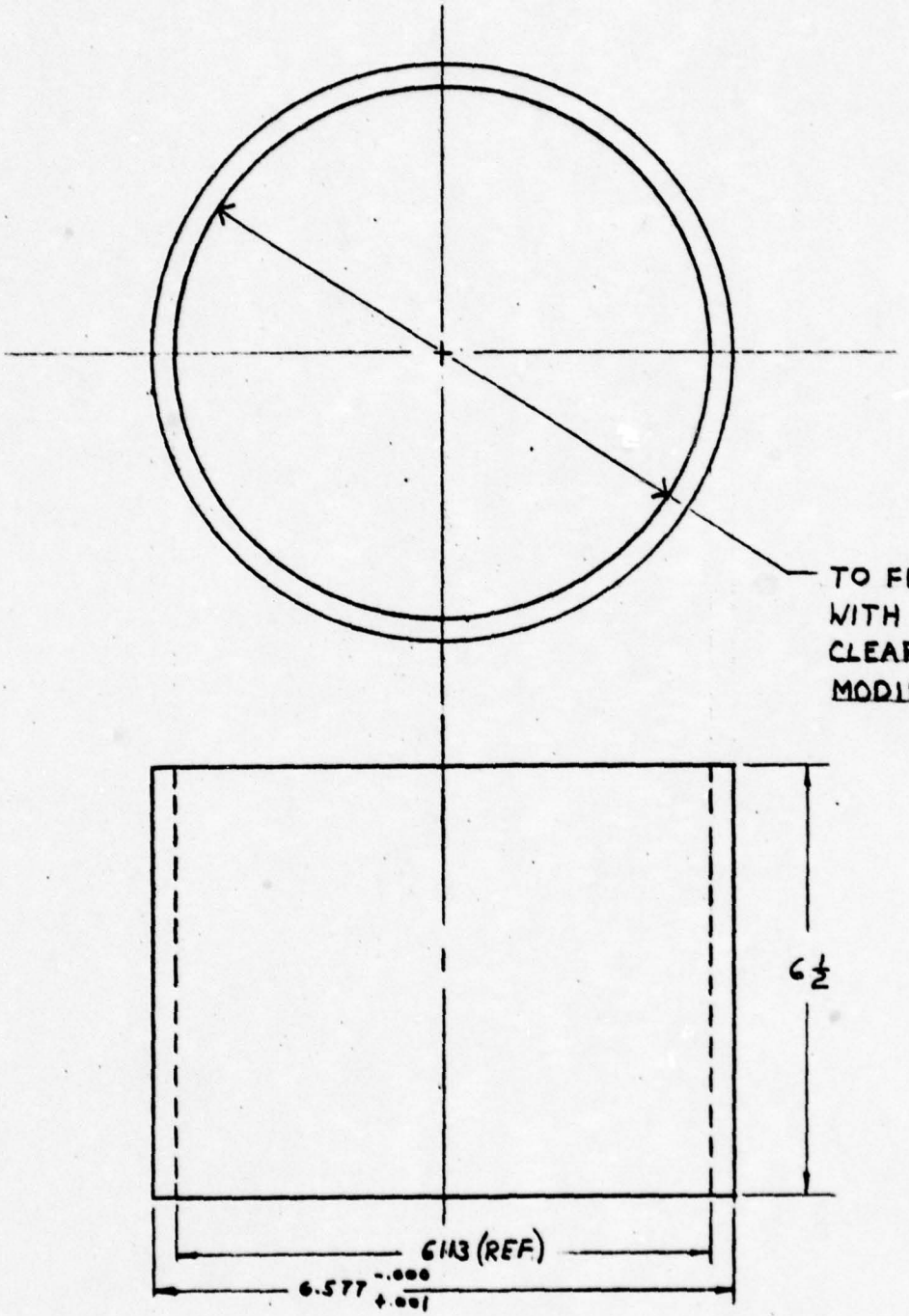

UNIVERSITY OF FLORIDA	
NAME: STATOR	NO. A2
MAT'L: ALUMINUM	
SCALE: 2" = 1"	DATE: JAN. 25, 1979
BY. FRANK LAUDADIO	

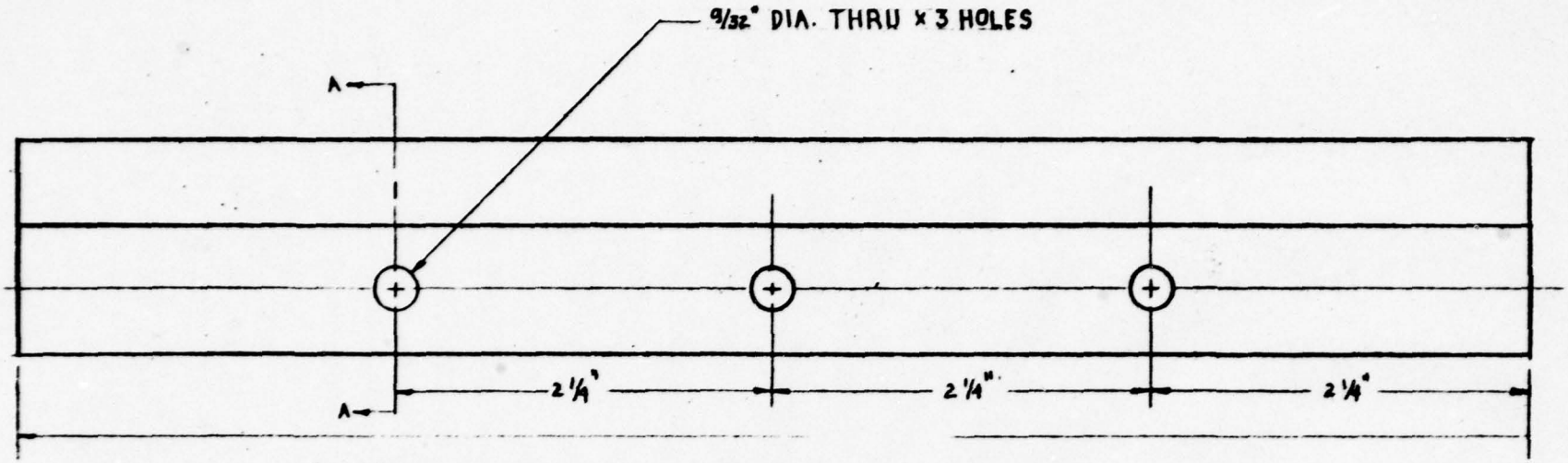

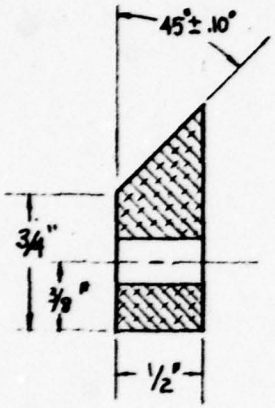

UNIVERSITY OF FLORIDA	
NAME : SLIDE GUIDE	NO : A3
MATERIAL ALUMINUM	
SCALE 1" = 1"	DATE 2-1-79
BY FRANK LAUDADIO	

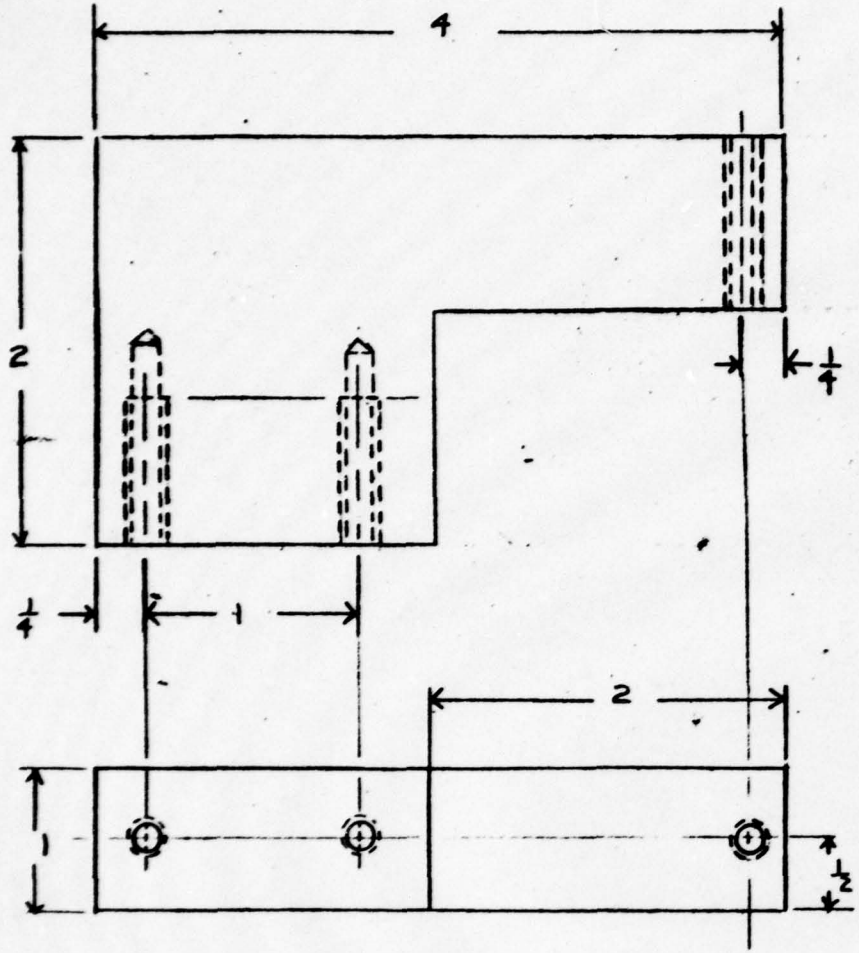

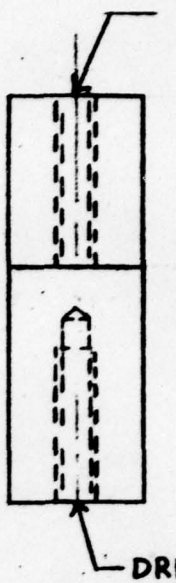

UNIVERSITY of FLORIDA	
NAME CLAMP	NO. A4
MAT'L ALUMINUM	
SCALE 1" = 1"	DATE 1-29-79
BY FRANK LAUDADIO	

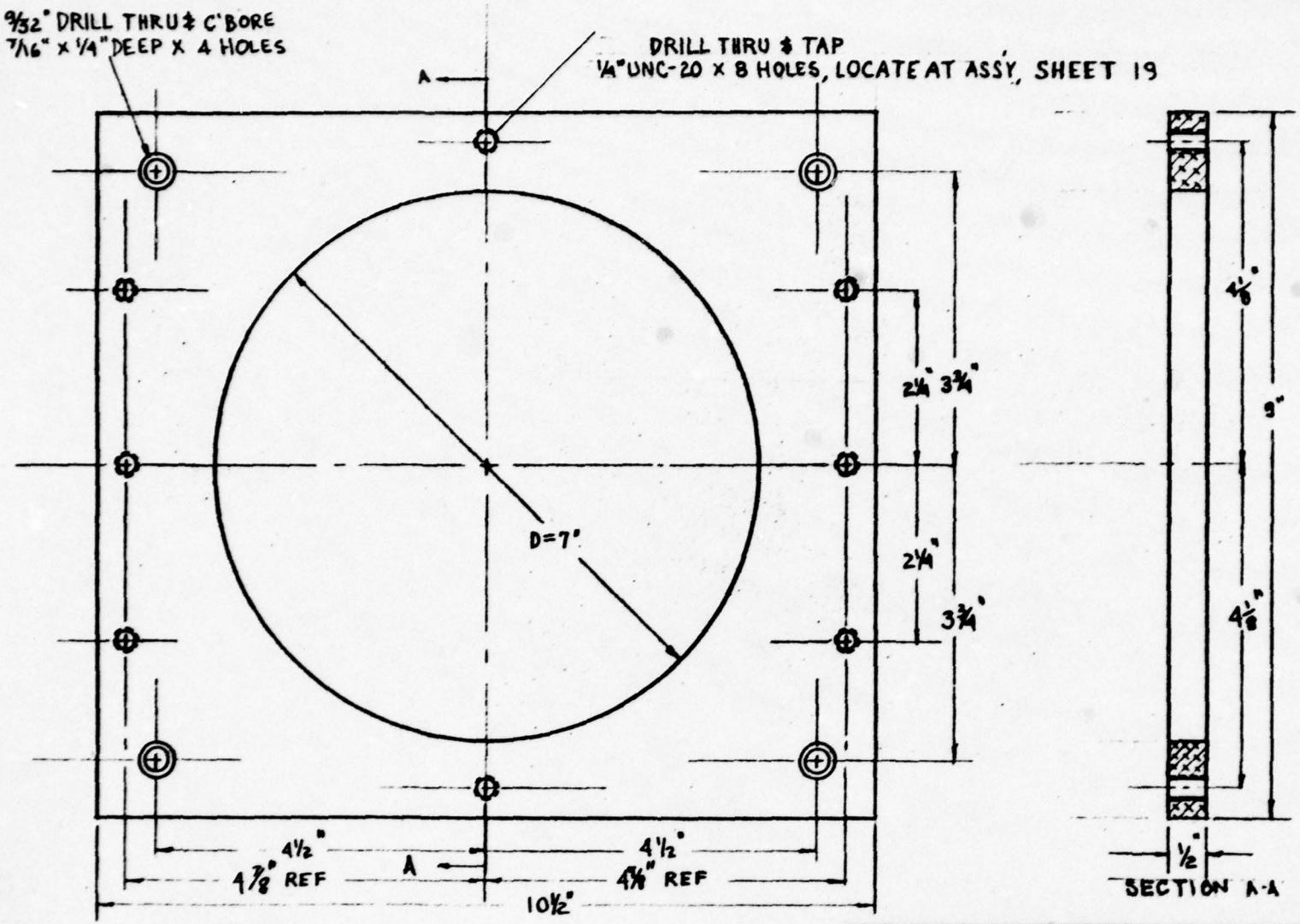

UNIVERSITY OF FLORIDA	
NAME: BOTTOM PLATE	NO. A5
MATERIAL: ALUMINUM	
SCALE: 1/2 SIZE	DATE: 2-1-79
BY: FRANK LAUDADIO	

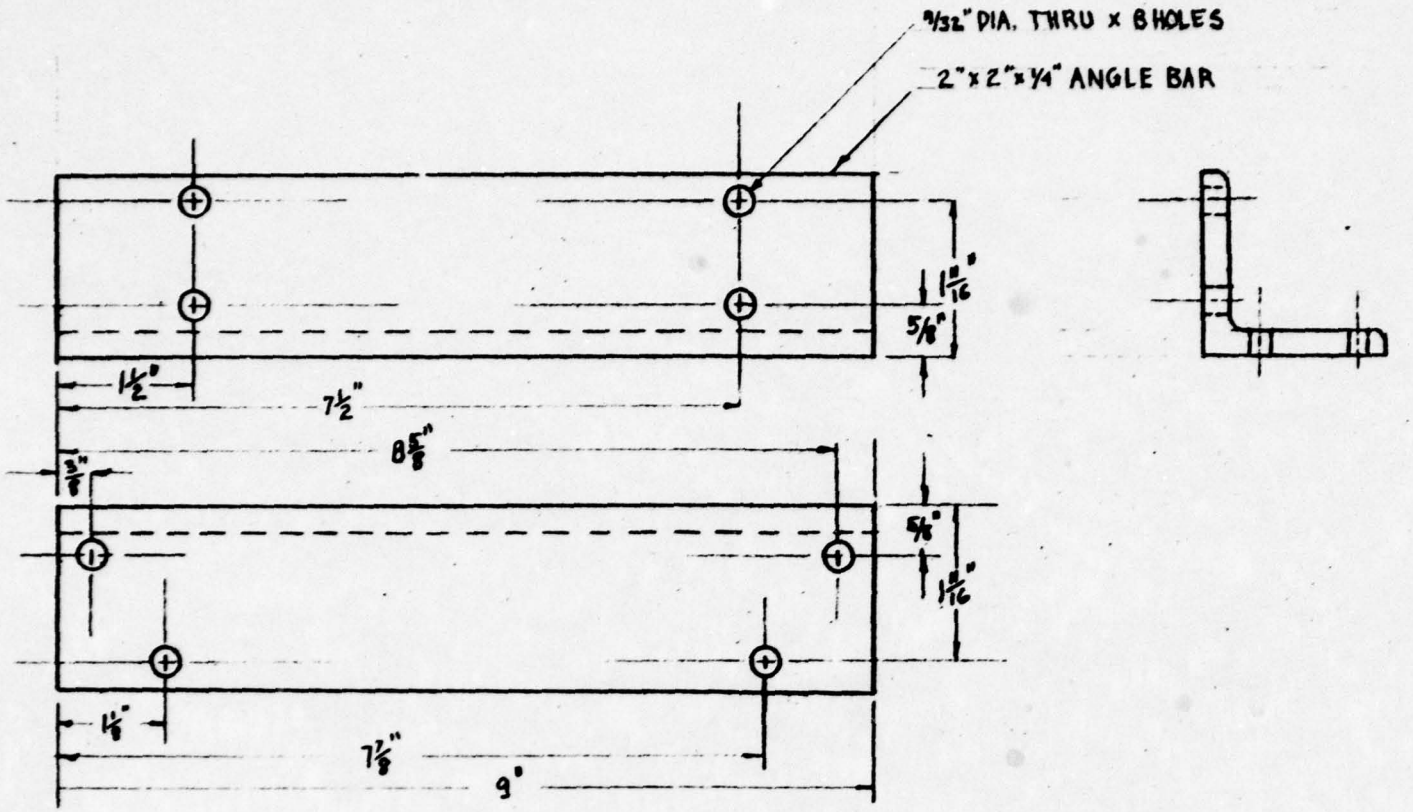

UNIVERSITY OF FLORIDA		
NAME: ANGLE BRACKET	NO. AG	QUAN: 2
MATERIAL: STEEL		
SCALE: 1/2 SIZE	DATE: 2-3-79	
BY: FRANK LAUDADIO		

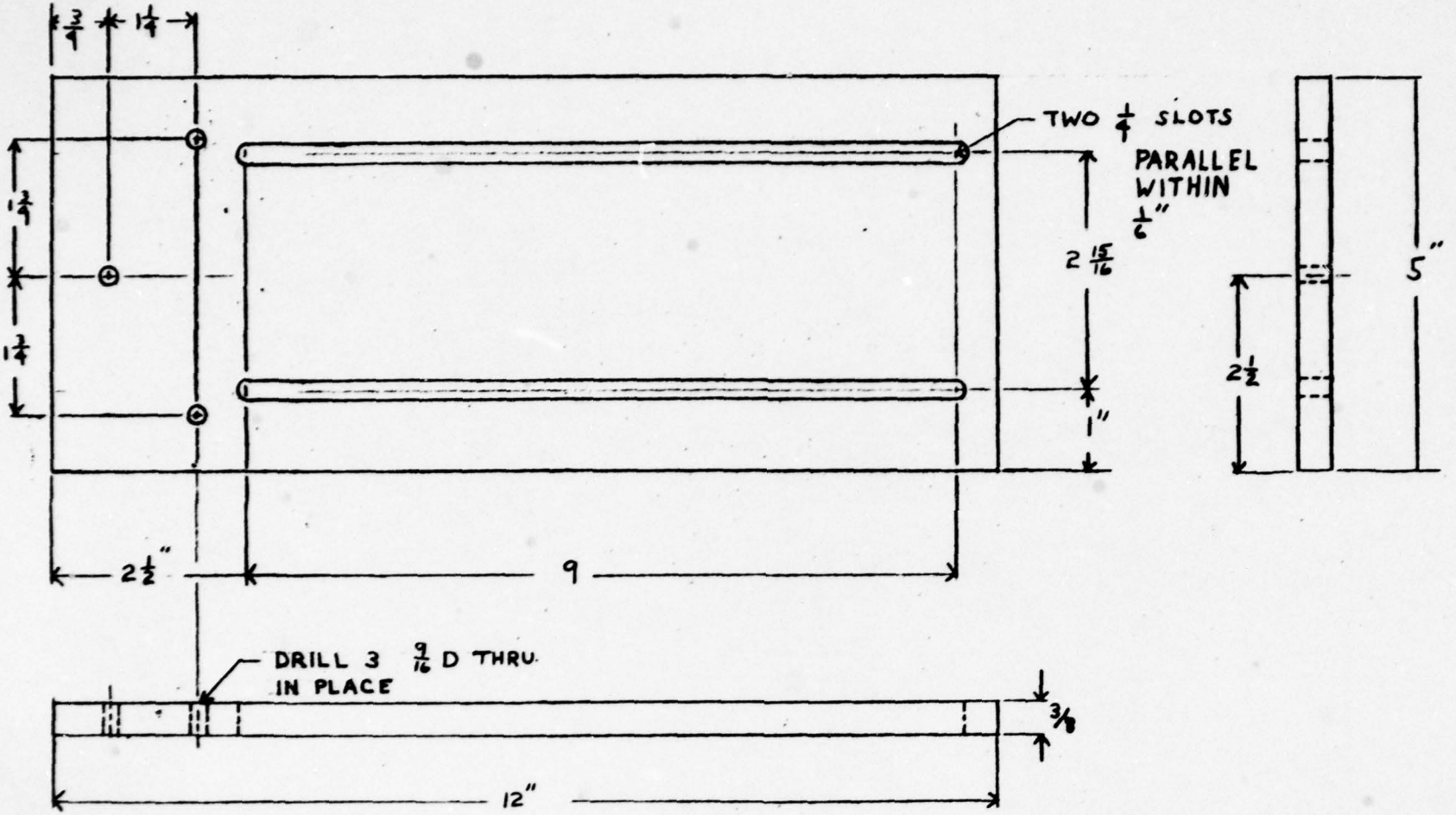

UNIVERSITY of FLORIDA	
PART NAME MOTOR MOUNT	
MAT'L ALUMINUM	NO A7
SCALE 1" = 2"	DATE 2-2-79
BY FRANK LAUDADIO	

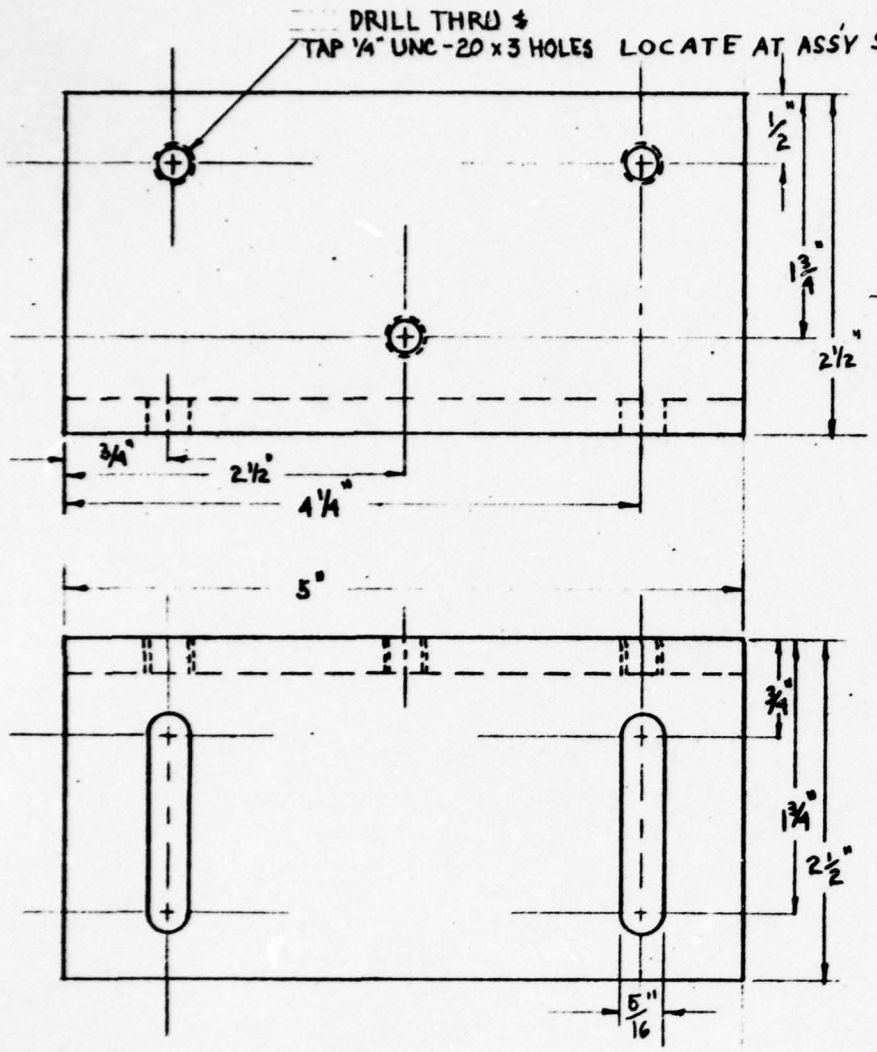

MOTOR MOUNT BRACKET A8 QUAN: 1
MAT'L STEEL

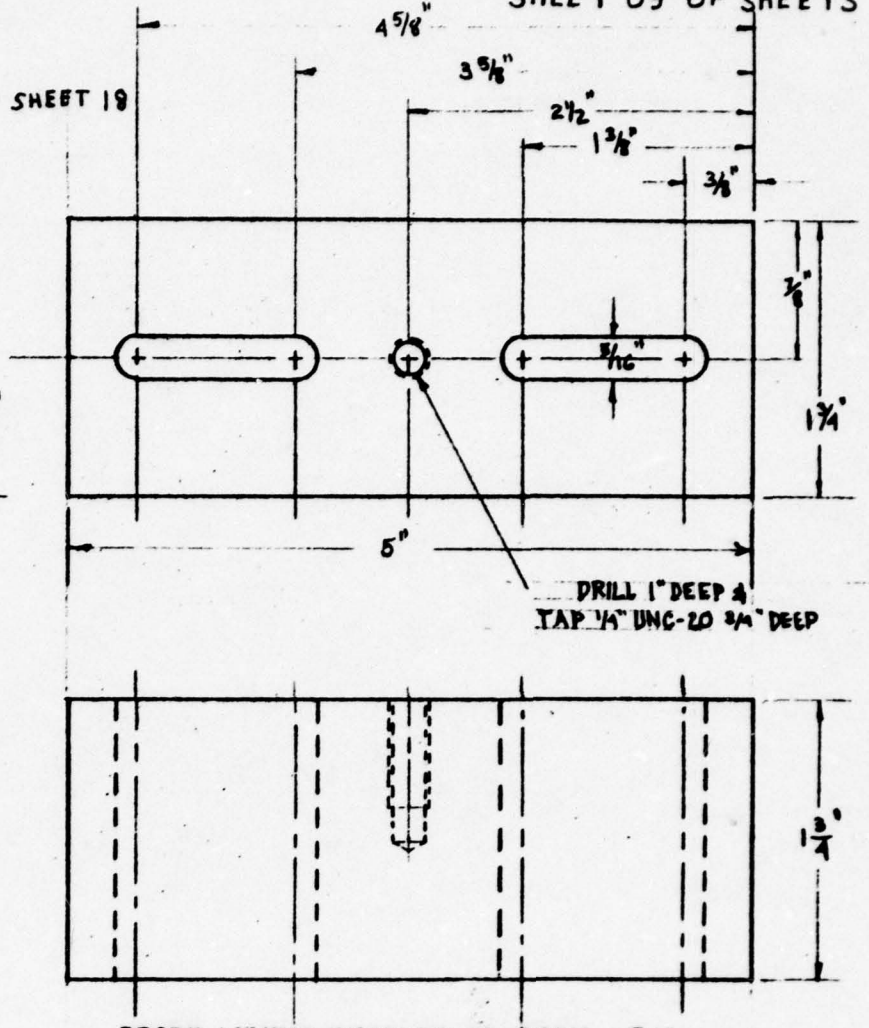

PROBE MOUNT SUPPORT A9 QUAN: 2
MAT'L: ALUMINUM

UNIVERSITY OF FLORIDA		
PART NAME: AS SHOWN	NO. AS SHOWN	QTY: AS SHOWN
MATERIAL: AS INDICATED		
SCALE: 3/4 SIZE	DATE: 2-3-79	
BY: FRANK LAUDADIO		

SHEET 10 OF SHEETS 34

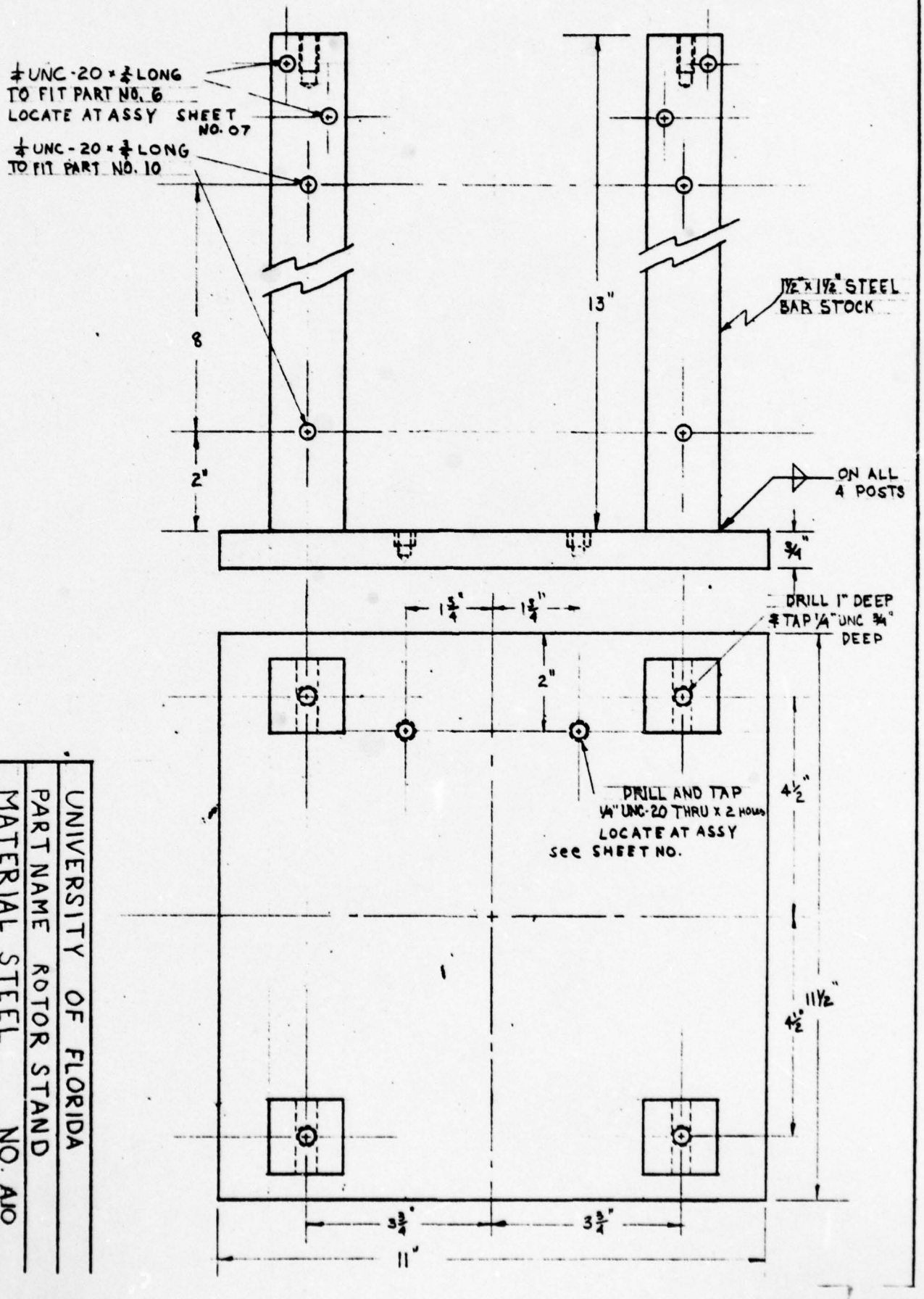

UNIVERSITY OF FLORIDA	
PART NAME ROTOR STAND	
MATERIAL STEEL	NO. A10
SCALE 3/8" = 1"	DATE 2-7-79
BY FRANK LAUDADIO	

SHEET 11 OF SHEETS 34

A 0.35 $^{+0.1}_{-0.0}$
B 0.4 $^{+0.1}_{-0.0}$
C 3.00 $^{+.01}_{-.00}$
D 0.625 $^{+1/16}_{-0.00}$
E 2.25 $^{+0.1}_{-0.0}$
F 0.50 $^{+1/8}_{-0.0}$
G 1.00 $^{+1/8}_{-0.0}$
H $3\frac{1}{4}$"
I 0.375 $^{+1/8}_{-0.0}$

T 0.3148 $^{+0.0000}_{-0.0002}$
U 3/8
V 0.29 $^{+0.0}_{-1/8}$
W 0.310 $^{+0.000}_{-0.002}$
X 5/16 FOR HEX JAM NUT
Y 0.314 PRESS FIT WITH NO. 23
Z 0.30 $^{+0.0}_{-1/8}$

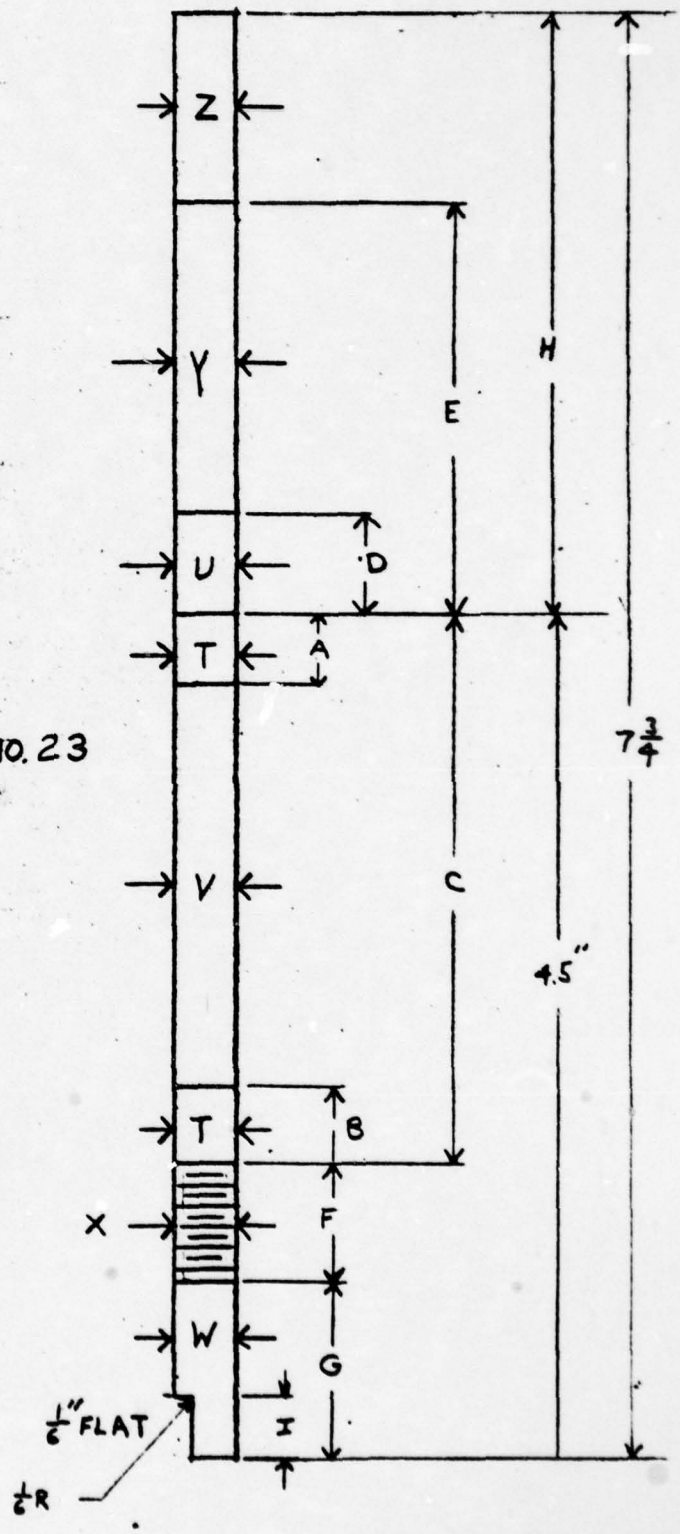

UNIVERSITY of FLORIDA
SHAFT NO. A11
SCALE 1" = 1"
MAT'L $\frac{3}{8}$" x 8" STEEL STOCK
BY HARVY LIPRIN

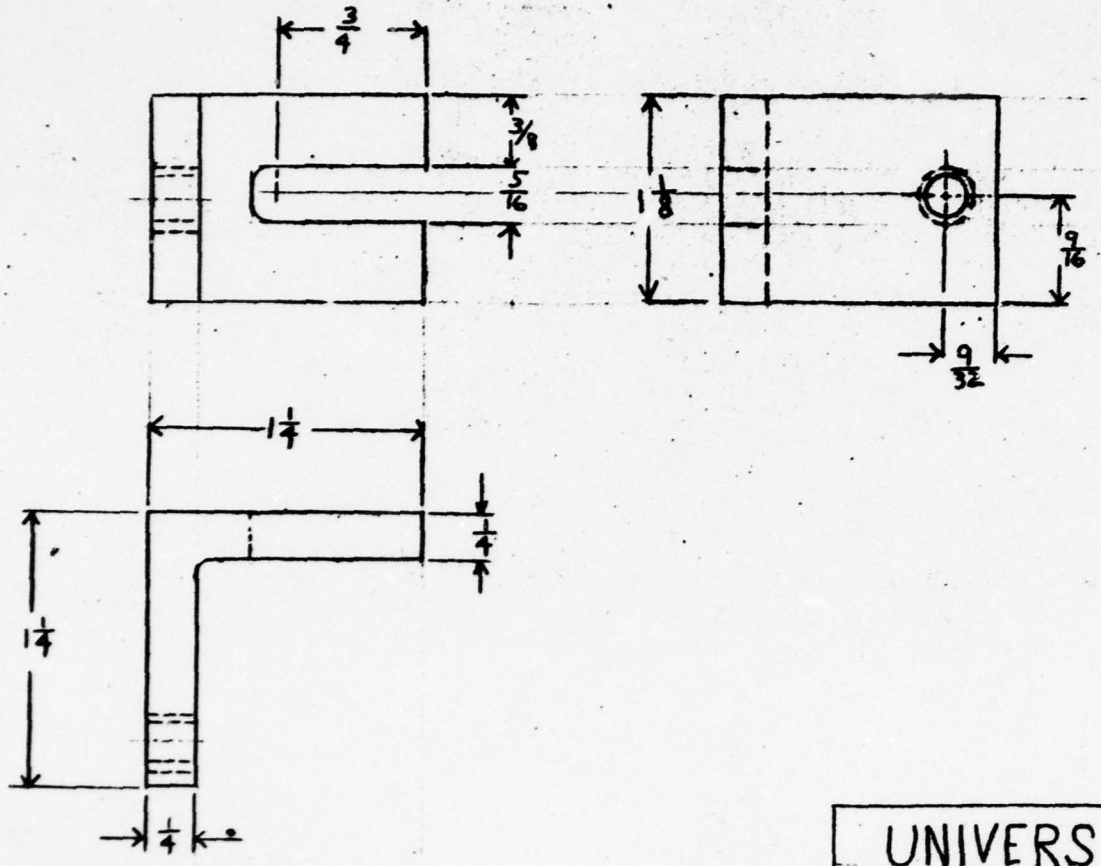

UNIVERSITY of FLORIDA	
PART NAME: ANGLE BRACKET	
MAT'L STEEL	NO. : A13
SCALE 1" = 1"	DATE 2-2-79
BY FRANK LAUDADIO	

B19

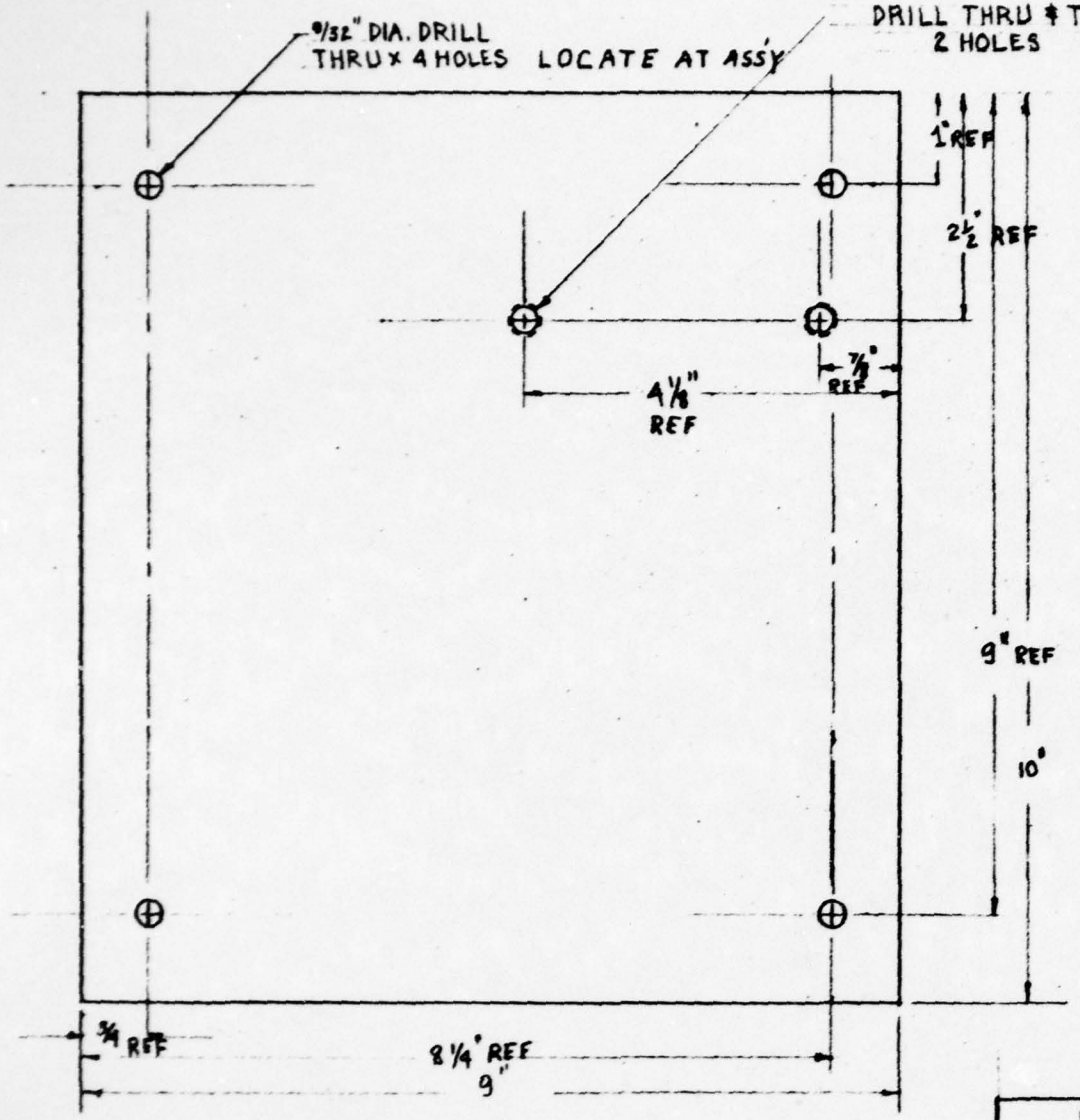

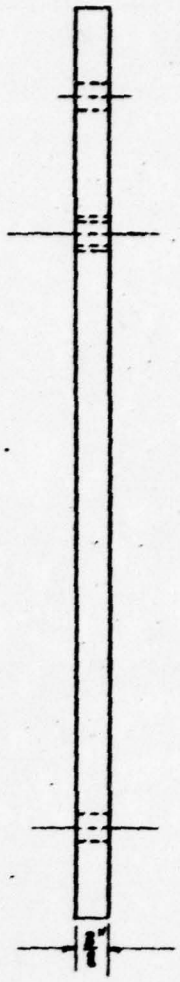

UNIVERSITY OF FLORIDA		
NAME: SIDE PLATE	NO. A12	QUAN: 2
MATERIAL: ALUMINUM		
SCALE: 1/2 SIZE	DATE: 2-3-79	
BY: FRANK LAUDADIO	*Laudadio*	

SHEET 14 OF SHEETS 34

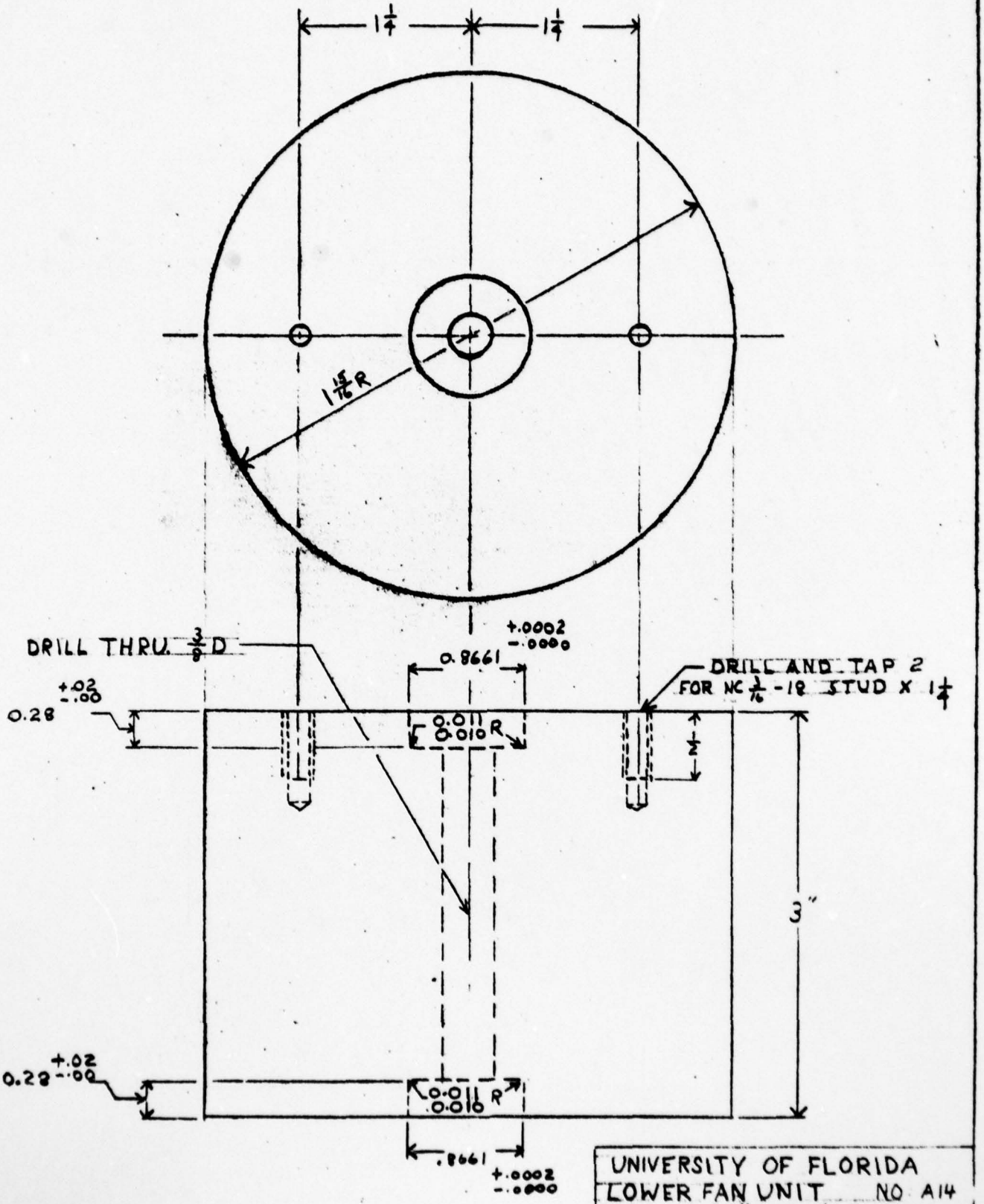

UNIVERSITY OF FLORIDA
LOWER FAN UNIT NO A14
SCALE 1"=1" MATL ALUMINUM
BY HARVY LIPTIN

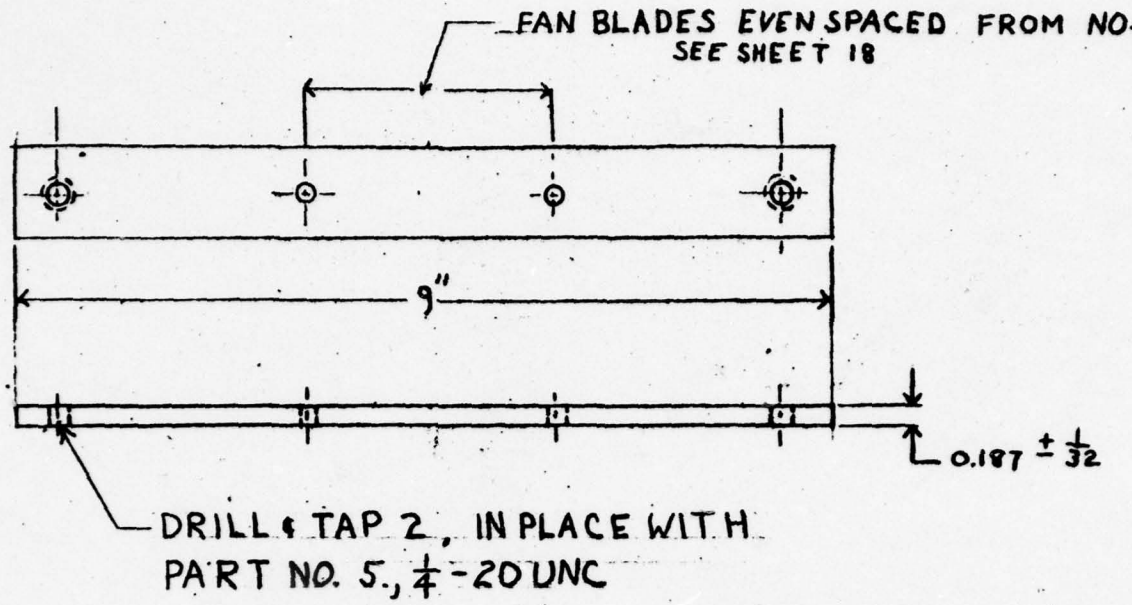

UNIVERSITY of FLORIDA
PART NAME: ELASTIC BEAM
MATERIAL: ALUMINUM NO. A15
SCALE 1" = 2" DATE 2-24-79
BY FRANK LAUDADIO

B22

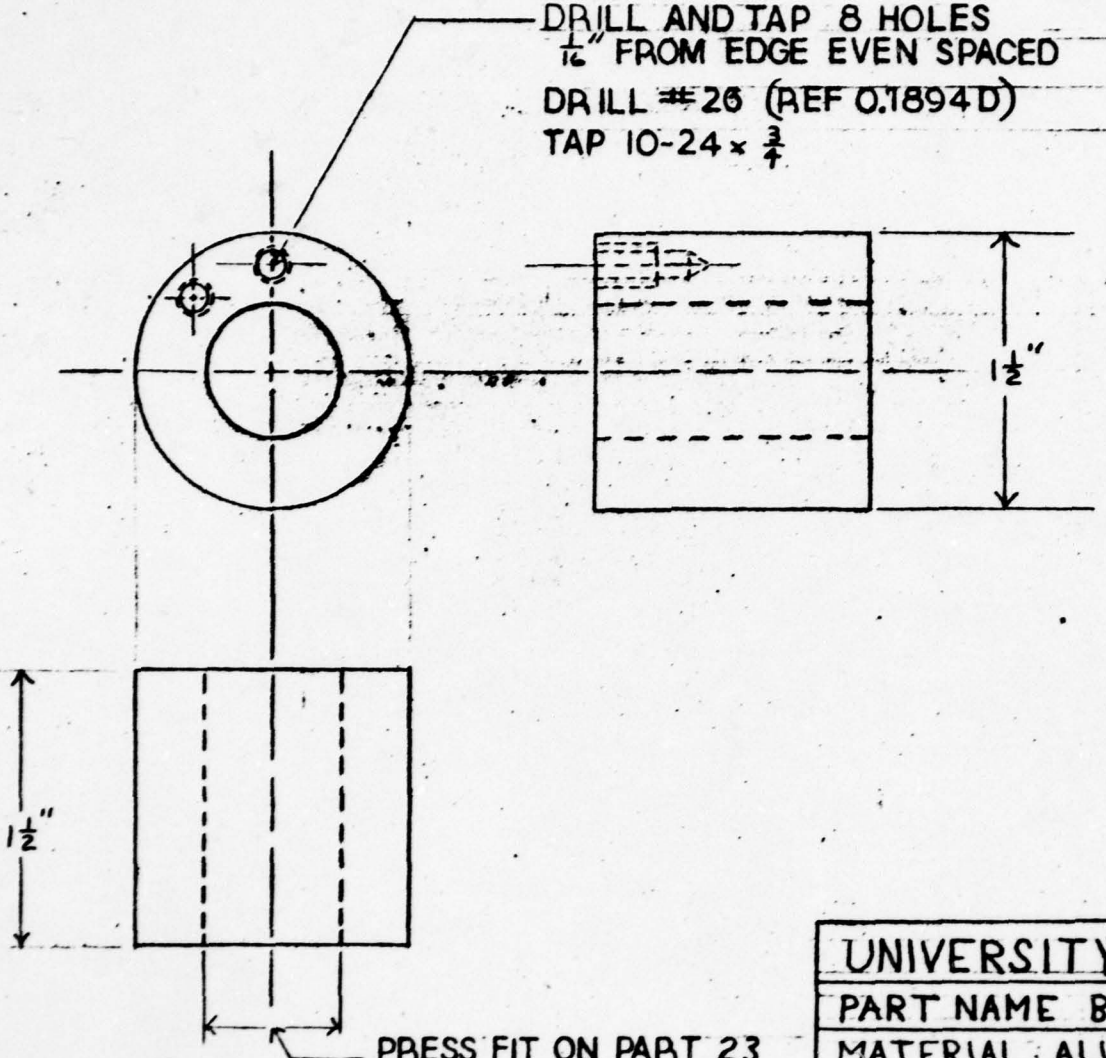

UNIVERSITY OF FLORIDA	
PART NAME BALANCING TOP	
MATERIAL ALUMINUM	NO A24
SCALE 1" = 1"	DATE 2-22-79
BY FRANK LAUDADIO	

B23

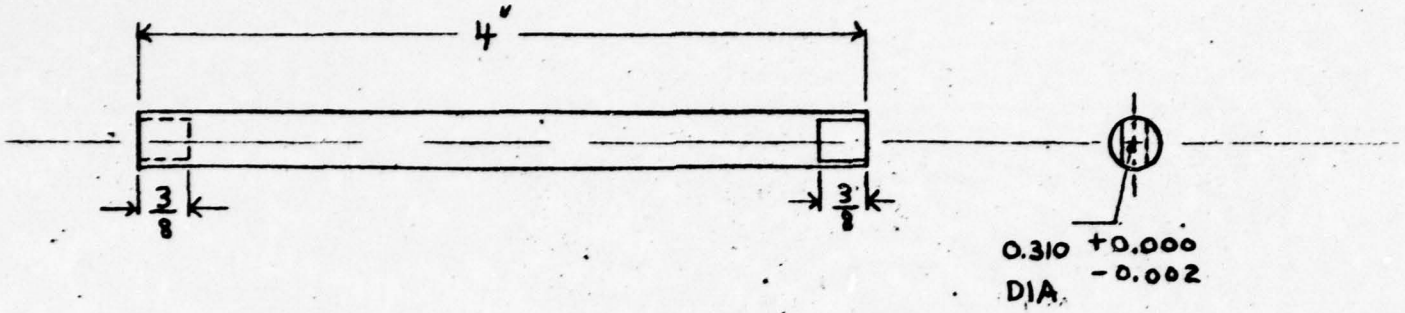

UNIVEVSITY of FLORIDA
PART NAME: QUILL SHAFT
MATERIAL: STEEL NO A25
SCALE 1"=1" DATE 3-2-79
bY Frank Lavadio

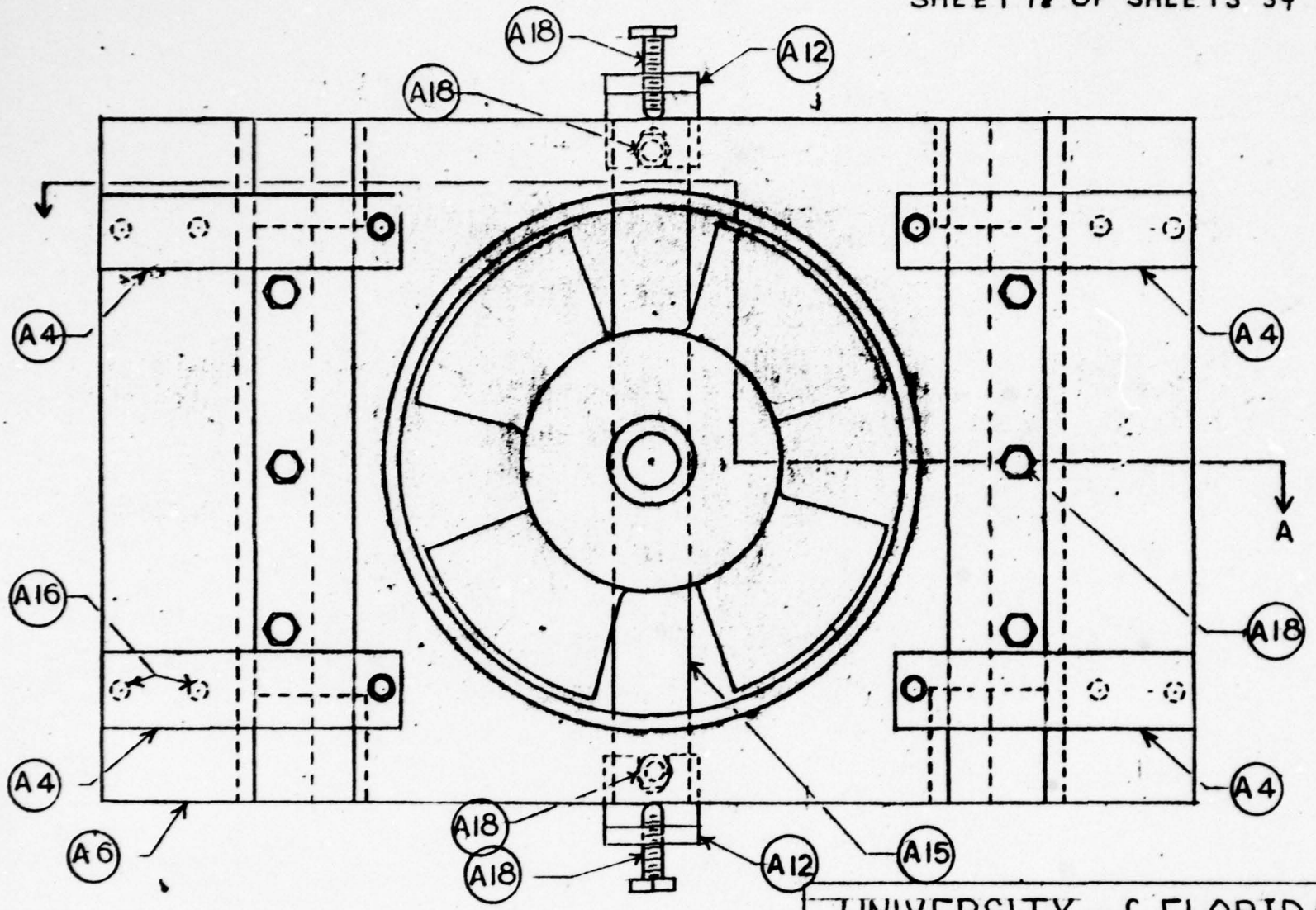

UNIVERSITY of FLORIDA

ASSEMBLY DRAWING

TOP VIEW

SCALE 1" = 2" DATE 2-23-79

BY FRANK LAUDADIO

B25

SHEET 19 OF SHEETS 34

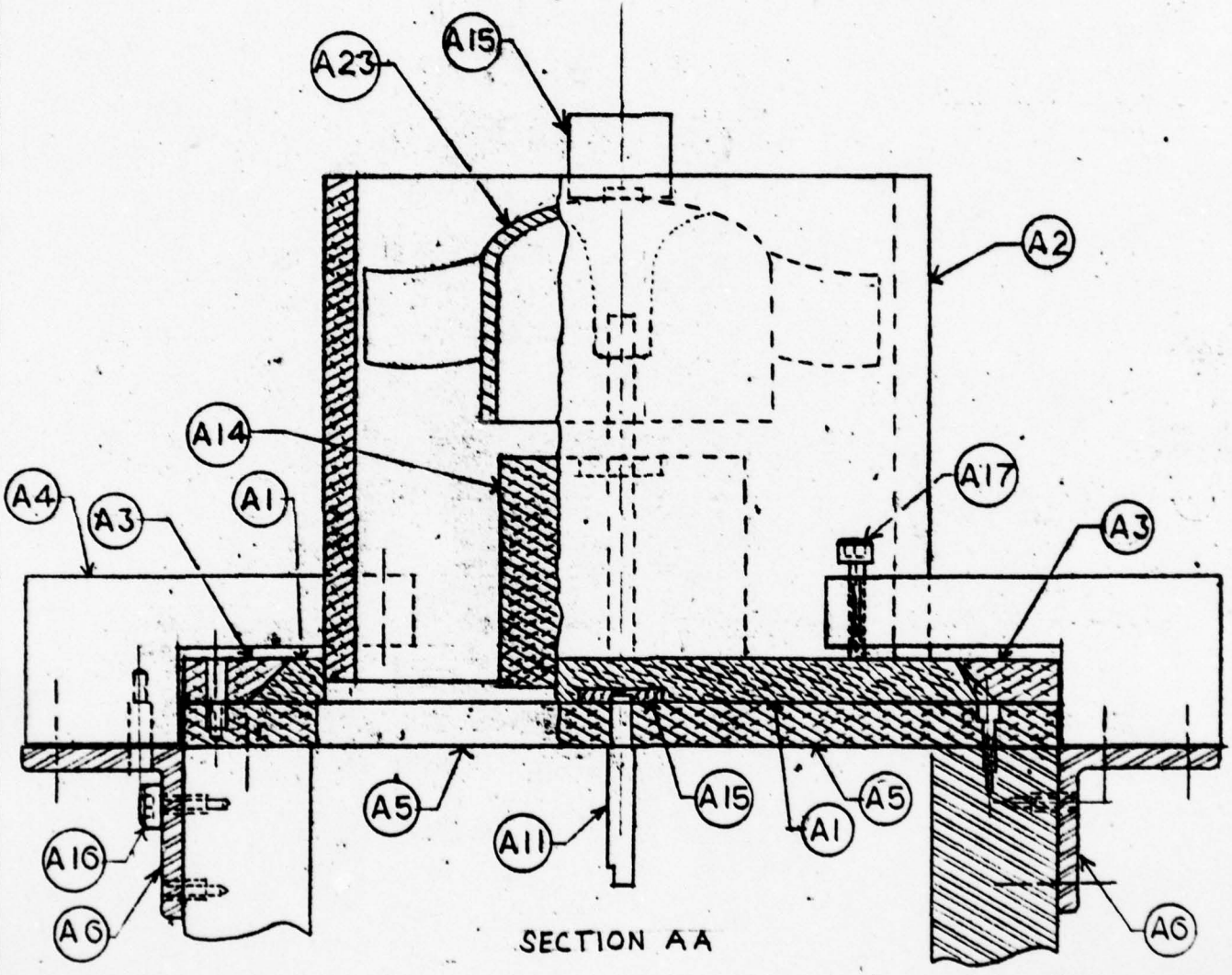

SECTION AA

UNIVERSITY of FLORIDA
ASSEMBLY DRAWING
SIDE VIEW TOP SECTION
SCALE 1" = 2" DATE 2-19-79
BY FRANK LAUDADIO

SHEET 20 of SHEETS 34

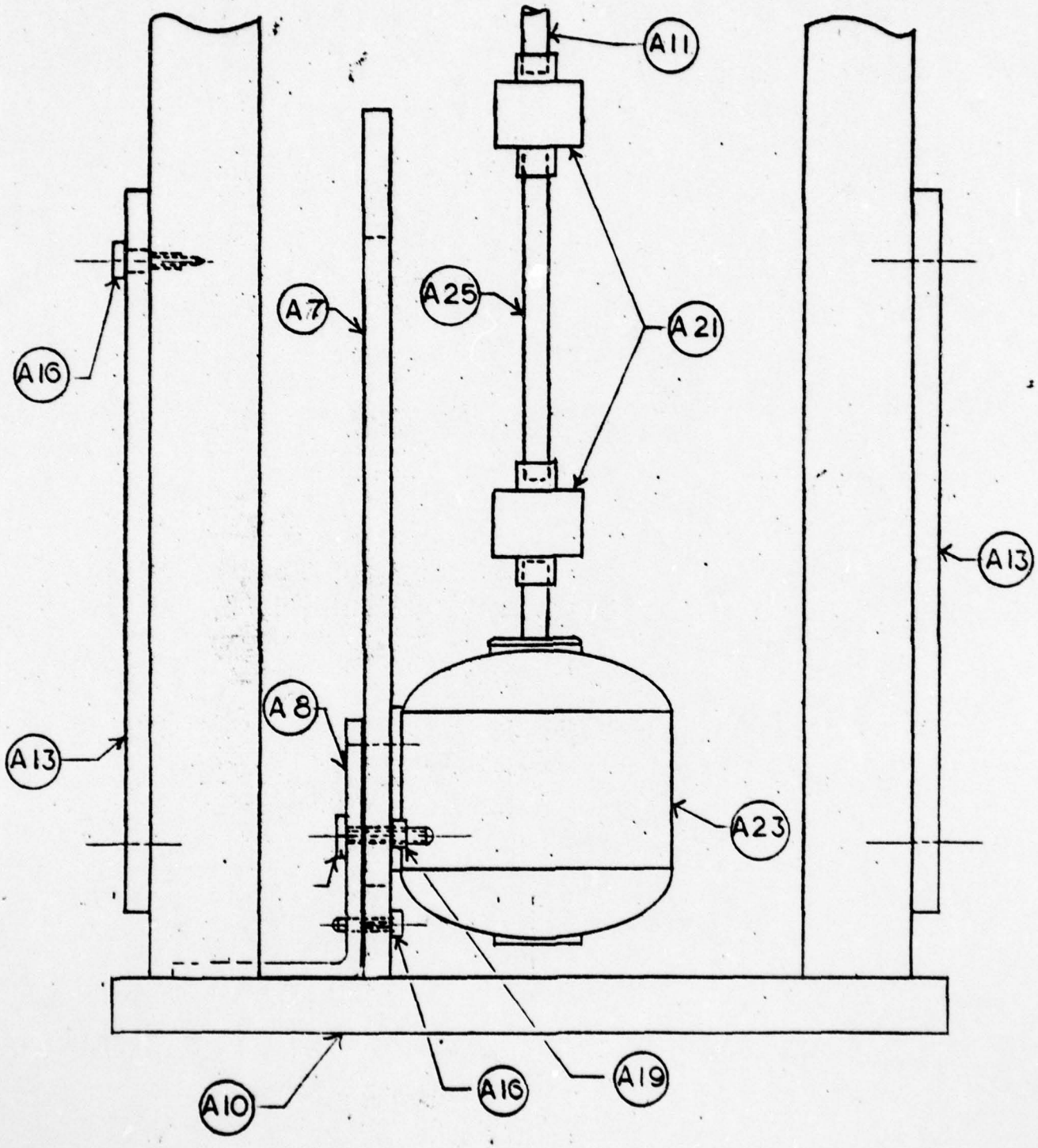

UNIVERSITY of FLORIDA
ASSEMBLY DRAWING
LOWER FRAME
SCALE 1" = 2" DATE 2-20-79
BY FRANK LAUDADIO

SHEET 21 of SHEETS

BILL of MATERIAL

PART NO.	QUANTITY	SHEET NO.	DESCRIPTION
B1	1	23	WALL MOUNT
B2	1	24	STRAIN BEAM
B3	1	25	HOLDER
B4	2	26	SPACER
B5	2	27	ARM
B6	2	28	LEG
B7	1	29	CORE
B8	1	30	TABLE MOUNT
B9	1	31	DYNO DISK
B10	1	32	BALANCE LOCK
B11	1	33	MOTOR MOUNT
B12	1	34	HOLDER TOP
B13	13	22	WALL MOUNTING SCREWS
B14	2	22	STRAIN GAGES
		MICRO-MEASUREMENTS VISHAY INTERTECHNOLOGY.	
		INC. PO BOX 306 · 38905 CHASE ROAD	
		ROMULUS, MICHIGAN 48174 (313) 941-3900	
		STOCK NO. EA-13-030CG-120	
B15	1400 TURNS	22	NO. 20 S.C.C. COPPER WIRE

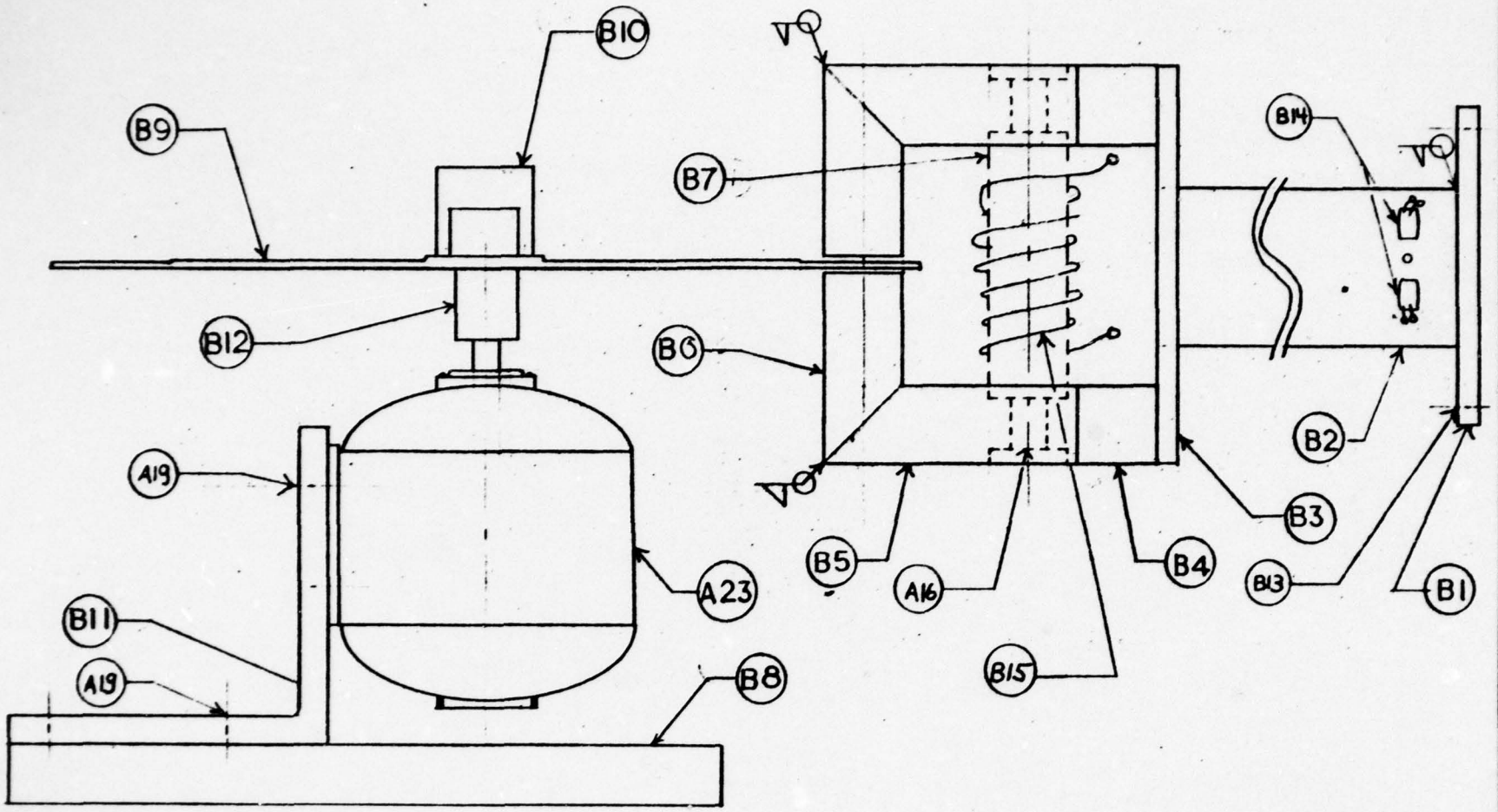

UNIVERSITY OF FLORIDA	
PARTNAME: DYNAMOMETER ASSY	
MAT'L: —	
SCALE: ½ SIZE	DATE: 2-7-79
BY: FRANK LAUDADIO	

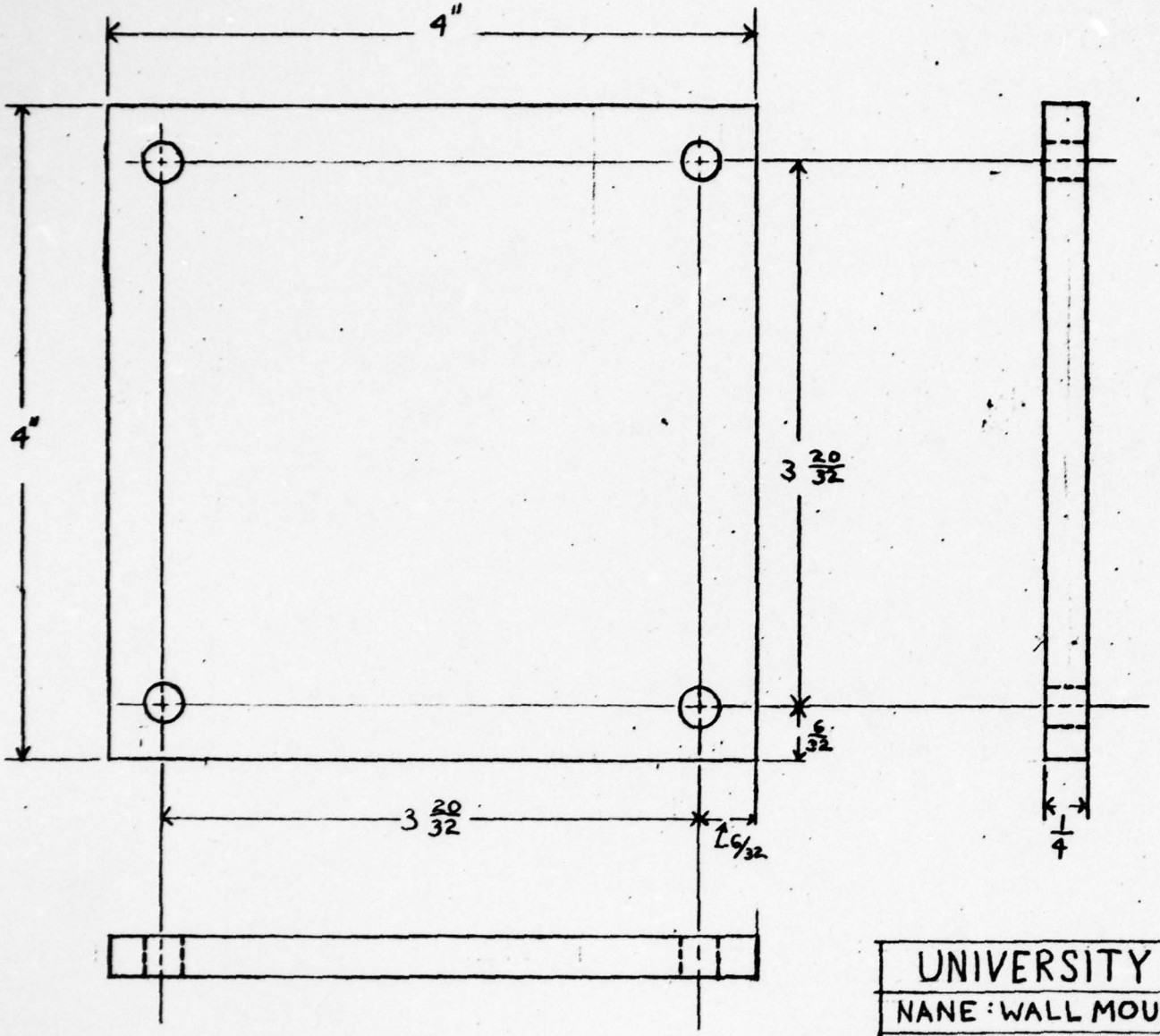

UNIVERSITY OF FLORIDA	
NANE: WALL MOUNT	NO: B1
MATERIAL: ALUMINUM	
SCALE 1"=1"	DATE 1-3-79
BY: FRANK LAUDADIO Frank Laudadio	

B30

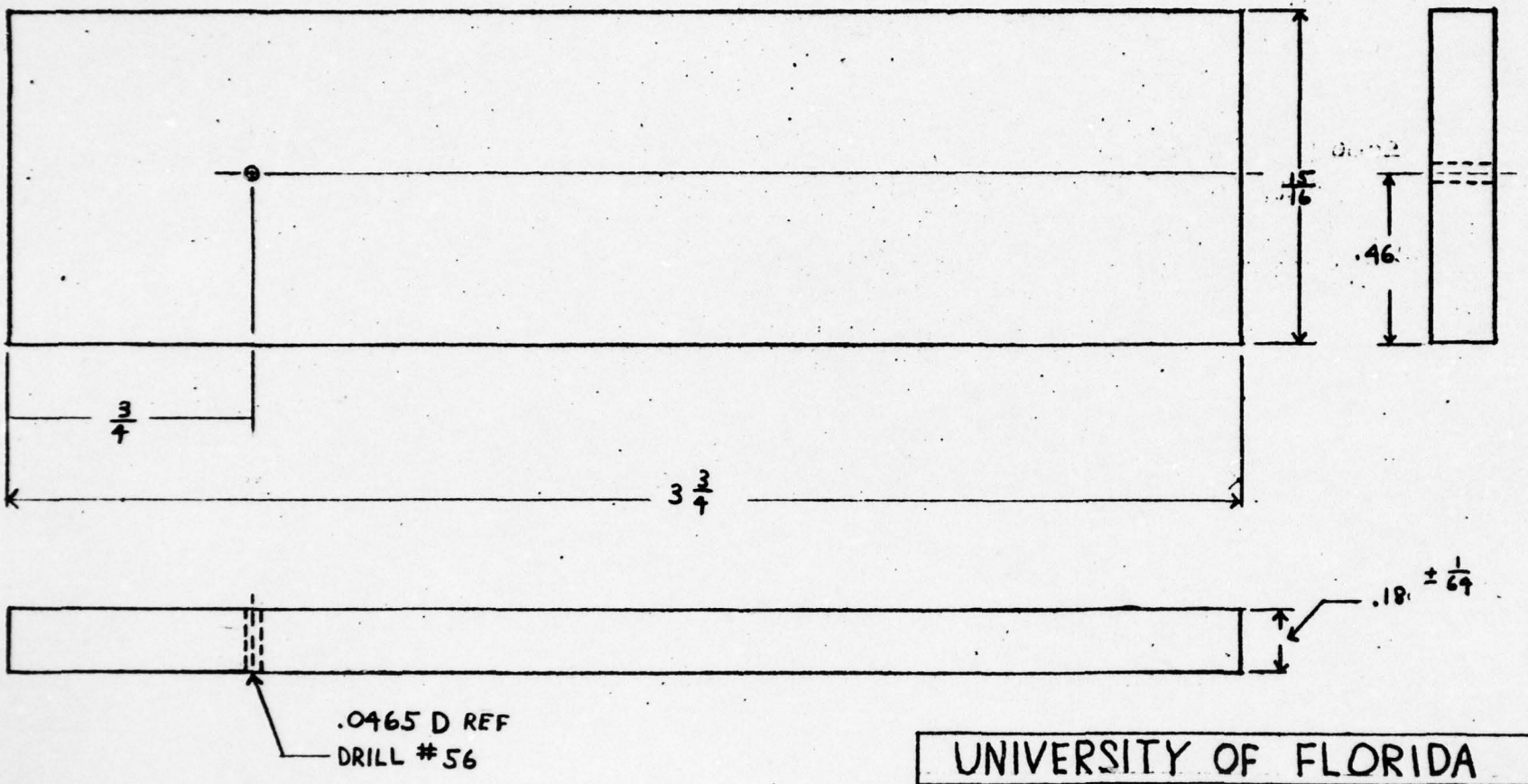

UNIVERSITY OF FLORIDA	
PART NAME : DUCTILE BEAM	NO. B2
MATERIAL : 6061 T6 ALUMINUM	
SCALE 1" = .5"	DATE 1-3-79
BY: FRANK LAUDADIO Frank Laudadio	

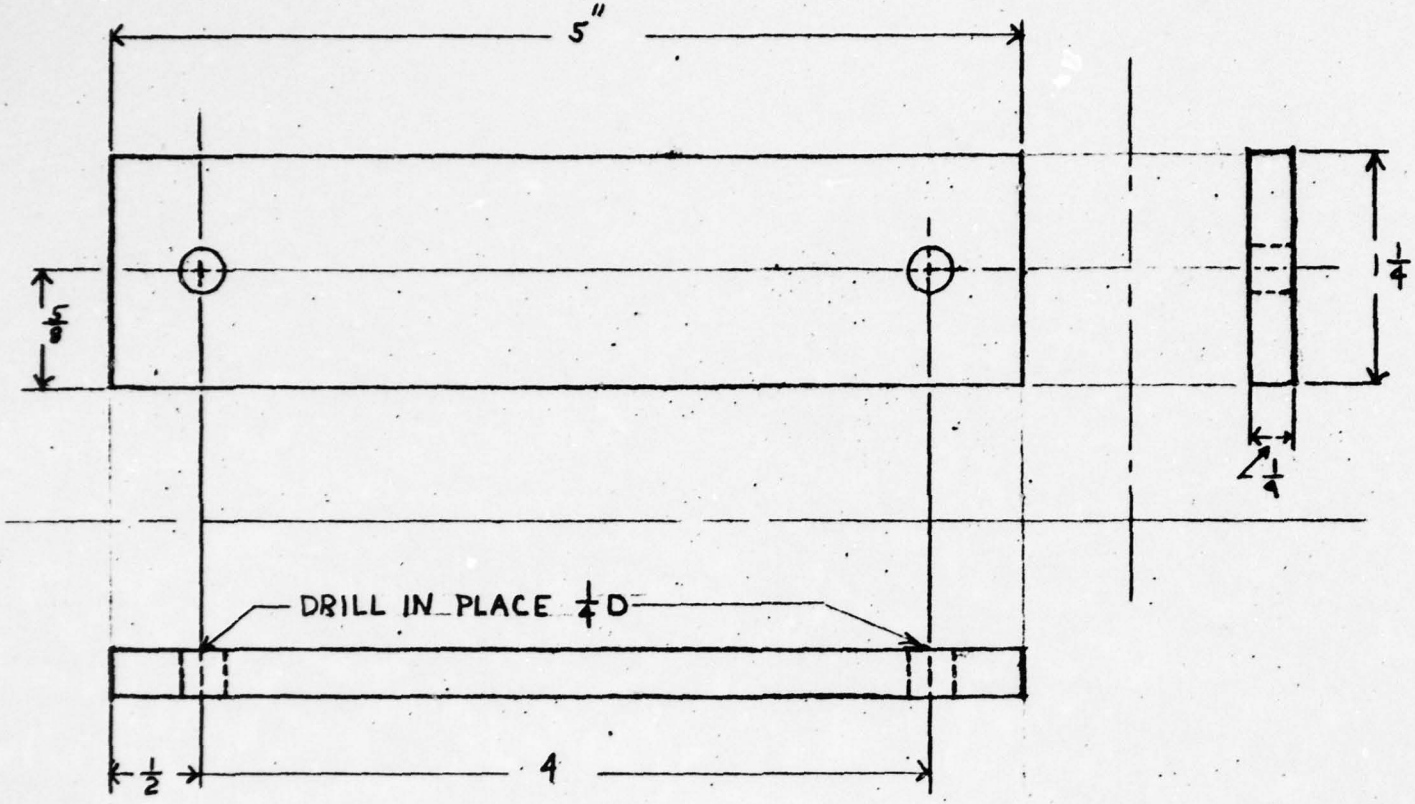

UNIVERSITY of FLORIDA	
PART NAME: HOLDER	NO: B3
MATERIAL ALUMINUM	
SCALE 1"=1"	DATE 1-16-78
BY FRANK LAUDADIO	

B32

AD-A071 716 FLORIDA UNIV GAINESVILLE ROTORDYNAMICS LAB F/G 20/11
INVESTIGATION OF LOAD-INDUCED NON-SYNCHRONOUS WHIRL INSTABILITI--ETC(U)
MAR 79 J M VANCE, G N SANDOR, K E ARD DAAG29-77-G-0217
UNCLASSIFIED ARO-15041.2-E NL

2 OF 2
AD A071716

END
DATE FILMED
8-79
DDC

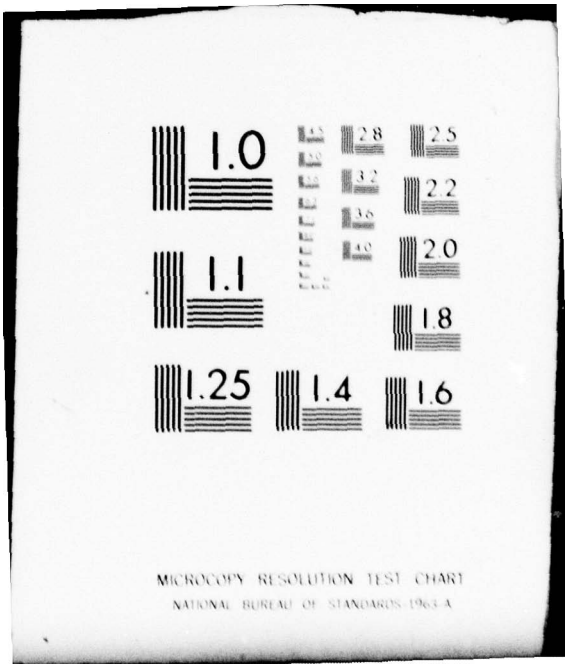
1.0
1.1
1.25
1.4
1.6
2.8
3.2
3.6
4.0
2.5
2.2
2.0
1.8
MICROCOPY RESOLUTION TEST CHART
NATIONAL BUREAU OF STANDARDS-1963-A

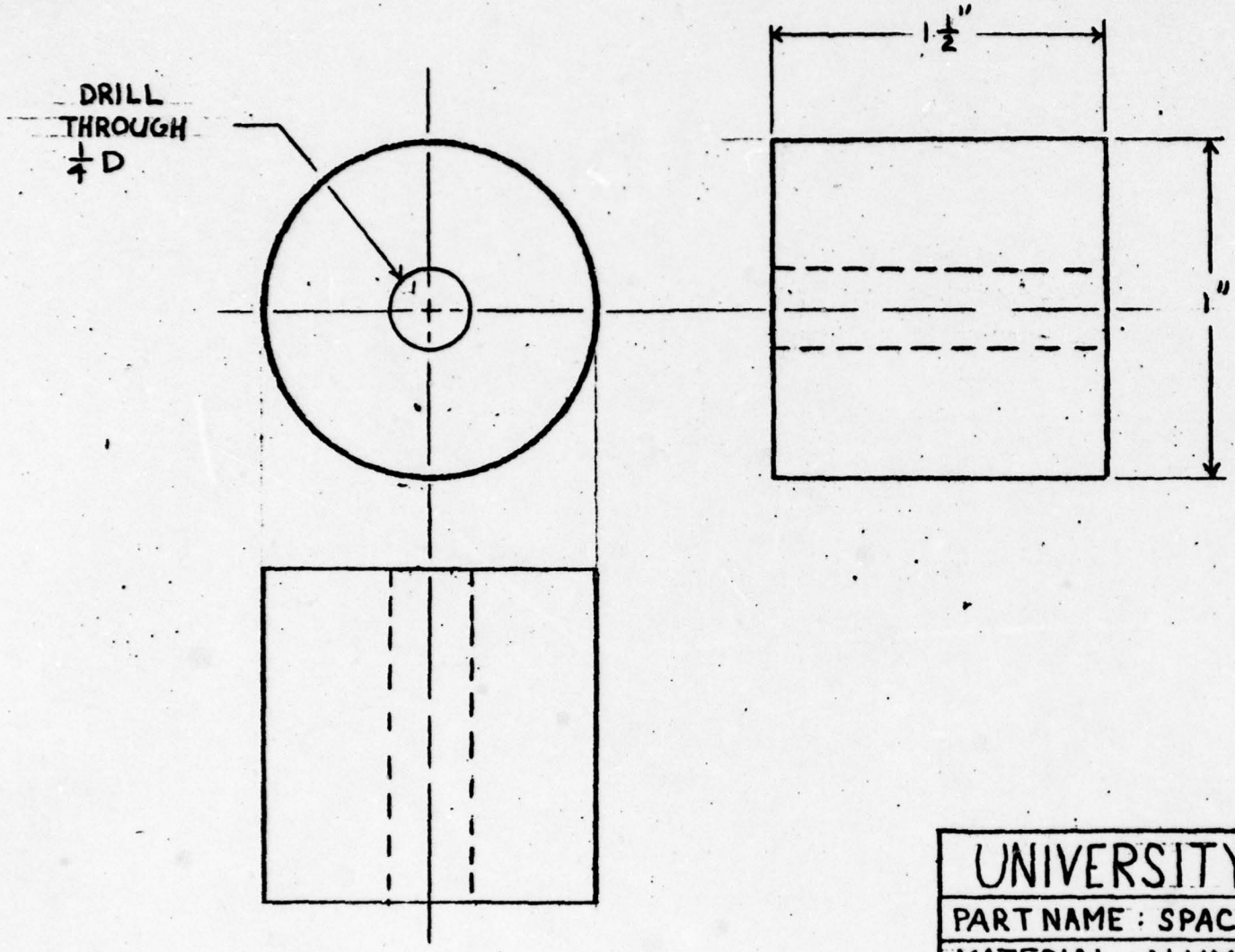

UNIVERSITY of FLORIDA	
PART NAME : SPACER	NO. B4
MATERIAL : ALUMINUM	
SCALE 2" = 1"	DATE 1-16-78
BY FRANK LAUDADIO	

B33

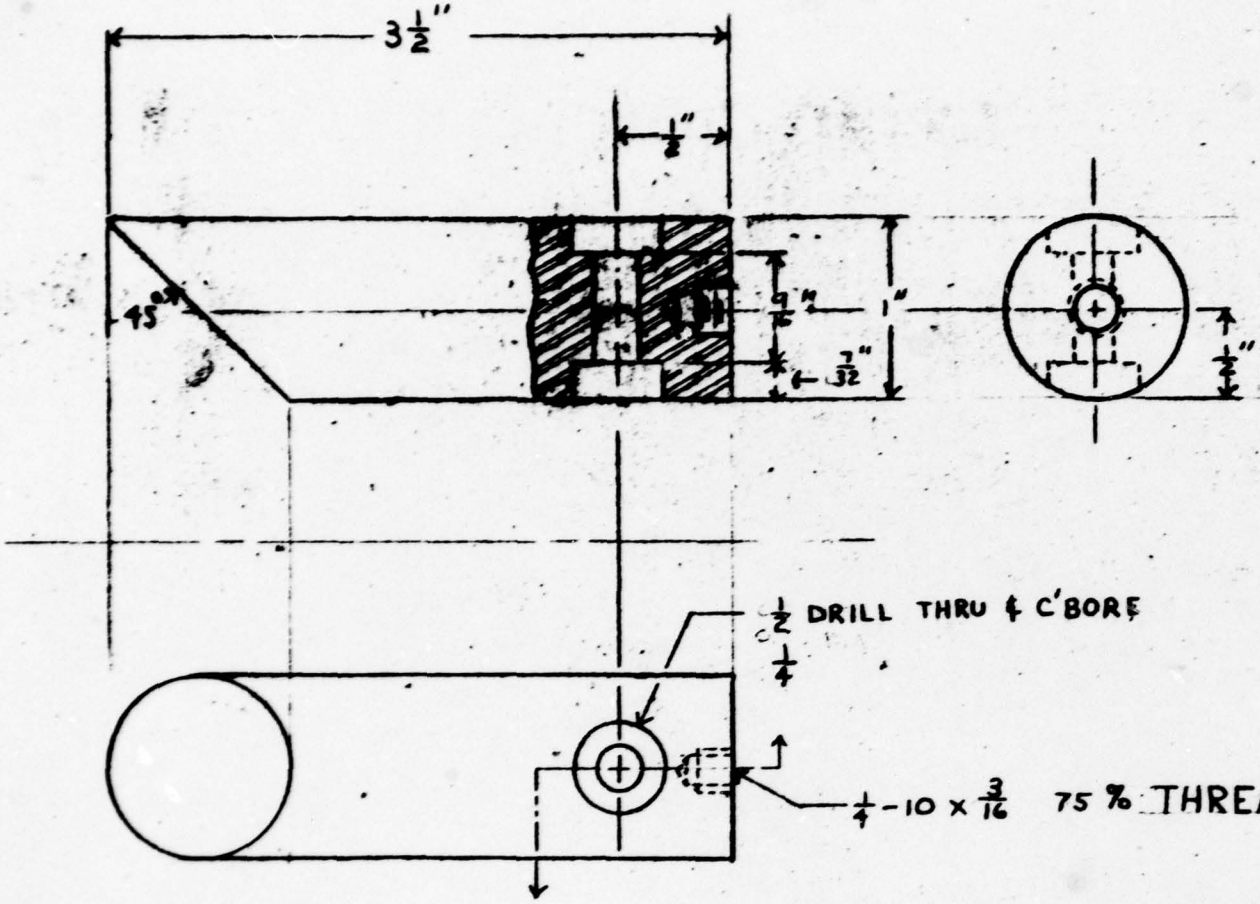

UNIVERSITY of FLORIDA	
PART NAME : ARM	NO.: B5
MATERIAL : STEEL	
SCALE 1"=1"	DATE 1-17-79
BY FRANK LAUDADIO *f Laudadio*	

B54

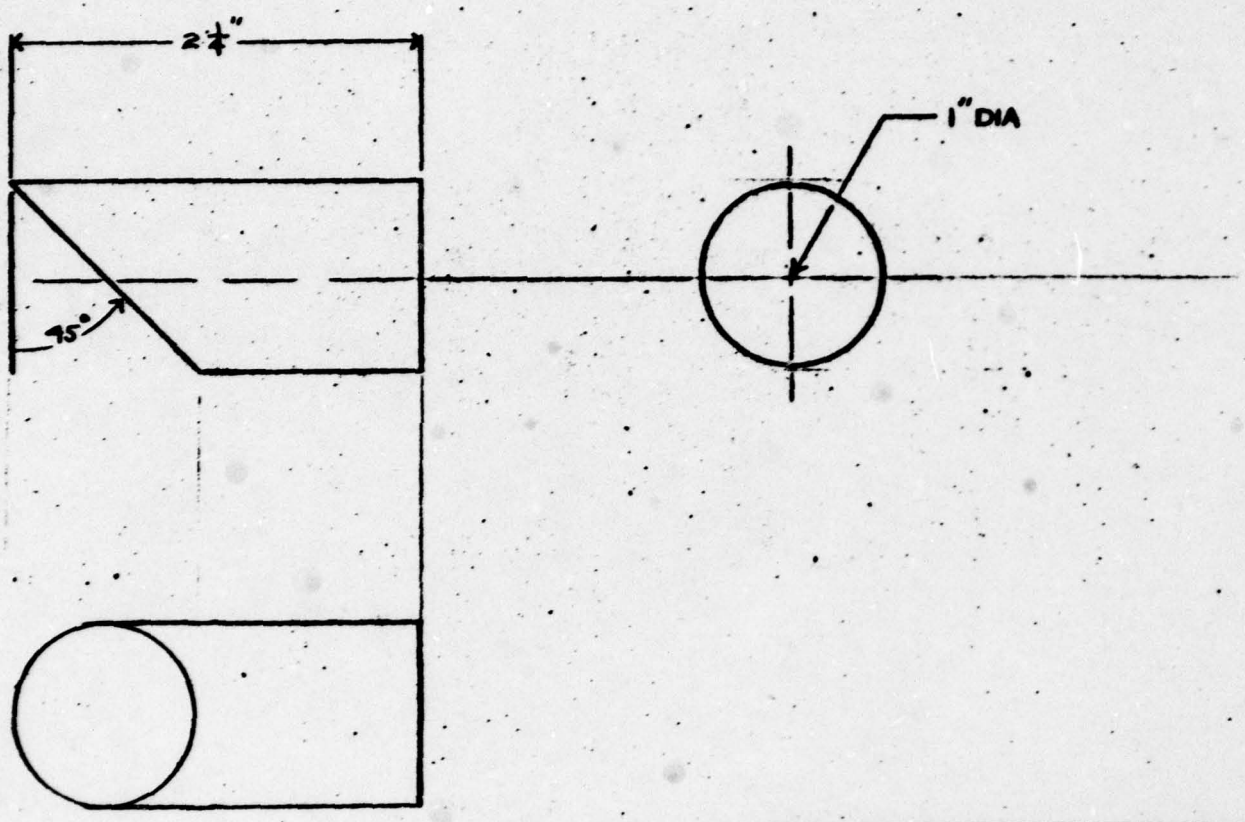

UNIVERSITY OF FLORIDA	
PART NAME LEG	
MATERIAL: STEEL	NO : B6
SCALE 1"=1"	DATE 1-22-79
BY FRANK LAUDADIO	

B55

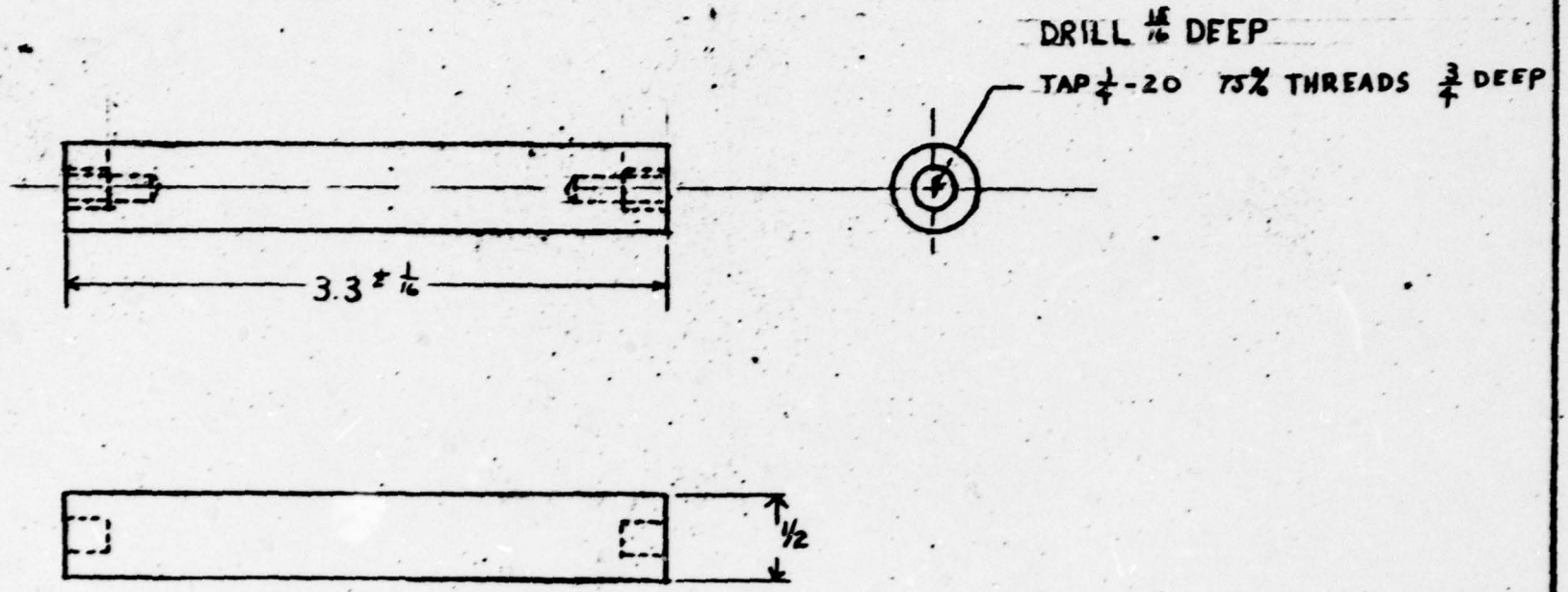

UNIVERSITY OF FLORIDA	
PART NAME : CORE	NO : B7
MATERIAL : STEEL	
SCALE 1" = 1"	DATE : 1-18-78
BY FRANK LAUDADIO	

B36

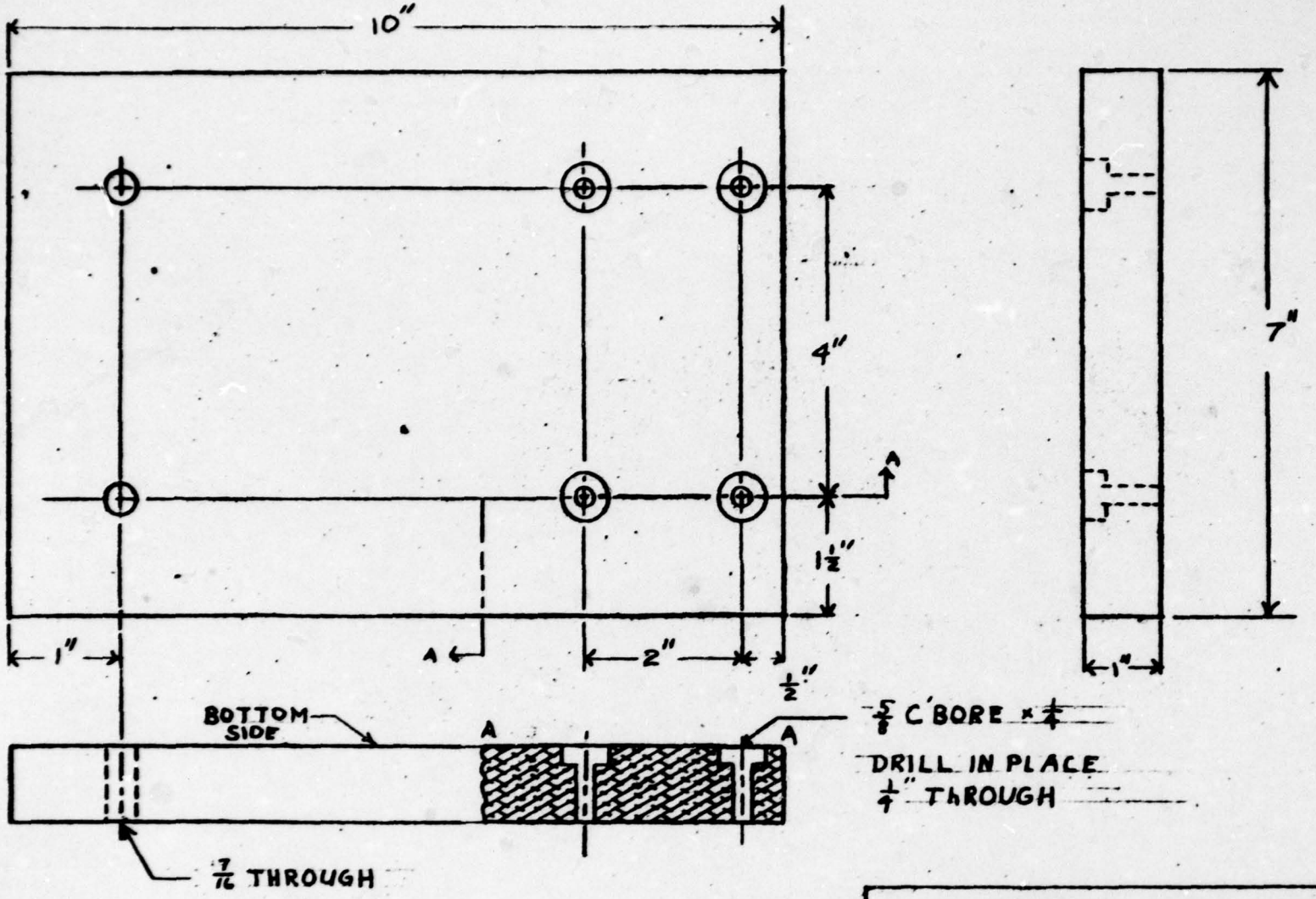

UNIVERSITY OF FLORIDA	
PART NAME : TABLE MOUNT	NO : B8
MATERIAL : ALUMINUM	
SCALE 2" = 1"	DATA 1-19-79
BY FRANK LAUDADIO	J. Laudadio

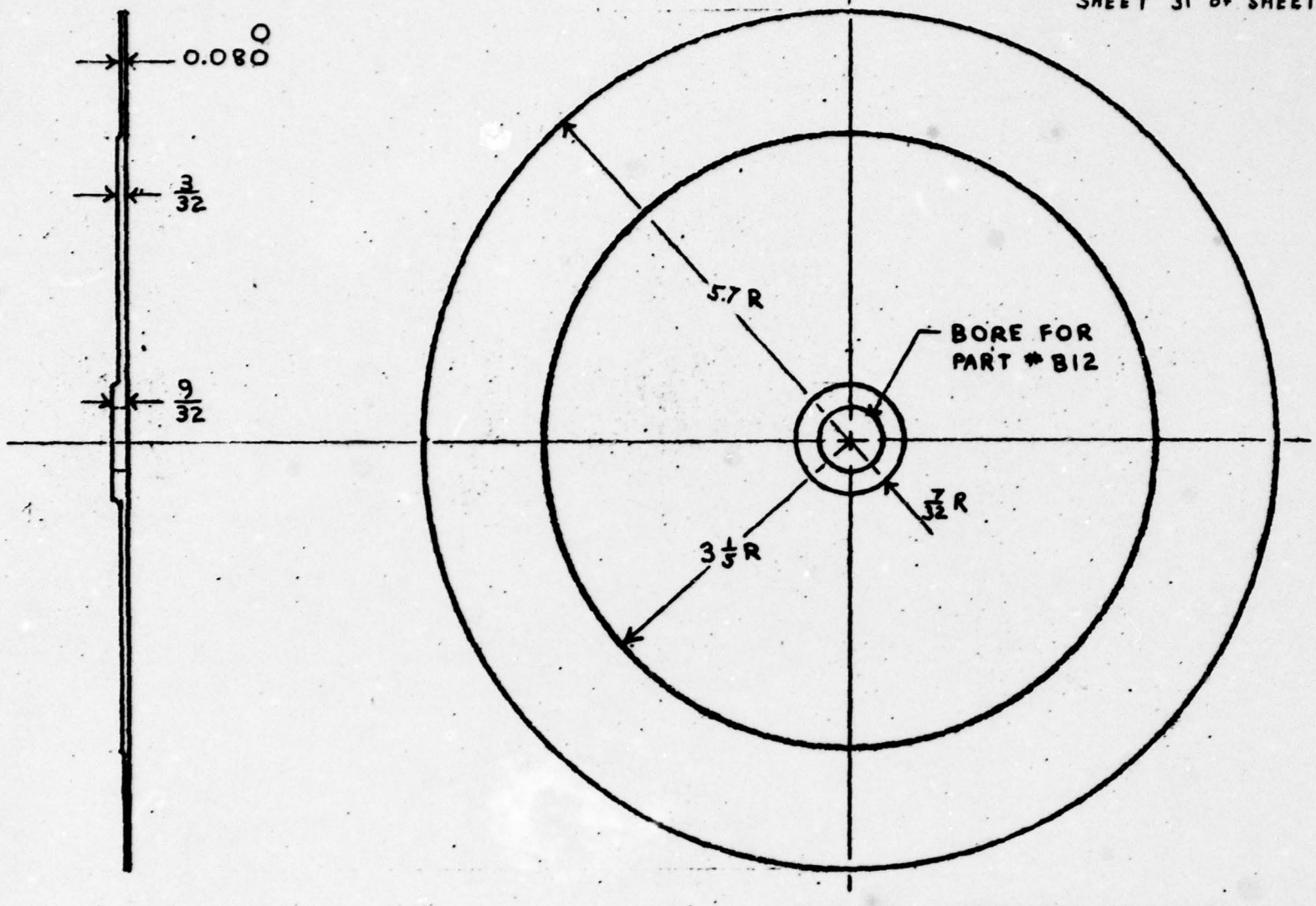

UNIVERSITY of FLORIDA	
PART NAME: DYNO DISK	NO: B9
MATERIAL: COPPER	
SCALE 1"=2"	DATE: 1-15-79
BY FRANK LAUDADIO	

B38

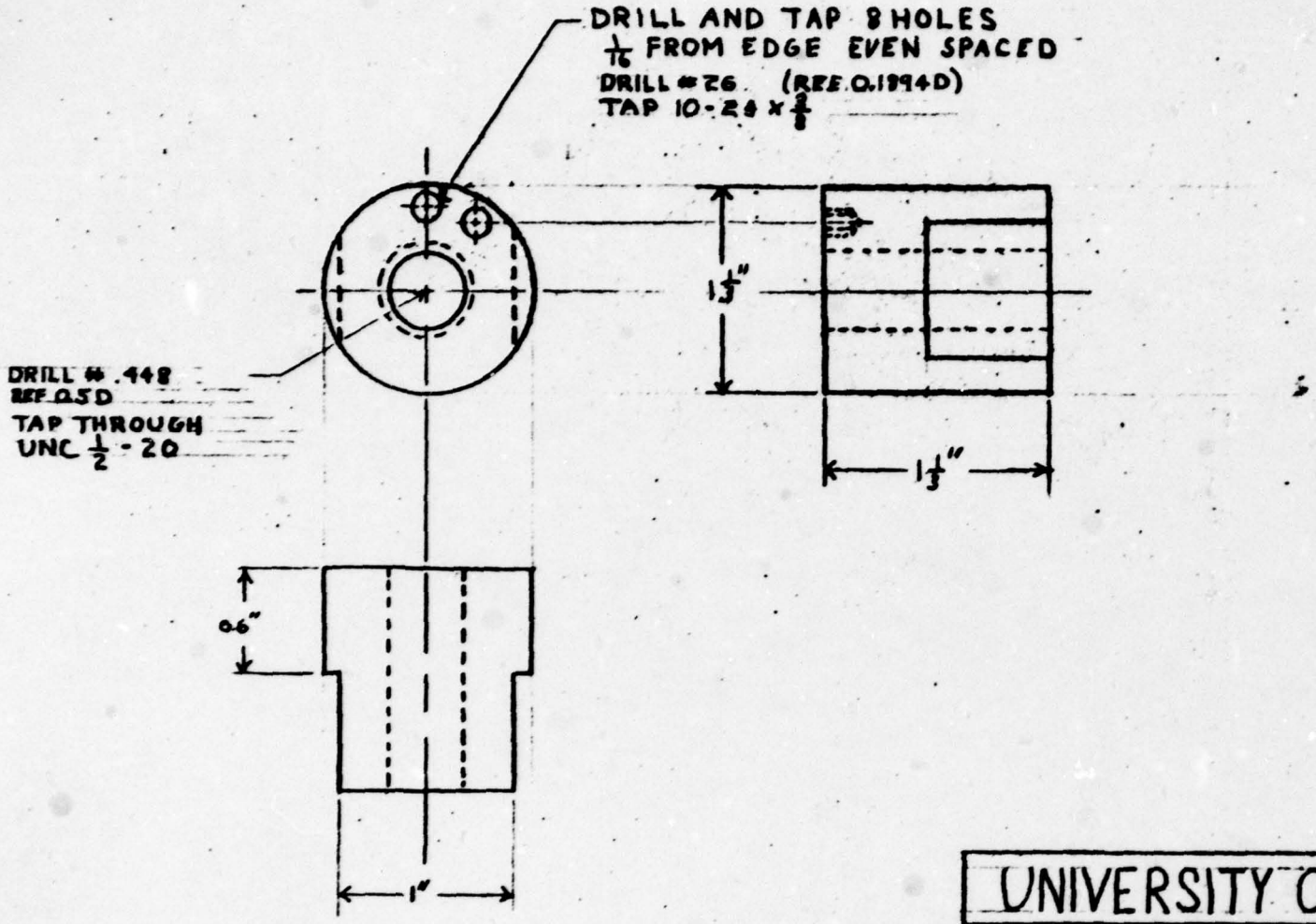

UNIVERSITY OF FLORIDA	
PART NAME : BALANCE LOCK NO B10	
MATERIAL : STEEL	
SCALE 1"=1"	DATE 1-16-78
BY FRANK LAUDADIO	F Laudadio

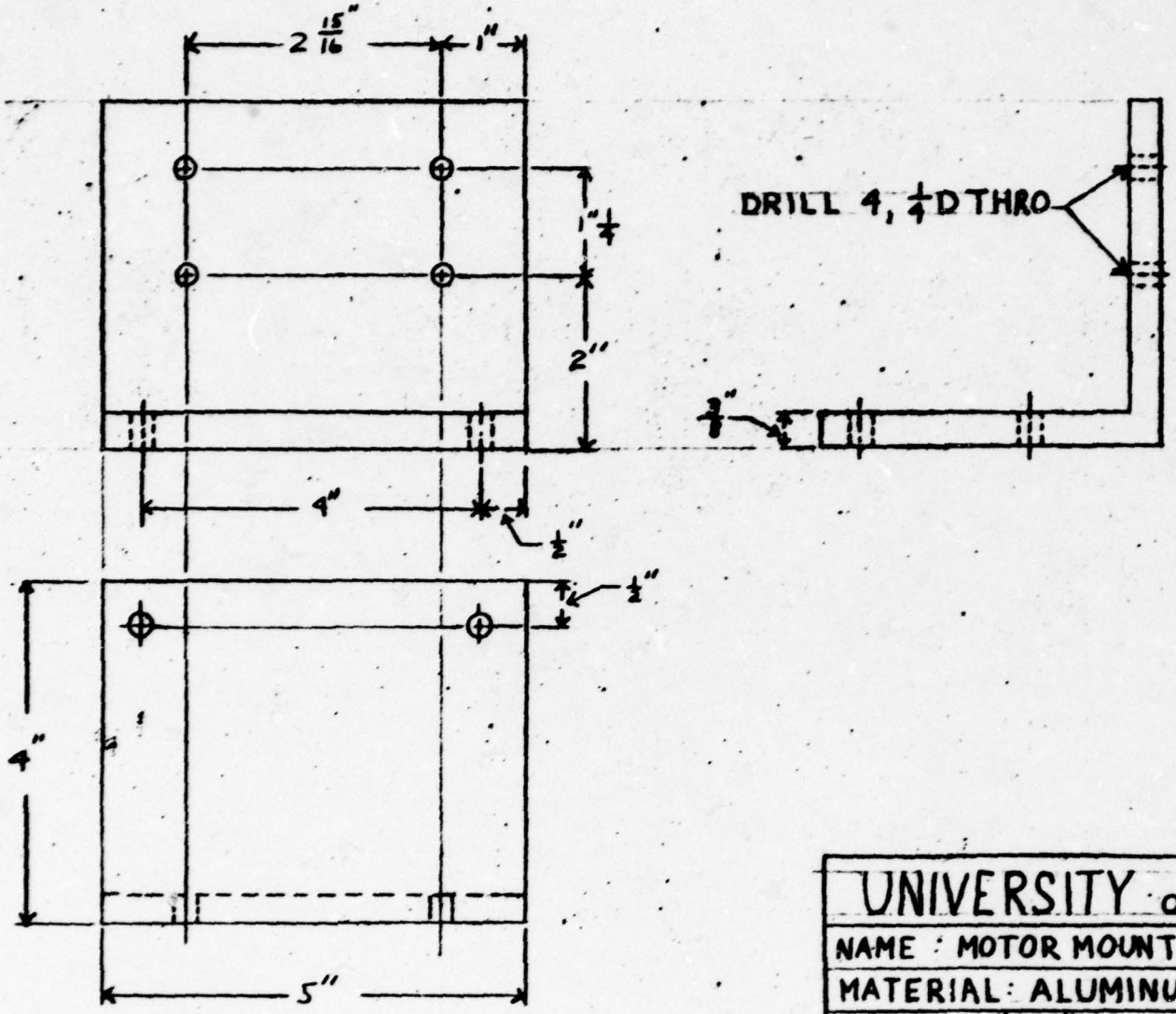

UNIVERSITY of FLORIDA	
NAME : MOTOR MOUNT	NO B11
MATERIAL: ALUMINUM	
SCALE 1" = 2"	DATE 1-22-79
BY FRANK LAUDADIO	

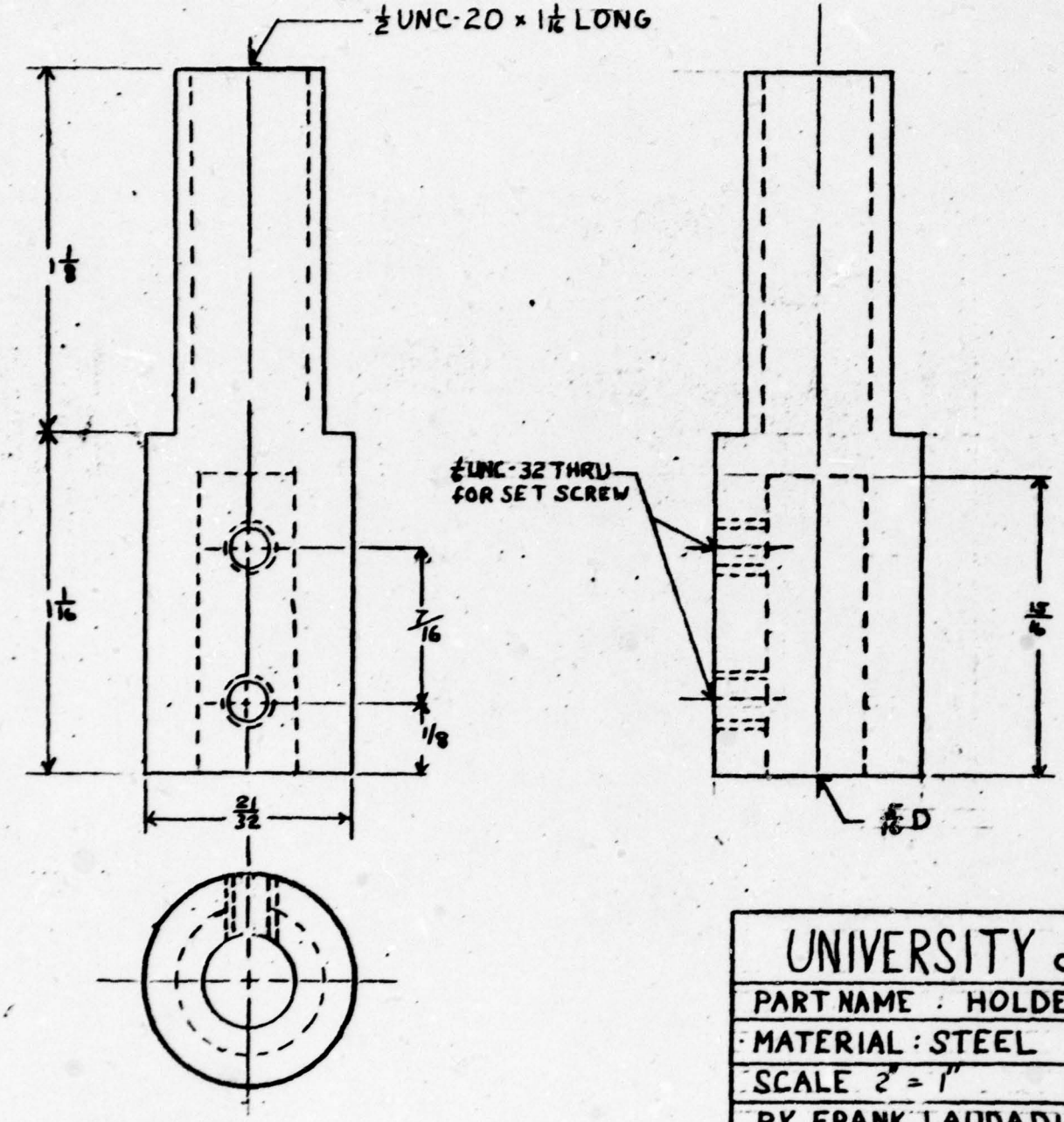

UNIVERSITY of FLORIDA	
PART NAME : HOLDER TOP	NO. B12
MATERIAL : STEEL	
SCALE 2" = 1"	DATE 1-23-79
BY FRANK LAUDADIO	

B11

Appendix C

Torquewhirl of a Flexible Shaft Rotor

Appendix C
Torquewhirl of a Flexible Shaft Rotor

Reference 1 gives an exact functional solution to the nonlinear differential equations of motion for a torque-loaded disk mounted on a straight rigid shaft, overhung from a flexible joint. This solution shows that load torque alone can produce nonsynchronous whirling, with amplitudes dependent on the ratio of torque to damping.

A model which more closely approximates a real machine, with a single overhung disk, is shown in Figure C-1. The shaft of length 1 is assumed to be flexible, but its mass is neglected as being insignificant compared to the disk.

Whereas the model of reference 1 has three degrees of freedom, the model of Figure C-1 has five. If a driving torque along the Z axis is reacted by a load torque aligned with the disk axis, then it might be supposed that the flexible shaft model has a solution for nonsynchronous whirl similar to that of reference 1.

To investigate this, consider generalized coordinates, x, y, θ, ϕ, ψ (Figures C-1 and C-2). The advantage of the Euler angles is that whirling is represented by constants, simplifying the search for a solution. The x,y coordinates do not have this advantage, and a whirling solution requires harmonic (time-dependent) functions. Therefore, consider replacing x,y by R,α, where R is the projection of $\overline{OG}$ on the xy plane and α is the angle XOG. the complete set of coordinates is then R, α, θ, ϕ, ψ, and the kinetic energy is expressed as

$$T = \frac{1}{2} M[\dot{R}^2 + (R\dot{\alpha})^2] + \frac{1}{2} I_x w_x^2 + \frac{1}{2} I_y w_y^2 + \frac{1}{2} I_z w_z^2,$$

where

$$w_x = \dot{\phi} \sin\theta \sin\psi + \dot{\theta} \cos\psi$$

$$w_y = \dot{\phi} \sin\theta \cos\psi - \dot{\theta} \sin\psi$$

$$w_z = \dot{\psi} + \dot{\phi} \cos\theta$$

The potential energy is elastic (strain) energy stored in the shaft, and will be a function

$$V = V(R, \alpha, \theta, \phi, \psi)$$

The potential energy is more easily written as $V(X, Y, \alpha_x, \alpha_y, \psi)$ where α_x, α_y are disk rotations about x and y. Therefore, it may be productive to derive transformations from x, y, α_x, α_y to R, α, θ, ϕ.

Since ψ is pure twist, it may appear in an uncoupled term.

The virtual work of the load torque produces the same generalized torques Q_ϕ and Q_ψ as in reference 1. Most of the external damping, however, will act on $\dot{R}$ and $R\dot{\alpha}$, rather than on $\dot{\theta}$ and $\dot{\phi}$.

A Simplifying Assumption

Considerable simplification is accomplished by assuming that the shaft remains in the plane BOG when it bends, thus reducing the degrees of freedom to four. An attractive set of coordinates is ℓ_e, θ, ϕ, ψ (see Figures C-1 and C-2) also, let $\Phi = \phi + \pi/2$ and the following relationships can be written:

$$x^2 + y^2 = \ell_e \sin\theta, \qquad \text{(C-1)}$$

$$\tan\phi = \frac{-x}{y}, \qquad \text{(C-2)}$$

$$\tan\phi = \frac{x}{y}\,, \tag{C-3}$$

$$\dot{\phi} = \phi = \frac{x\dot{y} - y\dot{x}}{x^2 + y^2} \tag{C-4}$$

$$w = \dot{\phi} + \dot{\psi} \tag{C-5}$$

The body rates are:

$$w_x = \dot{\phi}\,\sin\theta\sin\psi + \dot{\theta}\,\cos\psi, \tag{C-6}$$

$$w_y = \dot{\phi}\,\sin\theta\cos\psi - \dot{\theta}\,\sin\psi, \tag{C-7}$$

$$w_z = \dot{\psi} + \dot{\phi}\,\cos\theta. \tag{C-8}$$

Note that $w \neq w_z$.

The kinetic energy can now be written as

$$T = \frac{1}{2} M[(\dot{\ell}_e \sin\theta + \ell_e \dot{\theta} \cos\theta)^2 + (\dot{\phi}\,\ell_e \sin\theta)^2] + \frac{1}{2} I_x[\dot{\theta}^2 + \dot{\phi}^2 \sin^2\theta]$$

$$+ \frac{1}{2} I_z(\dot{\psi} + \dot{\phi}\cos\theta)^2 \tag{C-9}$$

for a symmetric rotor ($I_x = I_y$).

The potential energy is

$$V = V(\theta, \ell_e) \tag{C-10}$$

The virtual work of the damping forces is

$$\delta w = -C_d[\dot{\ell}_e \sin\theta + \dot{\ell}_e \cos\theta](\delta\ell_e \sin\theta + \ell_e\,\delta\,\theta\cos\theta)$$

$$- C_d[\ell_e\,\dot{\phi}\sin\theta](\ell_e \sin\theta)\,\delta\phi,$$

and the virtual work of the driving torque and load torque is the same as in reference 1.

The three differential equations of motion are obtained by substituting $L = T - V$ and the Q_i into

$$\frac{d}{dT}\left(\frac{\delta L}{\delta \dot{q}_i}\right) - \frac{\delta L}{\delta q_i} = Q_i, \quad i = 1, 2, 3$$

where $q_1 = \ell_e$, $q_2 = \theta$, $q_3 = \phi$, $q_4 = \psi$,

The solution should be similar to that of reference 1.

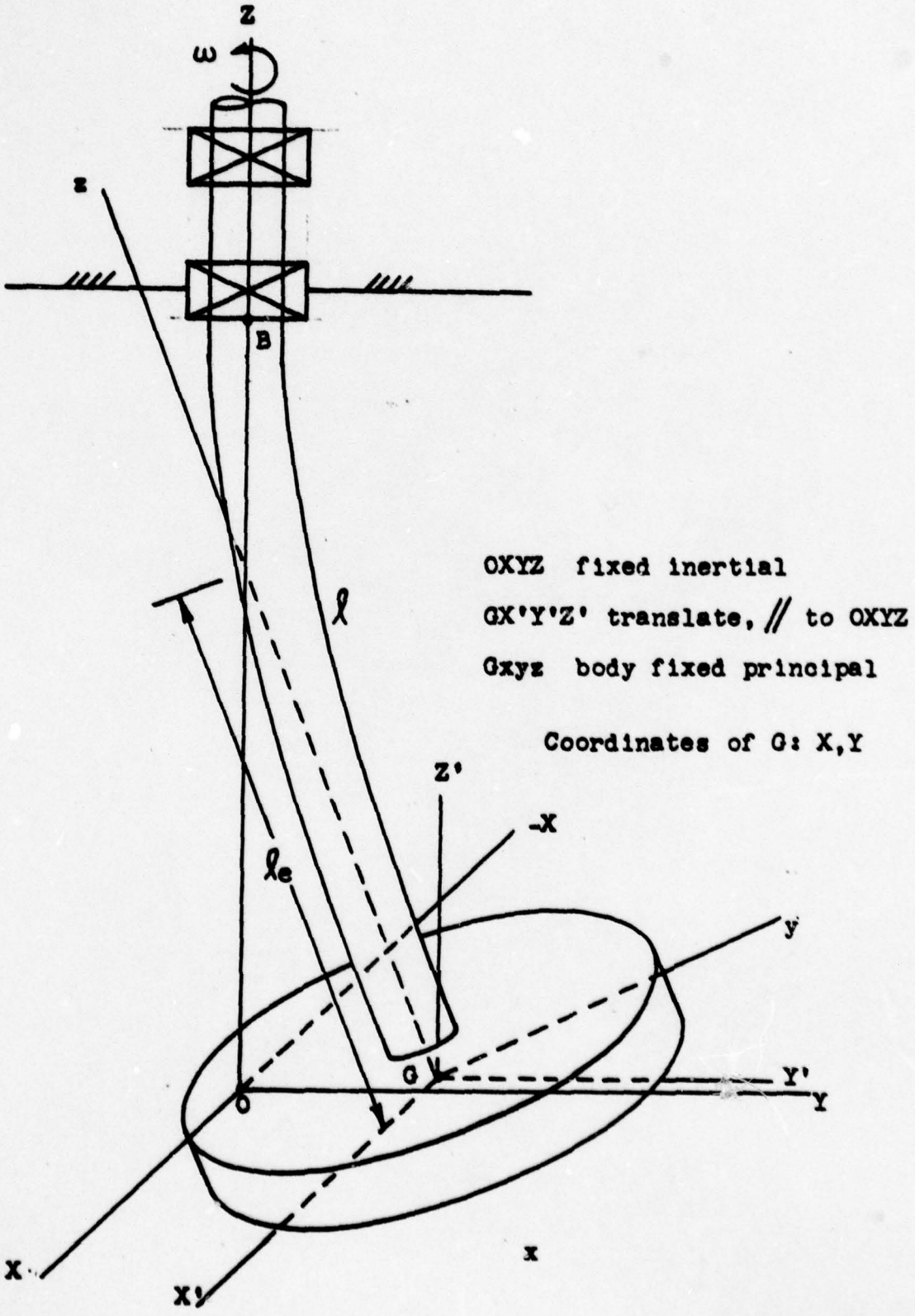

Figure C-1: Cartesian Coordinates

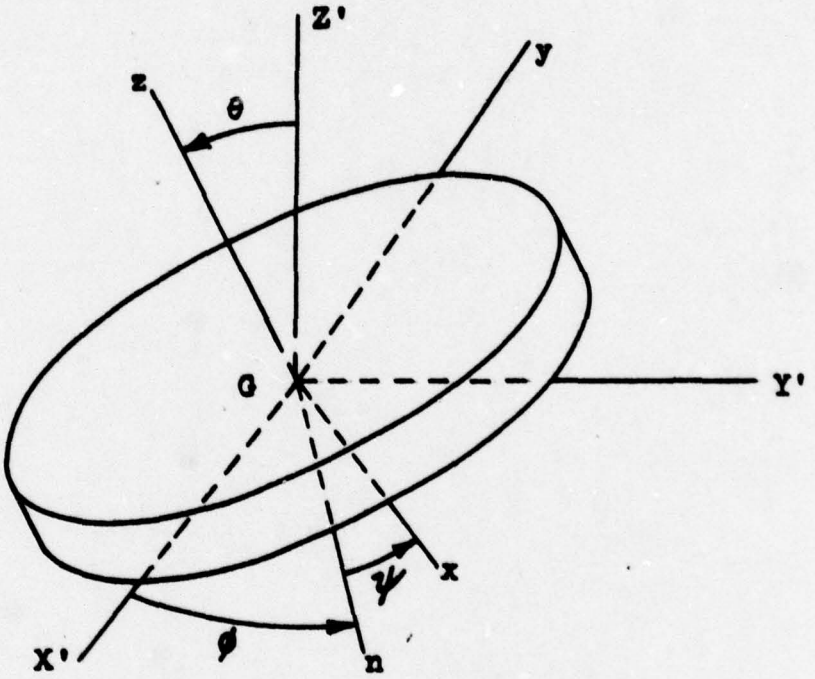

xyz originally coincident with X'Y'Z'

1. Rotate through ϕ about z(Z') (x goes to n)
2. Rotate about n(x) through θ
3. Rotate about z through ψ

Figure C-2: Euler angle coordinates

Appendix D

Torquewhirl Stability Predictions for Multi-Disk Rotors by the Transfer Matrix Method

Appendix D
Torquewhirl Stability Predictions for Multi-Disk Rotors by the Transfer Matrix Method

Lund (reference 14) has extended the Myklestad-Prohl transfer matrix method to rotor-bearing systems which include damping and destabilizing cross-coupled stiffness and damping coefficients. Whereas the Myklestad-Prohl method yields only the imaginary part of the eigenvalues (i.e. the natural frequencies), the Lund method yields complex eigenvalues (i.e. both the natural frequencies and the logarithmic decrement, which is a stability predictor).

Currently the greatest limitation of Lund's method (as with all other stability analyses) is the lack of accurate information about the types of destabilizing excitations which exist in real machines and which therefore are to be used as input to the computer program. Torquewhirl (reference 1) has recently been identified as one of these excitations. To put the torquewhirl forces into a Lund stability analysis, they must be formulated in terms of stiffness and damping coefficients.

The coordinates used in Lund's analysis are shown in Figure D-1. In general, the stiffness and damping coefficients are the matrices which define the forces and moments on each disk in the x and y directions.

For example, the force on a disk in the x direction, due to disk displacement and velocity, is

$$F_x = -K_{xx}X - K_{xy}Y - C_{xx}\dot{X} - C_{xy}\dot{Y} - K_{x\alpha}\alpha - K_{x\beta}\beta - C_{x\alpha}\dot{\alpha} - C_{x\beta}\dot{\beta}$$

and the matrix equation for the forces in all directions (on a single disk) is

$$\begin{Bmatrix} F_x \\ F_y \\ F_\alpha \\ F_\beta \end{Bmatrix} = - \begin{bmatrix} K_{xx} & K_{xy} & K_{x\alpha} & K_{x\beta} \\ K_{yx} & K_{yy} & K_{y\alpha} & K_{y\beta} \\ K_{\alpha x} & K_{\alpha y} & K_{\alpha\alpha} & K_{\alpha\beta} \\ K_{\beta x} & K_{\beta y} & K_{\beta\alpha} & K_{\beta\beta} \end{bmatrix} \begin{Bmatrix} x \\ y \\ \alpha \\ \beta \end{Bmatrix} - \begin{bmatrix} C_{xx} & C_{xy} & C_{x\alpha} & C_{x\beta} \\ C_{yx} & C_{yy} & C_{y\alpha} & C_{y\beta} \\ C_{\alpha x} & C_{\alpha y} & C_{\alpha\alpha} & C_{\alpha\beta} \\ C_{\beta x} & C_{\beta y} & C_{\beta\alpha} & C_{\beta\beta} \end{bmatrix} \begin{Bmatrix} \dot{X} \\ \dot{Y} \\ \dot{\alpha} \\ \dot{\beta} \end{Bmatrix},$$

where F_α and F_β are actually moments on the disk.

It can be seen that there are a total of thirty two stiffness and damping coefficients defining the forces and moments on each disk. The off-diagonal elements are called the cross-coupled coefficients.

For the rigid-shaft, flexible joint, torquewhirl model in reference 1, the disk rotation and translation coordinates are not independent (i.e. they are related by a kinematic constraint). The constraint equations are $R = \ell\theta$ in polar coordinates or $x^2 + y^2 = (\ell \sin\theta)^2$ in inertial coordinates.

Since the equations and generalized forces in reference 1 are written in terms of Euler angles ϕ, θ, and ψ, a coordinate transformation is required to derive the stiffness and damping coefficients, as follows (see Figure D-2):

First, the generalized torque Q_ϕ of reference 1 can be expressed as a tangential force (see Figure D-2)

$$F_\phi = Q_\phi/R,$$

and the generalized moment Q_θ can be expressed as a radial force

$$F_R = Q_\theta/\ell \cos\theta.$$

It is Q_ϕ (or F_ϕ) which contains the destabilizing torquewhirl forces. The transformation to x and y is

$$F_x = F_R \cos\phi - F_\phi \sin\phi$$

$$F_y = F_R \sin\phi + F_\phi \cos\phi$$

where

$$\sin\phi = \frac{y}{(x^2 + y^2)^{\frac{1}{2}}}$$

$$\cos\phi = \frac{x}{(x^2 + y^2)^{\frac{1}{2}}}$$

For the aerodynamic case (see reference 1), the generalized torque Q_ϕ is

$$Q_\phi = T_s - \bar{C}_L(\dot{\psi} + \dot{\phi}\cos\theta)^2 \cos\theta - \bar{C}_d(\ell^3 \sin^3\theta)\,\dot{\phi}^2,$$

where

T_s = shaft torque

$\bar{C}_L$ = disk load coefficient

$\bar{C}_d$ = nonlinear damping coefficient

The shaft speed w_s is

$$w_s = \dot{\psi} + \dot{\phi}.$$

The shaft torque equals the disk load torque so that

$$T_s = \bar{C}_L\,(\dot{\psi} + \dot{\phi}\cos\theta)^2$$

Therefore the generalized torque Q_ϕ can be expressed as

$$Q_\phi = T_s\,[1 - \cos\theta] - \bar{C}_d\,(\ell^3 \sin^3\theta)\,\dot{\phi}^2 .$$

Rigid-Shaft Model (Reference 1)

The destabilizing part of Q_ϕ is the first term from the expression just above. The equivalent tangential force F_ϕ is

$$F_\phi = \frac{Q_\phi}{R} = \frac{T_s(1 - \cos\theta)}{R}$$

The required relationships between R, θ, and α, β, and x, y are

$$R = (x^2 + y^2)$$

$$x = \alpha\ell$$

$$y = -\beta\ell$$

$$\text{and } \theta = (\alpha^2 + \beta^2)^{\frac{1}{2}}$$

Therefore, in terms of x and y, we can write

$$F_\phi = \frac{T_s\left[1 - \cos\frac{(x^2 + y^2)^{\frac{1}{2}}}{\ell}\right]}{(x^2 + y^2)^{\frac{1}{2}}}$$

Keeping only the first two terms of the cosine series yields

$$F_\phi = \frac{T_s}{2\ell^2}(x^2 + y^2)^{\frac{1}{2}}$$

or

$$F_x = -F_\phi \sin\phi = -\frac{T_s}{2\ell^2} y,$$

$$F_y = F_\phi \cos\phi = \frac{T_s}{2\ell^2} x$$

By inspection, it can be seen that the cross-coupled stiffnesses are

$$K_{xy} = \frac{T_s}{2\ell^2}$$

$$K_{yx} = -\frac{T_s}{2\ell^2}$$

It is interesting to note that K_{xy} and K_{yx} have the same form as Alford's coefficients for the effect of tip clearance asymmetry in axial flow turbomachinery (reference 7).

As a crude approximation, the above coefficients (K_{xy}, K_{yx}) could be used for a flexible-shaft model by taking ℓ as the axial distance from the disk plane to a virtual pivot point, as determined by the mode shape.

Flexible-Shaft Model

When the rotor flexibility is distributed along the shaft, there is no constraint between x, y and α, β (see Figure D-1). Therefore the virtual work of the destabilizing torque must be written in terms of x, y, α, and β. This requires that the virtual displacement $\delta\phi$ be written in terms of δx, δy, $\delta\alpha$, and $\delta\beta$.

Since the rotations of a disk are independent of the translations, it can be seen that δx and δy will not appear in $\delta\phi$. This leaves only the virtual angular displacements $\delta\alpha$ and $\delta\beta$ to be considered. A kinematical relationship between ϕ, α, and β is thus required.

Assuming this can be obtained, we proceed as follows:

For a multi-disk rotor, the destabilizing torque on the n^{th} disk is

$$Q_{\phi_n} = \eta_n T_s (1 - \cos\theta_n)$$

where

η_n = fraction of the shaft torque accounted for by the nth disk

$\theta_n = (\alpha_n^2 + \beta_n^2)^{1/2}$ (see Figure D-1)

Therefore the virtual work of the shaft torque on the n^{th} disk is

$$\delta w = \eta_n T_s (1 - \cos\theta_n) \delta\theta_n$$

$$= F_{\alpha_n} \delta\alpha_n + F_{\beta_n} \delta\beta_n$$

The cross-coupled stiffness coefficients will then be

$$K_{\alpha\beta} = - \frac{\delta F_{\alpha_n}}{\delta\beta_n}$$

$$K_{\beta\alpha} = - \frac{\delta F_{\beta_n}}{\delta\alpha_n}$$

Derivation of the Characteristic Polynomial from the Transfer Matrices

In the computer analysis of reference 14, the complex roots of the characteristic equation are obtained by a numerical iteration algorithm. In some cases involving a large number of mass stations along the rotor, the algorithm has been known to miss certain roots. Also, the roots are not determined in any particular order, and the higher order roots are less accurately determined.

These shortcomings suggest that it would be advantageous to have the characteristic polynomial available, so that more efficient computer subroutines ("rootfinders") could be used to determine the roots. Of course, the polynomial could be obtained by expanding the determinant of the large eigenmatrix, but this would require a very large computer storage array, thus losing one of the advantages of the transfer matrix method.

Also, electrical engineering and controls technology have produced a wide and powerful array of stability investigation techniques which use the characteristic polynomial as a starting point. There is no reason to doubt that many of these techniques would be useful for rotor dynamic stability studies.

Derivation of the characteristic polynomial by multiplication of fifteen or twenty (four by four) transfer matrices for a rotor is a challenging task. Attempts to derive functional expressions by direct multiplication have been successful only for four or less mass stations on the rotor. A numerical scheme is outlined in reference 15, but is implemented only for a simple undamped beam vibrating in one plane. Therefore the most recent efforts on this Grant have been directed toward developing a formal scheme to generate the numerical values of the polynomial coefficients on a digital computer.

To develop such a scheme, it was found helpful to begin with a somewhat simpler, although completely analogous, problem. This is the generation of polynomial coefficients for torsional vibration of a multi-disk rotor. Figure D-3 shows the model used.

The transfer equation across the n^{th} inertia station is

$$T'_n = T_n + S^2 I_n \theta_n + S\beta_n \theta_n + K_n \theta_n$$

where S is the complex eigenvalue.

Across the n^{th} (massless) shaft segment, the equations are

$$T_{n+1} = T'_n$$

and

$$\theta_{n+1} = \theta'_n + \frac{T'_n}{k_n + c_n S}$$

A numerical computation of the eigenvalues, by Hölzer's method, starts with an assumption for S along with setting the arbitrary amplitude $\theta_1 = 1$ at the left hand end. The transfer equations above are then used repetitively, from left to right along the length of the rotor, to calculate the right end boundary torque. If this torque is correct, the assumption for S is known to be an eigenvalue.

Here, the transfer equations are to be used to derive the coefficients of the characteristic polynomial, which has the form

$$a_o + a_1 S + a_2 S^2 + a_3 S^3 + \ldots + a_{N-2} S^{N-2}$$

for an N-inertia rotor with zero boundary torques. This can be achieved by either of the following two methods. (The case with no damping is illustrated for simplicity).

Method 1:

The amplitudes θ_n and θ_{n+1} are eliminated by substitution from the transfer equations to yield (for S = iw)

$$T'_n = T'_{n-1}\left(1 + \frac{I_n}{I_{n-1}} - w^2 \frac{I_n}{k_{n-1}}\right) - T'_{n-2} \frac{I_n}{I_{n-1}} .$$

Start at the left end where n = 1 and work to the right by substitution. For example, substitute T'_1 for T'_{n-2} and T'_2 for T'_{n-1} to generate T'_3. T'_1 and T'_2 are made especially simple by the assumption $\theta_1 = 1$. They are

$$T'_1 = -w^2 I_1$$

and

$$T'_2 = -w^2\left[I_1 + I_2\left(1 - w^2 \frac{I_1}{k_1}\right)\right] .$$

In the computer program, all parameters except w have numerical values. Coefficients of like powers of w are summed into an array as the multiplication progresses to the right end, where the boundary torque is zero.

Method 2:

The polynomial coefficients of the four-inertia rotor can be obtained in the following form, which suggests a pattern for the more general N-inertia system.

$$a_o = - \frac{k_1 k_2 k_3 (I_1 + I_2 + I_3 + I_4)}{I_1 I_2 I_3 I_4}$$

$$a_2 = \left[\frac{k_1 k_2 (I_1 + I_2 + I_3)}{I_1 I_2 I_3} + \frac{k_2 k_3 (I_2 + I_3 + I_4)}{I_2 I_3 I_4} + \frac{k_1 k_3 (I_3 + I_4)}{I_1 I_3 I_4} + \frac{k_1 k_3 (I_3 + I_4)}{I_2 I_3 I_4}\right]$$

$$a_4 = -\left[\frac{k_1(I_1 + I_2)}{I_1 I_2} + \frac{k_2(I_2 + I_3)}{I_2 I_3} + \frac{k_3(I_3 + I_4)}{I_3 I_4}\right]$$

$$a_6 = 1$$

Extending the pattern to a five-inertia rotor yields

$$a_o = \frac{k_1 k_2 k_3 k_4 (I_1 + I_2 + I_3 + I_4 + I_5)}{I_1 I_2 I_3 I_4 I_5}$$

etc.

It appears that methods analogous to the two methods above can be developed to generate the characteristic polynomial for rotor whirl stability predictions.

Figure D-1: Virtual Work in Terms of Coordinates Used in Lund's Program

The position of the disk is described by x, y, α, β (z is negligible and ω is constant)

x & y give position of CG

α & β give angular orientation of the disk (Lund calls them θ & ϕ)

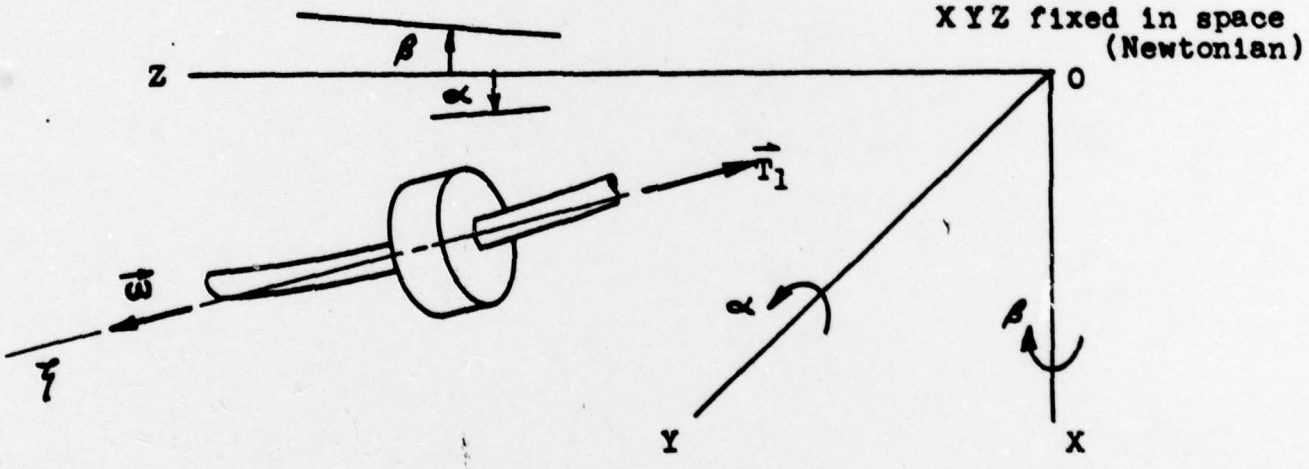

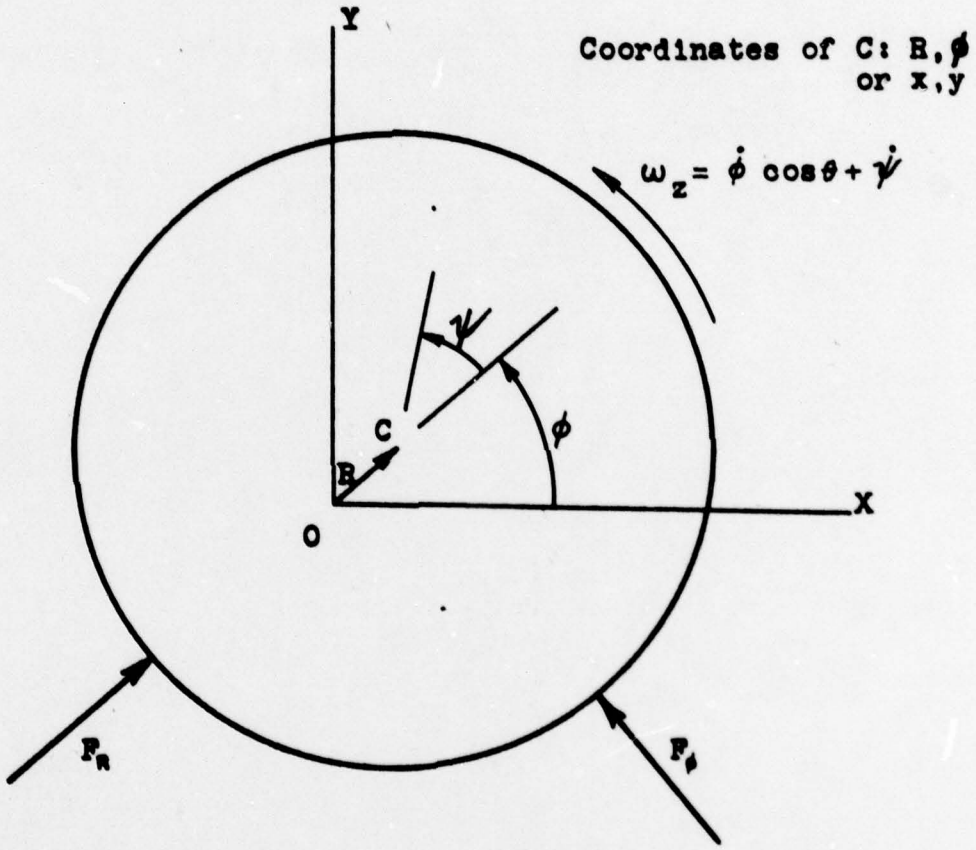

Figure D-2 : Radial and Tangential Forces on the Deflected Rotor Disk of Reference I.

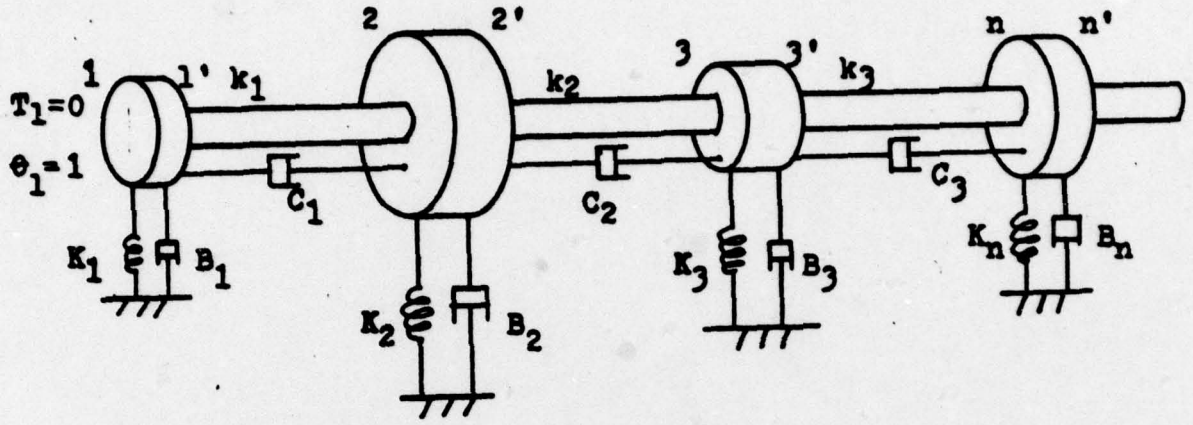

a) Discretized Model

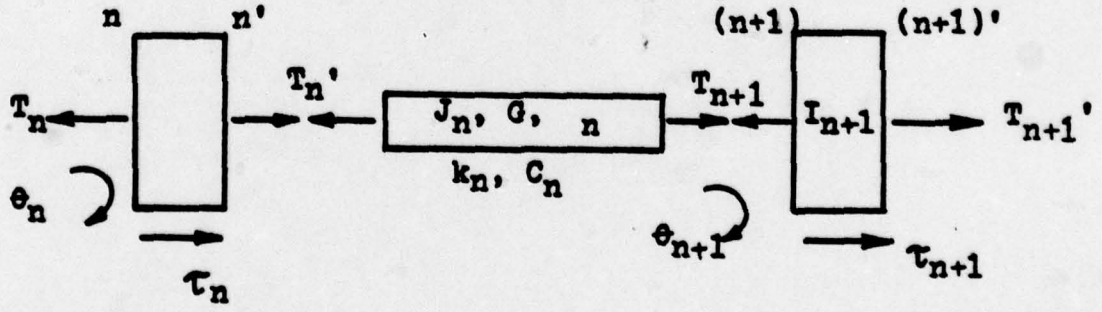

b) The nth station

Figure D-3: Rotor Model for Torsional Vibration